Leveraging Systems-level Metabolic Modeling and Machine Learning to Optimize Antibiotic Combination Therapy Design

by

Carolina H. Chung

A dissertation submitted in partial fulfillment
of the requirements for the degree of
Doctor of Philosophy
(Biomedical Engineering)
in the University of Michigan
2023

Doctoral Committee:

Associate Professor Sriram Chandrasekaran, Chair
Associate Professor Kelly B. Arnold
Associate Professor Deepak Nagrath
Associate Professor Evan Snitkin
Associate Professor Kevin Wood

Carolina H. Chung

chechung@umich.edu

ORCID iD: 0000-0003-2490-1842

Dedication

This dissertation is dedicated to my family, friends, and mentors who have supported me throughout my academic journey.

Acknowledgements

I would first and foremost like to thank my mom, dad, and sisters who have always been my #1 supporters in the advancement of my education. I would also like to acknowledge the friends that I have made throughout high school and college for helping me truly experience the meaning of camaraderie though challenging yet unforgettable experiences over the past decade. Most importantly, I would like to recognize all the mentoring figures who helped me navigate the maze that is higher education, namely:

- Cathy Whitlow, my high school biology teacher who showed me that college education was a definite possibility for me
- Prof. Monika Abramenko, my mathematics professor at UVA who revealed how rewarding and fulfilling teaching can be
- Prof. Kyongbum Lee and Prof. Carol Kumamoto, who graciously took me in as a summer undergraduate research intern at Tufts University (the first research experience that I ever had)
- Prof. Jason Papin and (now) Dr. Laura Dunphy, who helped nurture the researcher in me during my last year at UVA
- Last but not least, my dissertation committee who has guided me since the beginning of my graduate school experience into becoming a full-fledged independent researcher

I would especially like to thank Sriram, who was one of the best mentors that I could have ever asked for, and all the members in the Chandrasekaran Lab who I have built a long-lasting rapport with. Finally, I would like to acknowledge the generous support that I received from grants awarded to Sriram by the National Institutes of Health and the Beyster family who directly supported me as a 2022–2023 Beyster Fellow.

Table of Contents

List of Tables

List of Figures

List of Equations

Abstract

Over the past century, the rise of antibiotic resistance (AR) has closely followed the discovery of new antibiotics and has continued to increase as antibiotic development stalled within the past few decades. Combination therapy, which involves the prescription of two or more therapeutic agents, is a promising solution for combating AR. However, the process of designing effective combination therapies is plagued by several challenges, including: (a) the exponential explosion in the combinatorial space to search as the number of drugs and dosage levels to screen increases, (b) the heterogeneity in bacterial drug response due to differences in genetic and phenotypic states, and (c) the limited mechanistic insight that empirical methods for combination therapy design currently offer. For my dissertation research, I sought to optimize the design of antibiotic combination therapies by considering intrinsic and extrinsic factors that influence the bacterial response to drug treatment (**Chapter 1**). To this end, I developed two computational methods that predict drug interaction outcomes (e.g., synergy) in specific cell states and growth conditions.

The first approach is CARAMeL (**Chapter 2**), which stands for *Condition-specific Antibiotic Regimen Assessment using Mechanistic Learning*. CARAMeL leverages genome-scale metabolic models and machine learning to generate condition-specific drug interaction outcome predictions. Not only is CARAMeL better at generating accurate predictions for drug interaction outcomes against *Escherichia coli* and *Mycobacterium tuberculosis* compared to previous methods, but this approach is also the first to predict single-cell, media-specific, and sequential drug interaction outcomes. By evaluating how the outcome for individual drug combinations may

vary across different conditions, CARAMeL can identify drug combinations that are predicted to retain synergy regardless of fluctuations within the cell or the surrounding environment.

The second approach that I developed is called TACTIC (**Chapter 3**), which stands for *Transfer learning And Crowdsourcing to predict Therapeutic Interactions Cross-species*. TACTIC implements crowdsourcing and transfer learning to generate strain-specific drug interaction outcome predictions, which is accomplished by extending information between multiple bacteria based on genes that are orthologous between one another. Using drug interaction data measured across 12 phylogenetically diverse bacteria, I show that TACTIC can better predict drug interaction outcomes for unseen microbes compared to INDIGO (*INferring Drug Interactions using chemo-Genomics and Orthology*), a prior computational approach that serves as the foundation for TACTIC. With the ability to predict strain-specific drug interaction outcomes, I apply TACTIC to determine drug combinations that are predicted to have narrow-spectrum synergy; that is, selective synergistic outcomes against pathogenic (and not commensal) bacteria.

In **Chapter 4**, I demonstrate how CARAMeL and TACTIC can be leveraged to guide the design of clinically relevant combination therapies for the treatment of tuberculosis, one of the deadliest infectious diseases, and endophthalmitis, a serious eye infection that leads to blindness if improperly treated. Beyond the scope of the present work, CARAMeL and TACTIC hold the potential to aid the discovery of novel combination therapies with precise efficacy against other infectious diseases. To this end, both approaches are publicly available in adaptable formats that are primed for extended use by other research groups to optimize the design of antibiotic combination therapies. In the long-term future, CARAMeL and TACTIC could be extended to guide the design of combination therapies that are urgently needed outside of bacterial infections, including but not limited to fungal infections and cancer (**Chapter 5**).

Chapter 1 Introduction

1.1 Bacteriology 101

Bacteria are single-celled microorganisms that were amongst the first life forms on Earth, and they can reside within virtually any habitat. These organisms can generally be classified based on several characteristics related to their physiology and behavior (**Figure 1-1A**). For example, bacteria may be described by Gram staining, where Gram-positive bacteria possess a thick outer layer of peptidoglycan whereas Gram-negative bacteria are enclosed within a thin peptidoglycan layer covered by an additional outer membrane (Silhavy et al., 2010). Bacteria can also be characterized based on their growth rate, where fast-growing organisms (e.g., *Escherichia coli*) replicate within minutes while slow-growing organisms (e.g., *Mycobacterium tuberculosis*) require several hours to double in population size (M. Zhu & Dai, 2018). In relation to how bacteria interact with humans, these microorganisms can generally be classified as being commensal (i.e., harmless or health-promoting) or pathogenic (i.e., harmful or disease-causing) (Hornef, 2015).

Bacterial infections can occur through various routes, including but not limited to foreign bacteria entering a wound site or bacteria that naturally reside within a body becoming opportunistic due to an environmental change (e.g., host immunodeficiency). Antibiotics describe a class of drugs that specifically kill or neutralize bacteria by targeting different cellular mechanisms such as cell wall synthesis, DNA/RNA synthesis, and protein synthesis. Antibiotics, like bacteria, can be classified based on several criteria (**Figure 1-1B**). First and foremost, antibiotics are formally classified based on their mechanism of action (G. Kapoor et al., 2017). Antibiotics may also be described as having broad- or narrow-spectrum activity, where the former

applies to compounds that effectively kill or neutralize a phylogenetically diverse selection of bacteria and the latter describes compounds that selectively kill or neutralize a single species or group of bacteria (Melander et al., 2018). Additionally, antibiotics can be defined as being bactericidal (i.e., death-inducing) or bacteriostatic (i.e., growth-arresting) (Nemeth et al., 2015).

The bacterial response to antibiotic stress can be categorized into one of the following four phenotypes: susceptible, resistant, tolerant, or persistent (Brauner et al., 2016) (**Figure 1-1C**). A susceptible cell is effectively killed or neutralized by a given antibiotic, while the remaining three phenotypes describe a cell that can evade antibiotic stress in different ways. According to Brauner et al., these three phenotypes are distinguishable based on the minimum inhibitory concentration (MIC) and the minimum duration for killing (MDK) for a given cell population. The MIC measures the antibiotic concentration required to inhibit cell growth to a given extent (e.g., MIC_{99} = concentration that inhibits 99% of cell growth compared to an untreated cell). The MDK measures the duration of antibiotic exposure needed to kill a given proportion of a cell population (e.g., MDK_{99} = duration of antibiotic treatment that kills 99% of cells). Based on these two metrics, a resistant cell is one that has evolved to withstand a higher MIC than its susceptible equivalent, typically by inheriting genetic mutations that reduce antibiotic accumulation within itself or enzymatically inactivate the antibiotic. Tolerance describes the ability for a cell population to survive transient exposure to antibiotics and is characterized by the population having a higher MDK than a susceptible population, regardless of the MIC. Persistence is used to define a small cell sub-population (typically <1%) that survives antibiotic treatment at susceptible-level MIC but high MDK levels. Compared to resistant or tolerant cells, persistent cells are harder to characterize as their survival may be time- and/or dose-dependent.

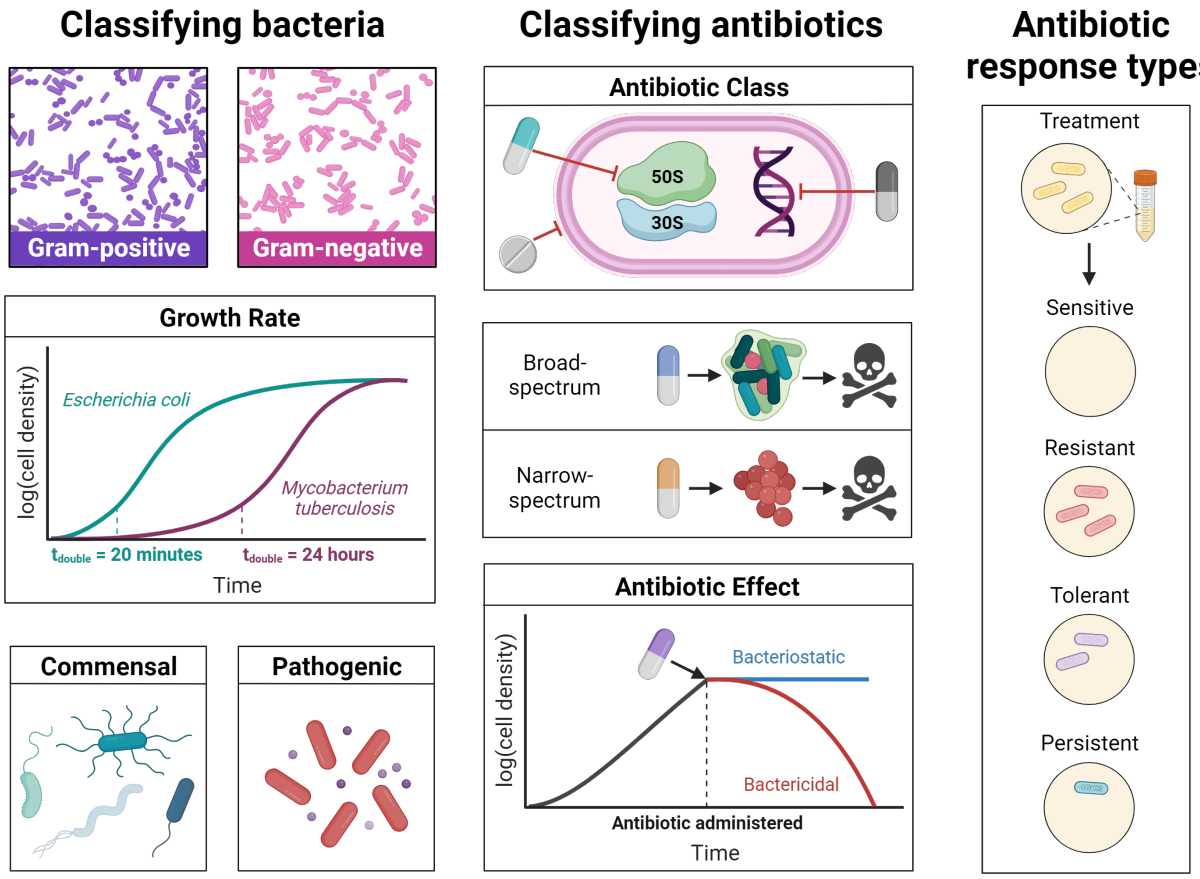

Figure 1-1 Classification of bacteria, antibiotics, and antibiotic response. (**A**) Bacteria are commonly classified based on their Gram stain (Gram-positive or Gram-negative), growth rate (fast or slow), and interaction with a host (commensal or pathogenic). (**B**) Antibiotics are classified based on their mechanism of action (DNA, protein, or cell wall inhibitors), extent of activity (broad- or narrow-spectrum), and mode of activity (bacteriostatic or bactericidal). (**C**) The bacterial response to antibiotic treatment can be categorized into four phenotypes: sensitive, resistant, tolerant, or persistent.

Given that tolerance and persistence are mainly defined by the MDK, these phenotypes only apply for cell response to bactericidal antibiotics. This dissertation describes topics and methodologies in context of the bacterial response to both bactericidal and bacteriostatic agents; hence, a cell that is described to overcome antibiotic stress can be assumed to be resistant unless it is clarified that a given cell population is tolerant or persistent.

1.2 Bacterial Metabolism Modulates Drug Resistance and Tolerance

Metabolism entails the collection of fundamental biochemical processes that enable organisms to consume and produce chemical compounds to sustain life. Metabolism is often depicted as an interconnected network of metabolites linked by enzymatic reactions, ranging from a moderate size (hundreds of metabolites/reactions) to being large and complex (thousands of metabolites/reactions) depending on the organism. For all living cells, the primary purpose of metabolism is to produce energy that is used to maintain cellular functions such as movement and enable cellular growth, development, and reproduction. Metabolic processes are carried out as a cell interacts with its surrounding environment, which includes both the immediately available nutrients as well as other cells that interact with one another through metabolite exchange. For the purpose of my dissertation, I focus on understanding and examining bacterial metabolism within the human body during infection.

In context of antibiotic resistance, bacterial metabolism can serve as a double-edged sword. On one side, it plays a key role in promoting survival and pathogenicity in new niches. For instance, *E. coli* possesses high metabolic versatility that enables the utilization of multiple carbon and nitrogen sources. As a result, *E. coli* is readily able to colonize different environments (e.g., intestinal tract, urinary tract) where it can become pathogenic (Fuchs et al., 2012). The nutrients available in the local environment also play a role in sustaining survival and promoting virulence (Brown et al., 2008). For instance, the nutrient composition in the urinary tract creates a harsher growth condition for *E. coli* in comparison to the native gut environment. However, uropathogenic *E. coli* (UPEC) strains have evolved metabolic adaptations that not only enable its survival but also enhance its virulence in causing urinary tract infections (UTIs) (Mann et al., 2017).

On the other side of the metaphorical double-edged sword, metabolism can enhance the bacterial susceptibility to antibiotics. For example, Kohanski et al. have proposed that metabolic activity plays a key role in modulating susceptibility to bactericidal drugs. Specifically, the authors have found that bactericidal antibiotic efficacy relies on tricarboxylic acid (TCA) cycle activity, as this enables production of hydroxyl radicals that damage cellular components (Kohanski et al., 2007). Similar findings on the involvement of metabolic activity, particularly in relation to oxidative stress, in drug efficacy have been reported for other organisms (Dharmaraja, 2017). Other studies have shown that global metabolic regulators can modulate bacterial susceptibility to antibiotics by changing membrane permeability (Martínez & Rojo, 2011). In contrast to a metabolically active state, which often potentiates antibiotic activity, cells can instead enter a dormant state where they are metabolically inactive. This cell state has been found to render bactericidal agents ineffective (Lopatkin et al., 2019) and may also explain the presence of persistent sub-populations (K. Lewis, 2006).

The information above provides a brief overview of metabolism and contextualizes its role in modulating bacterial behavior during disease and in response to antibiotics. This topic is discussed in further detail in **Chapter 2**, where the metabolic response to antibiotics serves as a pivotal component of the methodology that is presented. The role of metabolism in antibiotic resistance, tolerance, and persistence is revisited in **Chapter 4** in relation to how *M. tuberculosis* adapts to antibiotic stress.

1.3 Antibiotic Resistance: A Global Health Crisis

Antibiotic resistance (AR) refers to the phenomenon where bacteria become resistant to antibiotic treatments, therefore overcoming growth-inhibiting or death-inducing stresses. Resistance arises from extended exposure to antibiotics, which allow bacteria to evolve and genetically adapt to

promote their survival. Acquisition of resistance genes can occur via spontaneous mutations and horizontal gene transfer (HGT), where genetic material is laterally exchanged between bacteria (Blair et al., 2015). Specific manners through which HGT occurs includes conjugation (direct contact between bacteria), transduction (via viral vectors), and transformation (incorporation of exogenous genetic material). These genetic changes culminate to the development of resistance mechanisms that render antibiotic treatments ineffective in several ways (**Figure 1-2**), such as by: (a) activating new processes that avoid usage of the antibiotic target, (b) biochemically modifying an antibiotic via enzymatic action, (c) limiting the entry of antibiotics due to changes in membrane properties, (d) activating efflux pumps that remove antibiotics from the bacterial cytoplasm, and (e) modifying the antibiotic target to reduce binding affinity.

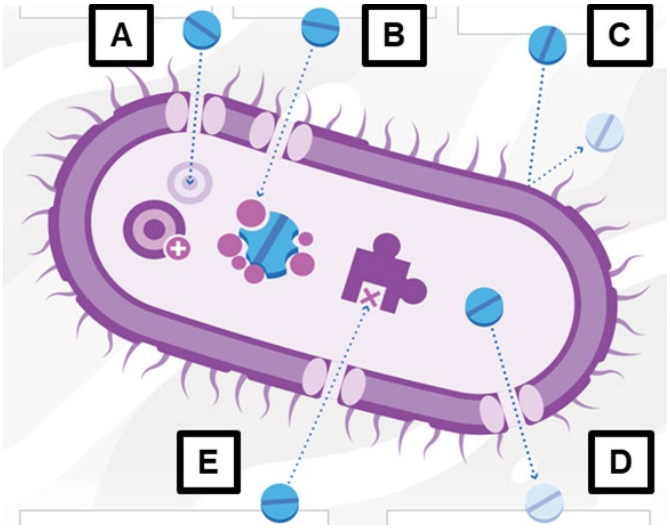

Figure 1-2 Resistance mechanisms against antibiotic treatment. Bacteria adopt various strategies to resist antibiotic treatment, including: (**A**) activation of processes that avoid usage of antibiotic target, (**B**) degradation of antibiotic via enzymatic action, (**C**) modification of membrane properties to limit antibiotic access, (**D**) expression of efflux pumps that remove the antibiotic, and (**E**) modification of the antibiotic target. Adapted from the CDC 2019 AR Threats Report (Centers for Disease Control and Prevention, 2019).

Among the various infectious diseases that afflict humans to this day, tuberculosis (TB) is one of the most devastating with a death toll of millions per year since pre-historic times (Barberis et al., 2017). TB is caused by *M. tuberculosis* (henceforth *M. tb*), a slow-growing pathogen that is

only known to infect humans (Comas et al., 2013). *M. tb* primarily resides within the lung and adopts one of two states: active, where it actively causes disease, or latent, where it enters a dormant period with minimal metabolic activity. TB is a notorious infectious disease that is difficult to treat, mainly due to three reasons. First, TB incidence is disparately dispersed with the vast majority of active TB cases occurring within low-income regions in Africa and Asia (World Health Organization, 2015). As a result, nearly one-third of all active disease cases go undetected, and potentially further spread TB, due to the scarcity of medical assistance that can be reached or afforded. Second, *M. tb* can develop varying levels of antibiotic resistance which are difficult and time-consuming to pinpoint. This is problematic because the resistance profile of *M. tb* is indicative of which antibiotic regimen should be prescribed to effectively clear the infection (Mirzayev et al., 2021). Third, the ability for *M. tb* to switch between active and latent phases enables it to persist within the human host, even after anti-TB treatment (Stewart et al., 2003). This can make it nearly impossible to completely clear TB infection, sometimes resulting in disease relapse throughout a patient's lifetime.

In addition to TB, both the Centers for Disease Control (CDC) and the World Health Organization (WHO) list other drug-resistant pathogens as critical threats, including but not limited to *E. coli, Pseudomonas aeruginosa,* and *Staphylococcus aureus* (Centers for Disease Control and Prevention, 2019; World Health Organization, 2014). These three organisms collectively represent multiple bacterial characteristics that promote pathogenicity and development of resistance mechanisms. For example, *E. coli* is a fast-growing Gram-negative species that naturally resides in the gut of large organisms and is often used as the model organism to study bacterial cells. Due to its high versatility and resilience in adapting to new environments, *E. coli* can behave as a commensal member of the intestinal lining or become pathogenic, causing

infections in the gut, blood, and urinary tract (Leimbach et al., 2013). Though *E. coli* is comparatively less threatening than bacteria such as *M. tb* in context of AR, *E. coli* is adept at accumulating resistance genes via HGT; this trait not only leads to multidrug-resistant strains, but also enables *E. coli* to serve as a reservoir of resistant determinants that can be shared with other bacteria (Poirel et al., 2018). *P. aeruginosa* is another Gram-negative species, though slower in growth than *E. coli*, that naturally resides in environmental niches (e.g., soil). *P. aeruginosa* is an exemplary case of an opportunistic pathogen, a microbe that does not cause disease under normal circumstances (e.g., healthy host) but becomes pathogenic when its surrounding environment changes (e.g., immunocompromised host). Due to this trait, *P. aeruginosa* can cause various types of infections such as bacteremia (blood infection) in burn victims, ulcerative keratitis (eye infection) in contact lens users, and chronic lung infection in cystic fibrosis patients (Lyczak et al., 2000). Unlike *E. coli* and *P. aeruginosa*, *S. aureus* is a Gram-positive species that is a commensal habitant of the nasal mucosa in humans (Wertheim et al., 2005). *S. aureus* causes infection when it invades the bloodstream or tissues underneath the mucosal layer, which can happen when this layer is disrupted during injury or surgery. In general, Gram-positive bacteria are more susceptible to antibiotic stress than Gram-negative counterparts, since the former lacks the outer membrane which serves as an additional resistive layer (Breijyeh et al., 2020). However, *S. aureus* has proven to be exceptionally resistive against antibiotic stress by rapidly acquiring resistance to various antibiotics shortly after exposure and has become notorious for causing epidemics of hospital-acquired infections worldwide (Chambers & DeLeo, 2009).

The content above is certainly not exhaustive in describing the current state of AR; however, it provides sufficient introductory information that is revisited in later chapters of this dissertation. Specifically, **Chapter 2** introduces a methodology that is constructed based on *E.*

coli. **Chapter 3** describes another methodology that is based on *E. coli* and *M. tb* data but extends applicability to other bacteria such as *P. aeruginosa* and *S. aureus*. **Chapter 4** focuses on leveraging both methodologies to design therapies that specifically counter drug-resistant *M. tb* in tuberculosis and identify narrow-spectrum therapies against *P. aeruginosa* in endophthalmitis (a serious eye infection).

1.4 Strategies to Combat Antibiotic Resistance

Current efforts to combat AR fall into two major categories: preventative measures and treatment options. Prevention tactics are heavily promoted by the CDC and the WHO, and these are widely implemented in both agricultural and clinical settings. Specific measures include: (a) increased sanitation when handling animals or caring for patients, (b) proper prescription and usage of antibiotic treatments, complemented by improved diagnostic technologies, and (c) administration of vaccines or antibody therapies to reduce infection rates (Centers for Disease Control and Prevention, 2019). On the treatment side, alternative options to the current method of treating bacterial infections are being explored, especially for highly resistant pathogens. Some examples include: (a) phage therapy, where genetically engineered bacteriophages are designed to target specific pathogens, (b) live therapeutics with health-promoting bacteria, such as fecal microbiota transplantation (FMT), and (c) combination therapy, where antibiotics are used in combination or are supplemented with another therapeutic agent (e.g., small peptides, nutrients).

Though each treatment option holds great potential for combating resistant bacterial pathogens, both phage therapy and live therapeutics are still poorly understood and hard to control. Consequently, their commercial viability is limited due to scalability issues and lack of widespread implementation guidelines (Lu & Koeris, 2011; Panchal et al., 2018). In contrast, combination therapy has the best potential for clinical application as this method optimizes the use of already

regulated therapeutics (Farha & Brown, 2019) and offers room for improved treatment efficacy through adjuvant supplementation (Tyers & Wright, 2019). Combination therapies can also engage multiple cellular targets to suppress growing resistance, which is difficult to achieve with a single active compound. In fact, combination therapies involving at least two and up to four antibiotics are commonly used to treat tuberculosis (Kerantzas & Jacobs, 2017). More broadly, combination therapies are widely used to treat other diseases such as viral infections (White et al., 2021) and cancer (Mokhtari et al., 2017).

1.4.1 Combination therapies strategically overcome drug resistance

The material in this section was partially adapted from the following article with adjustments:

> Cantrell, J. M., **Chung, C. H.**, & Chandrasekaran, S. (2022). Machine learning to design antimicrobial combination therapies: Promises and pitfalls. *Drug Discovery Today*, *27*(6), 1639-1651.

Combination therapies are discovered and designed by measuring how two or more drugs interact with one another. Drugs can be combined in a simultaneous or sequential fashion, where the former describes when drugs are formulated or prescribed together while the latter refers to when drugs are given in an order- and time-dependent manner. The vast majority of combination therapies that are used to treat bacterial infections are simultaneously prescribed. However, there is growing interest in designing sequential therapies in order to leverage collateral sensitivity (heightened susceptibility to one drug after adaptation to another drug) to mitigate drug resistance (Baym et al., 2016; Imamovic & Sommer, 2013; Lázár et al., 2018; Roemhild & Andersson, 2021). Nonetheless, established methods for discovering and designing combination therapies focus on investigating simultaneous drug interactions.

Checkerboard assays, or dose-response matrices, are commonly used to observe and measure interactions between two drugs (**Figure 1-3A**). Schematically, drugs are combined at different concentrations (i.e., dosages) along orthogonal directions of a well plate (i.e., matrix), and their impact on cell viability (i.e., response) is measured using optical density or colorimetric assays. The way that drugs interact when combined can be visualized as an isobologram (**Figure 1-3B**) and classified into one of three types of outcomes: synergy, additivity (i.e., neutral), or antagonism. For clinical use, the goal is to identify drug combinations that are synergistic, meaning that the drug combination achieves better efficacy (e.g., greater infection clearance) compared to the single agents. Using the data measured from checkerboard assays, drug interaction outcomes can be quantified using a mathematical model. Three foundational models, each possessing its own set of assumptions on how two drugs interact, are predominantly used to quantify drug interaction outcomes (Meyer et al., 2020). For the purposes of this dissertation, I describe two of these models in further detail: the Loewe Additivity Principle (Loewe & Muischnek, 1926) and the Bliss Independence Model (Bliss, 1939).

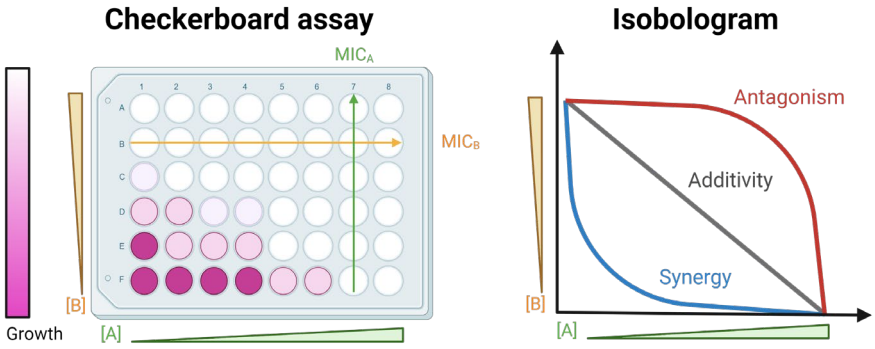

Figure 1-3 Evaluating combination therapy outcomes using a checkerboard assay. A checkerboard assay measures the interaction between two compounds (e.g., drugs A and B) by evaluating the cell response (e.g., growth) across a well-plate where each compound is dispensed at concentration levels ranging from 0 to the minimum inhibitory concentration (MIC) along a vertical or horizontal direction. (**B**) The drug interaction is visually inspected using an isobologram, which depicts the curve that achieves a specified effect level (e.g., 90% growth inhibition) along the concentration axes for the two compounds. Based on the Loewe Additivity Principle (Loewe & Muischnek, 1926), the deviation from the line of additivity (a downward diagonal line) indicates synergistic or antagonistic interactions depending on whether lower (concave curve) or higher (convex curve) drug concentrations achieve the desired effect, respectively.

The Loewe Additivity Principle assumes dose additivity for additive (i.e., neutral) drug interaction outcomes. This imposes three main assumptions: (1) a drug cannot interact with itself, (2) the effect achieved by the maximum concentration of one drug is the same as the other (e.g., $[Drug_A]$ = $[Drug_B]$ = 90% inhibition), and (3) the effect achieved in (2) is also achieved by combined ratios that sum to one (e.g., $0.5[Drug_A] + 0.5[Drug_B] = 0.7[Drug_A] + 0.3[Drug_B] = [Drug_A] = [Drug_B]$ = 90% inhibition). The third assumption is used to determine the drug interaction outcome, where synergy is defined by lower concentration ratios achieving the effect of the maximum concentration of the individual drugs (e.g., $0.3[Drug_A] + 0.4[Drug_B]$ = 90% inhibition). Mathematically, the Loewe Additivity Principle introduces the following equation, which compares the dosage required to reach a defined response level (e.g., % growth inhibition) when two drugs are combined versus when they act independently (**Equation 1-1**):

$$\frac{d_{A,x}}{D_{A,x}} + \frac{d_{B,x}}{D_{B,x}} = 1$$

Equation 1-1 Quantifying the interaction between two drugs based on the Loewe Additivity Principle.

where $d_{A,x}$ and $d_{B,x}$ represent the dosage required for each drug to achieve x% inhibition when combined, while $D_{A,x}$ and $D_{B,x}$ represent the dosage required for each drug to independently achieve x% inhibition. **Equation 1-1** classifies a combination as synergistic or antagonistic based on whether the growth inhibition is less than or more than one, respectively.

The Bliss Independence Model assumes response additivity for additive drug interaction outcomes using probabilistic rules. This model is applicable when the following three assumptions are met: (1) the individual probabilities of cells being affected by each individual drug are independent, (2) the dose-response curve for each individual drug is exponential, and (3) each drug targets a distinct pathway from the other. The drug interaction outcome is determined by

comparing the measured response (e.g., % growth inhibition) from the checkerboard assay against the expected response for a combination, which is calculated using the probabilities of the individual drugs. Mathematically, the Bliss model is represented as:

$$I_{AB} = I_A \times I_B$$

Equation 1-2 Quantifying the interaction between two drugs based on the Bliss Independence Model.

where I_{AB} is the expected response achieved by the combination based on the response achieved by each drug independently (I_A and I_B). Based on **Equation 1-2**, drug combinations are classified as synergistic or antagonistic based on whether they achieve a greater or lower desired response than expected, respectively.

The conventional approach for combination therapy screening primarily involves the use of checkerboard assays and quantification of drug interaction outcomes based on the Loewe and/or the Bliss model. Though this strategy has led to the establishment of over 400 FDA-approved drug combinations across many disease areas (P. Das et al., 2019), numerous challenges are implicated with this standard approach. First and foremost, experimentally searching for combination therapies has limited throughput and cannot scale to the exponential increase of the combinatorial search space upon incremental addition of drugs to screen. Second, without rational guidance of which drug combinations to test, the bench-to-clinic success rate can be very low. Third, checkerboard assays and mathematical formulae such as the Loewe and Bliss models were designed to evaluate pairwise (i.e., two-way) drug interactions; as a result, there is little consensus on how these methods can be extended to evaluate higher-order drug interactions. Last but not least, the conventional approach for combination therapy design cannot measure sequential drug interactions; hence, investigation into the potential for sequential therapies in overcoming drug resistance remains underexplored.

To address these challenges, I developed two computational methodologies for combination therapy design as part of my dissertation work. Both methodologies, which are described in **Chapters 2 and 3**, help to risk stratify drug combinations by predicting which drug combinations within a large combinatorial space (~thousands) are likely to yield synergy and proposing a smaller set (<50) for experimental validation. Both methodologies can also generate outcome predictions for higher-order drug interactions. Importantly, the methodology described in **Chapter 2** further accounts for sequential drug combinations when generating predictions for their interaction outcomes.

1.5 Computational Methods for Systems Biology and Drug Therapy Design

1.5.1 Genome-scale metabolic models simulate systems-level metabolism

The material in this section was partially adapted from the following article with adjustments:

> **Chung, C. H.**, Lin, D. W., Eames, A., & Chandrasekaran, S. (2021). Next-generation genome-scale metabolic modeling through integration of regulatory mechanisms. *Metabolites*, *11*(9), 606.

Genome-scale metabolic models (GEMs) are computational representations of metabolic networks accounting for the entirety of metabolic activity encoded within the genome for a given organism (Price et al., 2004). Principally, they involve a set of mass-balanced metabolic reactions and metabolites represented in a stoichiometric matrix. GEMs also include gene-protein-reaction (GPR) associations describing the relationship between thousands of genes, proteins, and reactions (Thiele & Palsson, 2010). GEMs facilitate quantitative, *in silico* simulations of how environmental and genetic changes influence cellular metabolism (N. E. Lewis et al., 2012). Since their introduction, over 6,000 GEMs have been reconstructed across bacteria, archaea, and eukarya (Fang et al., 2020).

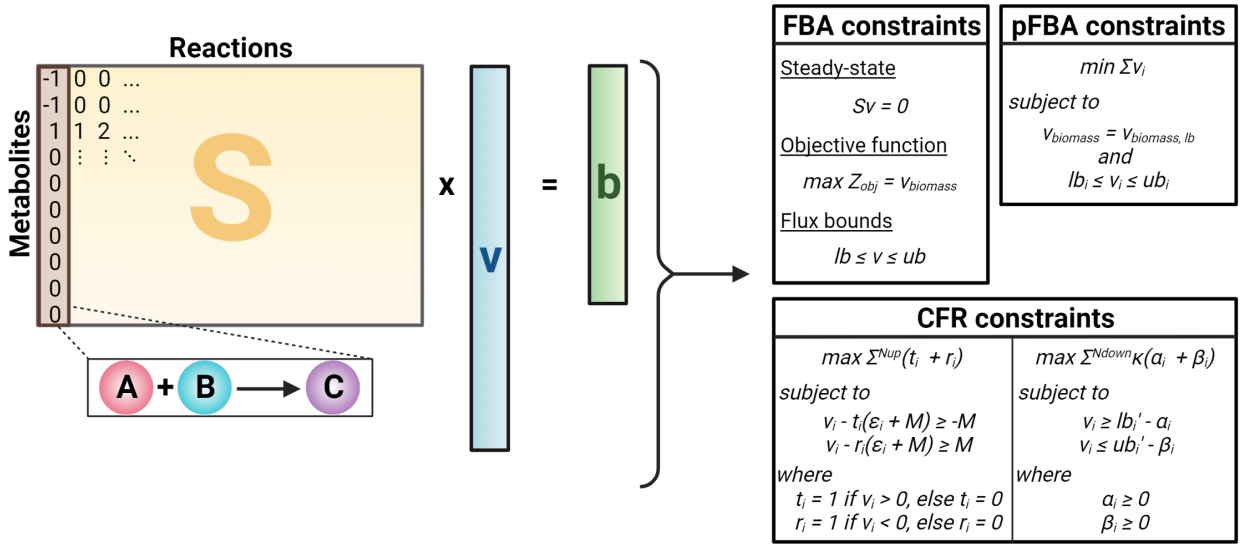

Figure 1-4 Mathematical framework of three constraint-based modeling (CBM) methods. Flux balance analysis (**FBA**) is a standard method to determine metabolic reaction flux solutions at steady-state by a cell that optimizes a defined objective function (e.g., maximize biomass). Parsimonioius FBA (**pFBA**) is another method that applies an additional constraint that minimizes the overall flux based on the assumption that the cell is efficiently modulating its metabolism. The constrain-flux-regulation (**CFR**) method incorporates FBA, pFBA, and additional constraints that maximize fluxes through up-regulated ("on") reactions while minimizing fluxes through down-regulated ("off") reactions. See main text for variable descriptions.

Constraint-based modeling (CBM) is the standard mathematical framework for reconstructing and analyzing GEMs, primarily through the addition of model constraints (N. E. Lewis et al., 2012) (**Figure 1-4**). The most basic form of CBM is flux balance analysis (FBA) (Orth et al., 2010). FBA begins with the stoichiometric matrix *S*, where rows signify metabolites and columns represent reactions. For each reaction (column), the stoichiometric coefficients of all metabolites involved in the reaction are set to a non-zero value. Specifically, positive coefficients indicate production of a metabolite while negative coefficients indicate consumption of a metabolite. A key assumption of FBA is steady-state metabolism in which each metabolite's production and consumption is balanced equally (Reimers & Reimers, 2016). Mathematically, FBA aims to simulate reaction fluxes at steady-state, which leads to solving the following system of equations (**Equation 1-3**):

$$S \cdot v = b$$

Equation 1-3 Constraining a genome-scale metabolic model based on flux balance analysis (FBA).

where *S* represents the stoichiometric matrix, *v* is the vector of reaction fluxes, and *b*, representative of changes in metabolite concentrations, is set to a zero vector to mathematically reflect steady-state metabolism.

Since the number of reactions exceeds the number of metabolites, the system is underdetermined and a large solution space exists; however, this can be narrowed by imposing additional constraints and specifying flux bounds. In FBA, linear optimization techniques are applied to solve a flux distribution that optimizes an objective function (Z_{obj}). To reflect evolutionary pressure, growth is typically maximized by defining a biomass objective function that consists of biomass precursors (Feist & Palsson, 2010). Other objectives such as maximization of ATP can also be used in FBA (Schuetz et al., 2007). These constraints are mathematically represented as follows (**Equation 1-4**):

$$Maximize\ Z_{obj} = v_{biomass}$$
$$s.t.\ lb\ < v < ub$$

Equation 1-4 Constraining a genome-scale metabolic model by specifying the objective function. s.t.: subject to.

where Z_{obj} is the objective function, $v_{biomass}$ is the flux through a user-defined biomass reaction, *v* is the vector of all reaction fluxes, *lb* is a vector of the lower bound flux limit, and *ub* is a vector of the upper bound flux limit.

Though FBA can generate flux solutions that match experimental data (Edwards et al., 2001; Schuetz et al., 2007), this method may still generate non-unique solutions. This predicament arises when multiple combinations of reaction fluxes can satisfy the above constraints and lead to

the same objective. To account for this uncertainty, other CBM methods that introduce additional constraints onto the flux solution space have been proposed (Bernstein et al., 2021). For the purposes of this dissertation, I describe one method called parsimonious FBA (pFBA) in further detail. pFBA adds another constraint layer to determine feasible flux ranges by assuming that cells maximize efficient enzyme usage to promote their growth (N. E. Lewis et al., 2010). This assumption is mathematically imposed by minimizing the overall flux in the system (**Equation 1-5**):

$$Minimize \sum_{i=1}^{N_{reactions}} v_i$$
$$s.t. v_{biomass} = v_{biomass,lb} \; and \; lb_i \leq v_i \leq ub_i$$

Equation 1-5 Constraining a genome-scale metabolic model based on parsimonious FBA (pFBA). s.t.: subject to.

where v_i is the flux through reaction i, $N_{reactions}$ is the total number of reactions, $v_{biomass}$ is the flux through the biomass reaction, $v_{biomass,lb}$ is the lower limit of the flux through the biomass reaction, lb_i is the lower flux bound for reaction i, and ub_i is the upper flux bound for reaction i. Of note, the flux solutions achieved using pFBA tend to emphasize a small number of high-flux reactions due to the underlying assumptions of pFBA. Nonetheless, pFBA has been shown to outperform other similar methods in predicting intracellular fluxes (Machado & Herrgård, 2014).

To further improve GEM accuracy in simulating metabolic reaction flux changes, CBM methods integrating omics data have been introduced (Ramon et al., 2018). Omics data refers to a large-scale collection of experimental measurements that provide systems-level understanding of a biological function. Different types of omics data help elucidate different facets of biological information, and these include genomics (gene-level), transcriptomics (gene transcript-level), proteomics (protein-level), and metabolomics (metabolite-level). A key component of the

methodology described in **Chapter 2** is constrain-flux-regulation (CFR), a CBM method that integrates omics data to simulate the metabolic response to a perturbation (Campit & Chandrasekaran, 2020; Shen, Cheek, et al., 2019). CFR imposes constraints that maximize fluxes through overactive reactions while minimizing fluxes through underactive reactions. Reaction activity can be directly provided into the CFR function by specifying which reactions are overactive or underactive; alternatively, this information can be inferred from transcriptomics (e.g., gene transcript) data where reactions associated with up-regulated genes indicate those that are overactive while reactions associated with down-regulated genes are assumed to be underactive. Mathematically, flux maximization for overactive reactions is imposed as follows (**Equation 1-6**):

$$Maximize \sum_{i=1}^{N_{up}} (t_i + r_i)$$
$$s.t. v_i - t_i(\varepsilon_i + M) \geq -M \; and \; v_i - r_i(\varepsilon_i + M) \geq M$$
$$where \; t_i = \begin{cases} 1 & if \; v_i > 0 \\ 0 & otherwise \end{cases}, r_i = \begin{cases} 1 & if \; v_i < 0 \\ 0 & otherwise \end{cases} \; and \; M \gg \varepsilon_i$$

Equation 1-6 Applying constrain-flux-regulation (CFR) for overactive reactions. s.t.: subject to.

where v_i is the flux through reaction i, N_{up} is the total number of overactive reactions, ε_i is the minimum flux through reaction i, t_i is set to 1 for reaction i if the flux directionality is positive, r_i is set to 1 for reaction i if the flux directionality is negative, and M is a constant much larger than ε_i (default: M = 10,000). The mathematical expression for minimizing fluxes through underactive reactions is as follows (**Equation 1-7**):

$$Maximize \sum_{i=1}^{N_{down}} \kappa(\alpha_i + \beta_i)$$
$$s.t. v_i \geq lb_i' - \alpha_i \; and \; v_i \leq ub_i' - \beta_i$$
$$where \; \alpha_i \geq 0 \; and \; \beta_i \geq 0$$

Equation 1-7 Applying constrain-flux-regulation (CFR) for underactive reactions. s.t.: subject to.

where v_i is the flux through reaction i, N_{down} is the total number of underactive reactions, α_i indicates the flux deviation for reaction i if the flux directionality is positive, β_i is the flux deviation for reaction i if the flux directionality is negative, κ is the penalty imposed onto α_i and β_i, lb_i' is the data-based lower flux bound for reaction i (default $lb_i' = 0$), and ub_i' is the data-based upper flux bound for reaction i (default $ub_i' = 0$). By default, CFR generates flux simulations that are defined by **Equations 1-6 and 1-7** while satisfying the constraint imposed by pFBA (**Equation 1-5**).

In summary, GEMs are computational models that linearly represent the metabolic network for a given organism. FBA is the most common CBM method that is used to simulate steady-state metabolic reaction fluxes that optimize a specified cellular objective (e.g., biomass) within feasible flux bound limits. Additional CBM methods such as pFBA and CFR can be imposed onto GEMs to simulate metabolic states that more closely resemble what is observed experimentally. These metabolic modeling concepts are pivotal for the methodology introduced in **Chapter 2**, which simulates the bacterial metabolic response to antibiotic exposure and growth within defined media (i.e., cell culture environment).

1.5.2 Brief primer on machine learning and its use for predictive modeling

The material in this section was partially adapted from the following article with adjustments:

Cantrell, J. M., **Chung, C. H.**, & Chandrasekaran, S. (2022). Machine learning to design antimicrobial combination therapies: Promises and pitfalls. *Drug Discovery Today*, *27*(6), 1639-1651.

Artificial intelligence (AI) describes a research area where computational machinery or systems are built to emulate different aspects of human intelligence such as thought, language, and vision (Muthukrishnan et al., 2020). Machine learning (ML) is a sub-field of AI that focuses on training computational machines to interpret a given dataset, and the level of information that is provided dictates which one of four types of ML is implemented (Morales & Escalante, 2022). The first is unsupervised learning, where a machine is given unlabeled data points and is tasked with identifying any meaningful patterns that may exist within the dataset. The second is supervised learning, where a machine is provided with labeled data points and is tasked with defining a function that connects each data point to its associated label. The third is semi-supervised learning, where the given dataset is partially labeled, and the machine is tasked with both goals of the prior two ML types (pattern recognition and function approximation). The last type of ML is reinforcement learning, where a machine acts as an agent within a defined environment and chooses a series of actions that maximize a defined reward and/or reduce a defined risk through trial-and-error.

For the purposes of this dissertation, additional information on unsupervised and supervised learning is specifically elaborated. Unsupervised learning is often used for clustering data points and/or reducing the dimensionality of a complex dataset. For instance, given single-cell gene expression data for a heterogeneous cell population (e.g., immune cells), an unsupervised ML model can deduce that several cell sub-populations (e.g., macrophages, T cells, B cells) characterized by distinctive gene expression profiles may exist. On the other hand, supervised

learning is typically applied for classification- or regression-based tasks where a model learns to associate data points with a discrete or continuous set of labels, respectively. For example, given information on patient-specific demographic and clinical measurements where the patient health status (e.g., healthy vs. diabetic) is known, a supervised ML model can learn a function that classifies a patient into a known sub-group. Alternatively, a supervised ML model could learn a function that infers a continuous value (e.g., blood glucose level) for a patient based on their information.

Given that supervised ML models serve as function approximators, they are often used for generalizing a learned function to predict labels for new input data. Before these models can be applied for predictive modeling, their performance as accurate function approximators is evaluated and optimized based on different metrics (Greener et al., 2021; Jiang et al., 2020). The general process for evaluating the performance for a supervised ML model begins with splitting the input data along with its labels into training and testing sets. The model is then subjected to training and optimization using the training dataset, then evaluated using the testing dataset. Finally, model performance is evaluated using different metrics based on the nature of the given supervised ML model (Gramatica & Sangion, 2016; Roy et al., 2015). For classification-based models, performance is often measured by inspecting the Receiver Operator Characteristic (ROC) curve, which visualizes the sensitivity (i.e., true positive rate) against the specificity (i.e., true negative rate) of model predictions. The area under the ROC curve (AUROC) can further serve as a quantitative measure, with values close to 1 indicating high model accuracy. For regression-based models, performance can be measured by the coefficient of determination (R^2), which calculates goodness-of-fit by comparing the expected output values against corresponding model-predicted values. The best R^2 measure is 1, meaning there is no difference between true and predicted values.

Of note, the square-root of the R^2 value indicates the correlation between true vs. model-predicted values, which is another measure for evaluating regression-based model performance.

The information described above provides a tailored understanding of ML that is constructive for understanding the methodologies introduced in **Chapters 2 and 3**. Both methodologies leverage supervised ML to build models predictive of drug interaction outcomes, either as a classification-based task (e.g., predicting synergy) or a regression-based task (e.g., predicting the Loewe- or Bliss-based drug interaction score) (**Figure 5**). Of note, both methodologies specifically leverage Random Forests as the base ML algorithm to define functions that approximate drug interaction outcomes given feature information that uniquely characterize distinct drug combinations. Briefly, Random Forests is an ensemble algorithm that consolidates the outputs from multiple decision trees to yield robust predictions (Breiman, 2001). Each tree is constructed using a random sample of data points, which are then split based on their features to attain the best class purity (for classification) or minimize the error between true vs. predicted values (for regression).

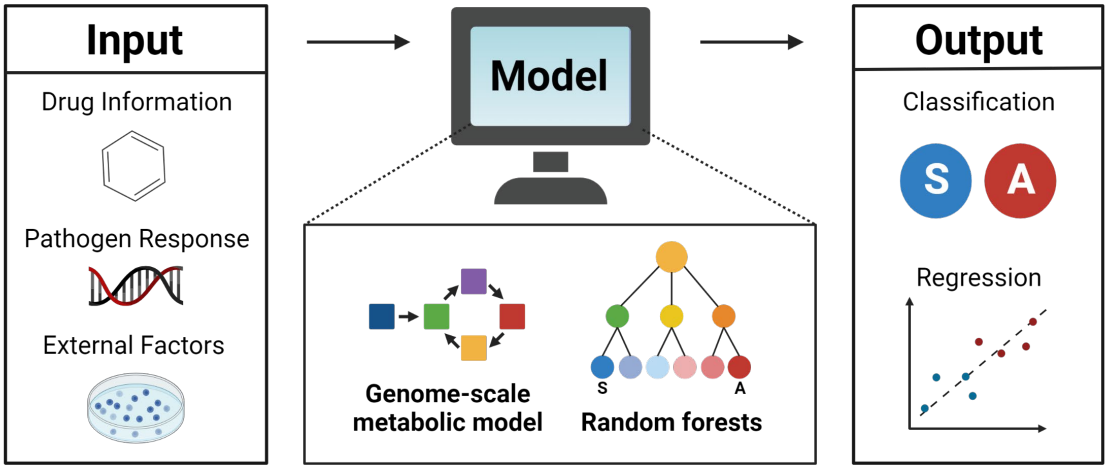

Figure 1-5 Schematic for the computational design of combination therapies. Based on a supervised learning approach, computational methods such as genome-scale metabolic models and random forests models can learn to associate patterns in drug information, pathogen response to treatment, and external factors (e.g., growth environment) to drug interaction outcomes such as synergy (S) or antagonism (A).

1.6 Dissertation Objectives

For my dissertation research, I sought to optimize the design of combination therapies effective in overcoming antibiotic resistance by considering intrinsic and extrinsic factors that influence the bacterial response to drug treatment. In pursuit of this goal, I developed two computational methods that prioritize different design objectives. The first method, which is fully described in **Chapter 2**, incorporates genome-scale metabolic modeling to understand how bacteria metabolically adapt in response to different conditions such as drug treatment or growth within specific environments. By providing this information into a ML model, I introduce a methodology that can predict condition-specific drug interaction outcomes. In **Chapter 3**, I describe the second computational method that leverages two ML concepts, namely crowdsourcing and transfer learning, that enables a model to predict strain-specific drug interaction outcomes. To demonstrate their utility, I apply both computational methods to determine synergistic drug combinations in the context of treating tuberculosis and endophthalmitis, a serious eye infection, in **Chapter 4**. In **Chapter 5**, I summarize my research findings and discuss limitations entailed with these two methodologies. I also provide suggestions on future research directions that can improve or expand my models for combination therapy design.

Chapter 2 A Flux-based Machine Learning Model to Simulate the Impact of Pathogen Metabolic Heterogeneity on Drug Interactions

The material in this chapter was adapted from the following article with minor adjustments:

> **Chung, C. H.**, & Chandrasekaran, S. (2022). A flux-based machine learning model to simulate the impact of pathogen metabolic heterogeneity on drug interactions. *PNAS nexus*, *1*(3), pgac132.

2.1 Abstract

Drug combinations are a promising strategy to counter antibiotic resistance. However, current experimental and computational approaches do not account for the entire complexity involved in combination therapy design, such as the effect of pathogen metabolic heterogeneity, changes in the growth environment, drug treatment order and time interval. To address these limitations, we present a comprehensive approach that uses genome-scale metabolic modeling and machine learning to guide combination therapy design. Our mechanistic approach (a) accommodates diverse data types, (b) accounts for time- and order-specific interactions, and (c) accurately predicts drug interactions in various growth conditions and their robustness to pathogen metabolic heterogeneity. Our approach achieved high accuracy (AUC = 0.83 for synergy, AUC = 0.98 for antagonism) in predicting drug interactions for *E. coli* cultured in 57 metabolic conditions based on experimental validation. The entropy in bacterial metabolic response was predictive of combination therapy outcomes across time scales and growth conditions. Simulation of metabolic heterogeneity using population FBA identified two sub-populations of *E. coli* cells defined by the

levels of three proteins (eno, fadB and fabD) in glycolysis and lipid metabolism that influence cell tolerance to a broad range of antibiotic combinations. Analysis of the vast landscape of condition-specific drug interactions revealed a set of 24 robustly synergistic drug combinations with potential for clinical use.

2.2 Significance

Worldwide, 700,000 people die each year from drug-resistant infections. Drug combinations have great potential to reduce the spread of drug-resistant bacteria. However, their potency is impacted by both the pathogen growth environment and the heterogeneity in pathogen metabolism. The metabolic heterogeneity in a pathogen population allows them to survive antibiotic treatment. Here we present a flexible machine-learning framework that utilizes diverse data types to effectively search through the large design space of both sequential and simultaneous combination therapies across hundreds of simulated growth conditions and pathogen metabolic states. Our approach can serve as a useful guide for the selection of robustly synergistic drug combinations.

2.3 Introduction

Antimicrobial resistance (AMR) occurs due to extended exposure to antibiotics, which allows bacteria to evolve resistance mechanisms that render antibiotic treatments ineffective (Blair et al., 2015). In the context of AMR, bacterial metabolism plays a key role. Cell-to-cell variation in metabolism within a population can be beneficial in responding to antibiotic stress (Balaban et al., 2013; Kussell et al., 2005), and several pathogens take on a distinct metabolic state *in vivo* to tolerate antibiotics (Cohen et al., 2013; Rittershaus et al., 2013). It is important to note that tolerant cells are predicted to be the source of drug-resistant pathogens (Cohen et al., 2013; Gill et al.,

2015; Holmes et al., 2016). In addition to stochasticity in metabolic activity within a population, extrinsic factors such as the metabolic environment also influence antibiotic efficacy (Martínez & Rojo, 2011; J. H. Yang, Bening, et al., 2017; J. H. Yang, Bhargava, et al., 2017). For example, the availability of oxygen and extracellular metabolites modulate potency of antibiotics (Martínez & Rojo, 2011). Metabolism can thus promote pathogen survival through adaptable use of nutrients in the local environment (Brown et al., 2008; Fuchs et al., 2012). Bacterial metabolism also impacts susceptibility to antibiotics through the production of reactive oxygen species (Dharmaraja, 2017; Kohanski et al., 2007) or changes in membrane permeability (Martínez & Rojo, 2011). Of note, these metabolic responses are also tied to entropy (i.e., disorder) in the bacterial stress response, which has been shown to be a generalizable predictor for antibiotic sensitivity (Z. Zhu et al., 2020). Altogether, these individual findings suggest that modeling bacterial metabolism in response to antibiotics may be insightful for the design of novel treatments that mitigate resistance.

Combination therapy, which involves the use of two or more therapeutics, holds great potential for combating resistant pathogens as it not only leverages already regulated therapeutics (Farha & Brown, 2019), but also offers room for improved efficacy (Tyers & Wright, 2019). Further, combination therapy could be optimized to selectively target resistant pathogens via collateral sensitivity, which has been shown to overcome multi-drug resistance in cancer (Pluchino et al., 2012; Vijayaraghavalu et al., 2013). Collateral sensitivity entails the increased sensitivity to a therapeutic that results from initial treatment with another stress agent (Pál et al., 2015). This phenomenon has been observed across various diseases and organisms (Deeks, 2003; Gadamski et al., 2000; Lukens et al., 2014; Pluchino et al., 2012), and in context of AMR, could be leveraged to prevent and mitigate resistance (Baym et al., 2016). Theoretical studies have also predicted that

antibiotic combinations can be effective in heterogeneous populations and reduce the rise of resistance more effectively than monotherapy (Ankomah et al., 2013; Baym et al., 2016). However, these studies do not provide a guideline to identify promising combinations among thousands of possible candidates. Combination therapies are traditionally identified using experimental methods; however, this approach quickly becomes infeasible when considering the vast combinatorial search space, the effects of the growth media, pathogen metabolic heterogeneity, and time-/order-dependence for treatment efficacy.

With the advent of high-throughput omics data and application of machine learning (ML), it is now possible to expedite the search for effective combination therapies. ML has also been applied to reveal mechanistic insights into antibiotic mechanisms of action (Ribeiro da Cunha et al., 2021; J. H. Yang et al., 2019) and identify novel antibacterial compounds (El Zahed & Brown, 2018; Stokes et al., 2020). In the past decade, several groups have used these methods to computationally design combination therapies in context of cancer (Chua et al., 2017; Lee et al., 2012; Regan-Fendt et al., 2019; Yuan et al., 2021; Zhang et al., 2021; X.-M. Zhao et al., 2011) and AMR (Chandrasekaran et al., 2016; Cokol et al., 2018; Ma et al., 2019). For the latter case, prior models have been shown to generate predictions that accurately correspond to experimental and clinical efficacy against *Escherichia coli* and *Mycobacterium tuberculosis*, thus offering effective reduction of the search space for combination therapies against AMR (Chandrasekaran et al., 2016; Ma et al., 2019). However, these approaches are limited by the availability of omics data measuring the bacterial response to antibiotic treatment. The combined drug effect on bacterial growth has also only been assessed in a limited number of growth environments (Cokol et al., 2018). Moreover, current models have primarily focused on simultaneous combinations; consequently, the potential of designing time- and order-dependent combination therapies that promote collateral

sensitivity remains unexplored. Since combination therapy is increasingly used to treat many medical conditions such as tuberculosis (TB), Gram-negative, and biofilm-associated infections (Boyd & Nailor, 2011; Dheda et al., 2016; Forrest & Tamura, 2010; Solomkin et al., 2010), it is essential to consider how various metabolic factors (e.g., cell-to-cell heterogeneity, growth environment) influence the efficacy of different drug combinations. Computational tools are hence necessary to identify antibiotic treatments that are robustly efficacious across heterogeneous environments (Bumann, 2015; Eisenreich et al., 2010).

To address these limitations, we present an approach that integrates genome-scale metabolic models (GEMs) into ML model development to determine effective combination therapies. Using GEMs allows us to integrate diverse data types and account for different pathogen metabolic states and growth conditions. GEMs are computational models built from gene-protein-reaction associations of metabolic genes present in the genome of an organism (Price et al., 2004). Additionally, they include annotation of traditional antibiotic targets such as cell wall synthesis, DNA replication, and RNA transcription. Model constraints, such as from omics data or nutrient availability, can be imposed to simulate bacterial metabolism in response to different perturbations (Dahal et al., 2020; N. E. Lewis et al., 2012). Our approach using GEMs and ML provides a systems-level perspective of the bacterial response to antibiotic treatment in condition-specific cases. This is critical for designing efficacious combination therapies, since experimentally measured susceptibility to antibiotics may not always translate into efficacy *in vivo*. We further extend our approach to predict outcomes for sequential combination therapies, which can be designed into cyclic antibiotic regimens that mitigate resistance (Baym et al., 2016). Finally, we showcase how our models reveal mechanistic insights that explain treatment potency and can be leveraged to finetune data-driven combination therapy design.

2.4 Results

2.4.1 The CARAMeL approach for combination therapy design

Our approach, called *Condition-specific Antibiotic Regimen Assessment using Mechanistic Learning* (CARAMeL), involves a two-step modeling process: (a) simulating metabolic flux data using GEMs and (b) developing a ML model to predict combination therapy outcomes using flux from GEMs. For the first part, omics data and metabolite composition of the extracellular environment serve as GEM inputs to determine flux profiles in response to drug treatment and growth in defined media, respectively (**Figure 2-1A**). For the second part, GEM-derived flux profiles and drug interaction data serve as inputs to train a ML model that predicts interaction outcomes for novel drug combinations ((**Figure 2-1B**). We developed ML models predictive of combination therapy outcomes for *E. coli* and *M. tb* using the Random Forests algorithm. We specifically chose this ML method as it can handle small datasets and determine feature importance, i.e., how much each feature contributes to the accuracy in model predictions. The feature importance can reveal mechanistic insights into the factors driving combination therapy outcomes.

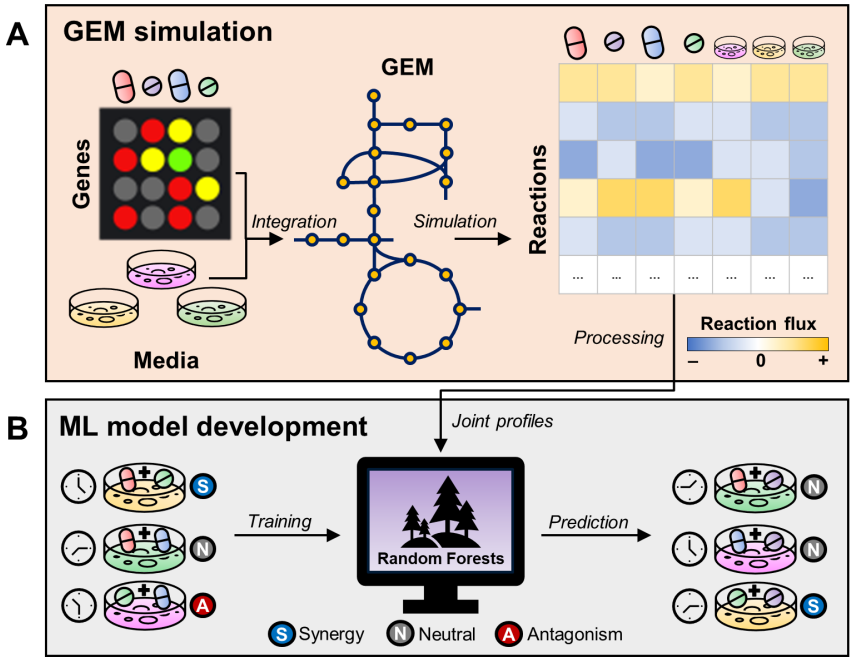

Figure 2-1 CARAMeL approach schematic. The *Condition-specific Antibiotic Regimen Assessment using Mechanistic Learning* (CARAMeL) approach involves a two-step process: (**A**) omics data (e.g., transcriptomics) measured for single drug treatments and information on growth media composition are integrated into a genome-scale metabolic model (GEM) to simulate metabolic flux changes. (**B**) This information, along with drug interaction data, serve as inputs to train a machine learning (ML) model; the trained model can then be used to predict outcomes for novel drug interactions.

We determined metabolic flux profiles in response to drug treatment and condition-specific growth by constraining the *E. coli* GEM iJO1366 (Orth et al., 2011) and the *M. tb* GEM iEK1011 (Kavvas et al., 2018). For drug flux profiles, we imposed chemogenomic data for *E. coli* (Nichols et al., 2011) and transcriptomic data for *M. tb* (Ma et al., 2019) as GEM constraints. Briefly, chemogenomic data measures single-gene knockout (KO) fitness while transcriptomics data measures genome-wide expression of genes. By selecting genes for which there was differential fitness or expression in response to a specific treatment, we could infer a set of differentially regulated genes for individual drugs. For transcriptomic data, positive and negative differential expression directly corresponded with up- and down-regulation, respectively. For chemogenomic data, we assumed that gene KOs that result in low fitness are likely to be up- regulated upon drug treatment, while gene KOs that enhance fitness were likely to be down-regulated. This assumption

is based on the cost-benefit gene expression model proposed by Dekel & Alon (Dekel & Alon, 2005). Direct comparison of flux profiles simulated from a chemogenomic-based approach against flux profiles simulated with transcriptomics and proteomics data confirmed that these assumptions were valid (**Figure S2-1**) (Maeda et al., 2020; Mori et al., 2021; Suzuki et al., 2014). To determine growth media flux profiles, the availability of metabolites within a media condition was used to constrain the GEMs. Specifically, we modified the uptake rate for exchange reactions providing key metabolites (e.g., glycerol exchange for M9 glycerol media) to allow cellular intake (see Methods for further details).

Prior to ML model development, we processed drug and media flux profiles to determine joint profiles for all combinations of interest. Joint profiles are comprised of four pieces of information: (a) the combined effect of all treatments (i.e., sigma scores), (b) the unique effect of individual treatments (i.e., delta scores), (c) the overall metabolic entropy (i.e., entropy scores), and (d) time interval (relevant for time- and order-dependent combinations). To determine sigma and delta scores, we adapted a strategy previously used for creating joint chemogenomic profiles (Chandrasekaran et al., 2016; Cokol et al., 2018). Specifically, we binarized drug and media flux profiles based on differential flux activity in comparison to baseline (i.e., GEM simulation without additional constraints). Sigma scores were defined as the union of binarized flux profiles for all treatments involved in a combination. Delta scores were defined as the symmetric difference between flux profiles (see Methods for details). To account for metabolic entropy, we first calculated entropy as defined by Zhu et al. (Z. Zhu et al., 2020) for each drug and media flux profile. We then defined entropy scores as the mean and sum of entropy among all treatments involved in a combination. Finally, the time feature was defined as the time interval between the first and last treatments for a combination (see Methods and **Figure S2-2** for further details).

Using feature (i.e., joint profiles) and outcome (i.e., interaction scores, IS) information for a set of drug combinations, we trained ML models to associate feature patterns to drug combination outcomes. Next, we used the trained ML models to predict outcomes for new drug combinations based on their feature information alone. We then compared our predictions against experimental data by calculating the Spearman correlation. We also assessed model performance by calculating the area under the receiver operating curve (AUROC) for both synergy and antagonism. High and positive values for both metrics indicate that model predictions correspond well with actual drug interaction outcomes.

2.4.2 CARAMeL predicts drug interactions with high accuracy

We benchmarked CARAMeL against previous approaches by directly comparing our prediction accuracy against those reported in literature and those re-calculated using omics data directly instead of using flux data. For these comparisons, we trained ML models and evaluated their performance for five different cases:

1. Predicting novel pairwise drug interaction outcomes for *E. coli* (Chandrasekaran et al., 2016)
2. Predicting novel three-way drug interaction outcomes for *E. coli* (Cokol et al., 2018)
3. Predicting pairwise drug interaction outcomes for *E. coli* cultured in a novel nutrient condition (M9 glycerol media) (Cokol et al., 2018)
4. Predicting novel pairwise and three-way interaction outcomes for *M. tb* (Ma et al., 2019)
5. Predicting interaction outcomes for multi-drug TB regimens used in clinical trials (Bonnett et al., 2017)

Of note, the first, second, and fourth cases tested the model's ability to predict unseen combinations involving test drugs with new mechanisms of action. The third case assessed whether the model could predict drug interaction outcomes in a new growth environment, while the fifth case ascertained if predicted outcomes corresponded with clinical efficacy. **Figure 2-2** summarizes our findings for all analyses listed above. For all these studies, the same train-test datasets were used for evaluating CARAMeL against the original methods to ensure direct comparison. The same thresholds for synergy and antagonism defined in the original studies were also used in all these comparisons. When re-evaluating omic-based approaches, we followed the exact procedure as reported in their respective original literature (Chandrasekaran et al., 2016; Cokol et al., 2018; Ma et al., 2019). To ensure fair comparison between CARAMeL and omic-based approaches, we also evaluated the omic-based methods for different parameter values and report the overall best results for all datasets (**Table S2-1**). Further discussion on ML model development and results, including the specific train-test allocation of interaction data reported in literature for each case, is provided below.

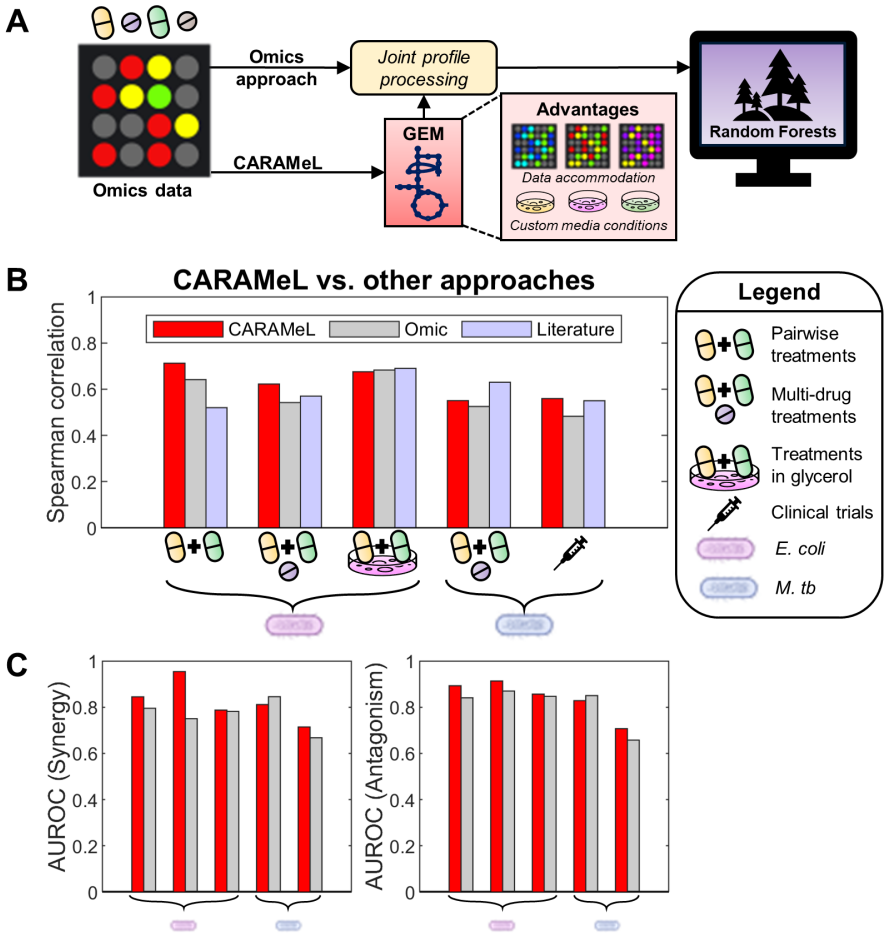

Figure 2-2 CARAMeL was benchmarked against other predictive approaches. (**A**) CARAMeL differs from previous omics-based approaches by using simulated metabolic flux data to define the joint profiles that are used in the random forests model. CARAMeL also provides advantages over the omics-based approaches, including the accommodation of diverse data types (e.g., chemogenomics, transcriptomics) and evaluation of user-defined media effects. (**B**) The Spearman correlation between actual outcomes and model predictions are shown and compared between three approaches: CARAMeL (this study), omics (determined using chemogenomic or transcriptomic data as input), and literature (reported in literature). (**C**) The area under the receiver operating curve (AUROC) for classifying interactions as synergistic or antagonistic is also directly compared between CARAMeL and omic-based approaches.

For case 1, we used drug interaction data previously measured for 171 pairwise combinations involving 19 drugs that cover a diverse set of targets (Chandrasekaran et al., 2016) (**Table S2-2**). Out of this total, 105 interactions involving 15 drugs were used for model training and the remaining 66 interactions, which involved four new drugs that introduced new mechanisms of action (e.g., RNA synthesis), were used for model validation. The CARAMeL model yielded significant correlations between experimental and predicted scores (R = 0.71, p ~ 10-11, **Figure**

S2-3A). Model predictions also yielded high AUROC values for classifying synergy (IS < -0.5, AUROC = 0.84) and antagonism (IS > 2, AUROC = 0.89) () based on thresholds defined in the original study. Of note, these results were considerably better than those reported in literature (R = 0.52) (Chandrasekaran et al., 2016) and those re-calculated using the omic-based approach (R = 0.64) (**Figure 2-2A**).

For case 2, we re-trained the CARAMeL model using 171 pairwise interactions to predict 56 three-way combinations involving eight antibiotics (Cokol et al., 2018) (**Table S2-2**). Our model generated accurate predictions (R = 0.62, p ~ 10-7, **Figure S2-3C**) and notably identified synergistic interactions (IS < -0.2, AUROC = 0.95, Fig. **Figure S2-3D**) with higher accuracy than the omics-based approach (AUROC = 0.76, **Figure 2-2B**).

For case 3, the CARAMeL model was once again re-trained with the 171 pairwise interactions and additional pairwise data measured for *E. coli* cultured in M9 glucose and lysogeny broth (LB) media. We then applied our model to predict 55 pairwise interaction outcomes for *E. coli* cultured in M9 glycerol media. Our model yielded results comparable to those from literature (Cokol et al., 2018) and re-determined using omics data across all three performance measures (R = 0.68, p ~ 10-8, **Figure 2-2**, **Figure S2-3E**, and **Figure S2-3F**).

For case 4, we trained a CARAMeL model using combination data for *M. tb* treated with 196 pairwise to five-way interactions involving 40 drugs (Ma et al., 2019) (**Table S2-3**). We then used data for 36 unseen interactions for model validation. The CARAMeL model yielded predictions that significantly correlated with experimental data (R = 0.55, p ~ 10-4, **Figure S2-4A**) and performed well in classifying synergistic (IS < 0.9, AUROC = 0.81) and antagonistic (IS > 1.1, AUROC = 0.83) interactions (**Figure S2-4B**). Though the CARAMeL-based correlation is slightly lower than that reported in literature (Ma et al., 2019) (R = 0.63), our model classified both

synergistic and antagonistic interactions with high accuracies that are comparable to a model trained on omics data (**Figure 2-2C**).

For case 5, we used the same CARAMeL model from case 4 to predict interaction outcomes for 57 multi-drug TB regimens involving nine drugs prescribed in separate clinical trials (Bonnett et al., 2017) (**Table S2-3**). Of note, interaction outcomes for this dataset measured regimen efficacy based on sputum clearance after two months of treatment. We found that model predictions were significantly correlated ($R = 0.56$, $p \sim 10\text{-}6$, **Figure S2-4C**) with sputum clearance, and that model predictions classified as synergistic ($IS < 0.9$) captured most of the efficacious treatments (sputum clearance > 80%) amongst all 57 TB regimens (**Figure S2-4D**). These results were comparable to both literature- (Ma et al., 2019) and omic-based results across all three performance measurements (**Figure 2-2**).

Overall, we found that our approach retained high accuracies in predicting combination therapy outcomes for a diverse set of test cases based on *E. coli* and *M. tb* data. This is striking considering that CARAMeL solely relies on simulated metabolic information, which was determined using only ~25–35% of available omics data.

2.4.3 Using CARAMeL to predict sequential interactions

Current approaches for predicting combination therapy outcomes focus on drug treatments that are given simultaneously. Here, we extended our approach to predict treatment efficacy for time- and order-dependent (i.e., sequential) interactions. In contrast to simultaneous combinations, the order and length of each drug treatment dictates how a pathogen adapts itself, and in turn, influences its sensitivity to successive drug treatments. As such, interaction outcomes are interpreted as leading to collateral sensitivity (analogous to synergy) or cross-resistance (analogous to antagonism). For this task, we used data for *E. coli* evolved in single drug treatments over three

timespans (10, 21, and 90 days) then subsequently treated with a second drug (Imamovic & Sommer, 2013; Oz et al., 2014; Suzuki et al., 2014). To account for both time- and order-dependent drug effect, we re-defined the delta scores for sequential joint profiles. Briefly, delta scores were defined as the difference in binarized drug profiles scaled by the time interval between treatments (mathematically defined for pairwise sequences below):

$$\delta = \frac{t_2 v_2 - t_1 v_1}{t_2 - t_1}$$

Equation 2-1 Delta score calculation for sequential drug interactions.

where δ = delta scores, t = length of treatment time, and v = binarized flux profile.

To initially assess how well the CARAMeL approach could predict sequential treatment outcomes, we first conducted a 10-fold cross-validation of the sequential data (N = 628), which involved 27 unique drugs (**Table S2-4**). We found that CARAMeL predictions moderately, but significantly, correlated with experimental outcomes ($R = 0.49$, $p < 10\text{-}16$, **Figure 2-3A**). Further, the model performed well in determining whether a sequential interaction resulted in collateral sensitivity (IS < -0.1, AUROC = 0.73) or cross-resistance (IS > 0.1, AUROC = 0.75) (**Figure 2-3D**).

We next evaluated the extent of our model's predictive power by conducting two types of leave-out analyses: (a) leave-first-drug-out and (b) leave-second-drug-out. The first case tested whether the model could generalize sequential treatment outcomes for an unknown evolved strain, while the second case assessed whether the model could generalize the immediate effect of a drug on strains evolved in other drugs. For a leave-out analysis, all interactions involving the drug of interest in the appropriate sequence position (first or second) were left out of model training and instead predicted for by the trained model. Similar to the cross-validation analysis, model performance was measured by the overall Spearman correlation and AUROC values for collateral

sensitivity and cross-resistance. We found that both leave-out analyses yielded accuracies similar to those attained from cross-validation (**Figures 2-3B**, **2-3C**, **2-3E** and **2-3F**). Overall, these results indicate that CARAMeL generates robust and accurate predictions for sequential interactions.

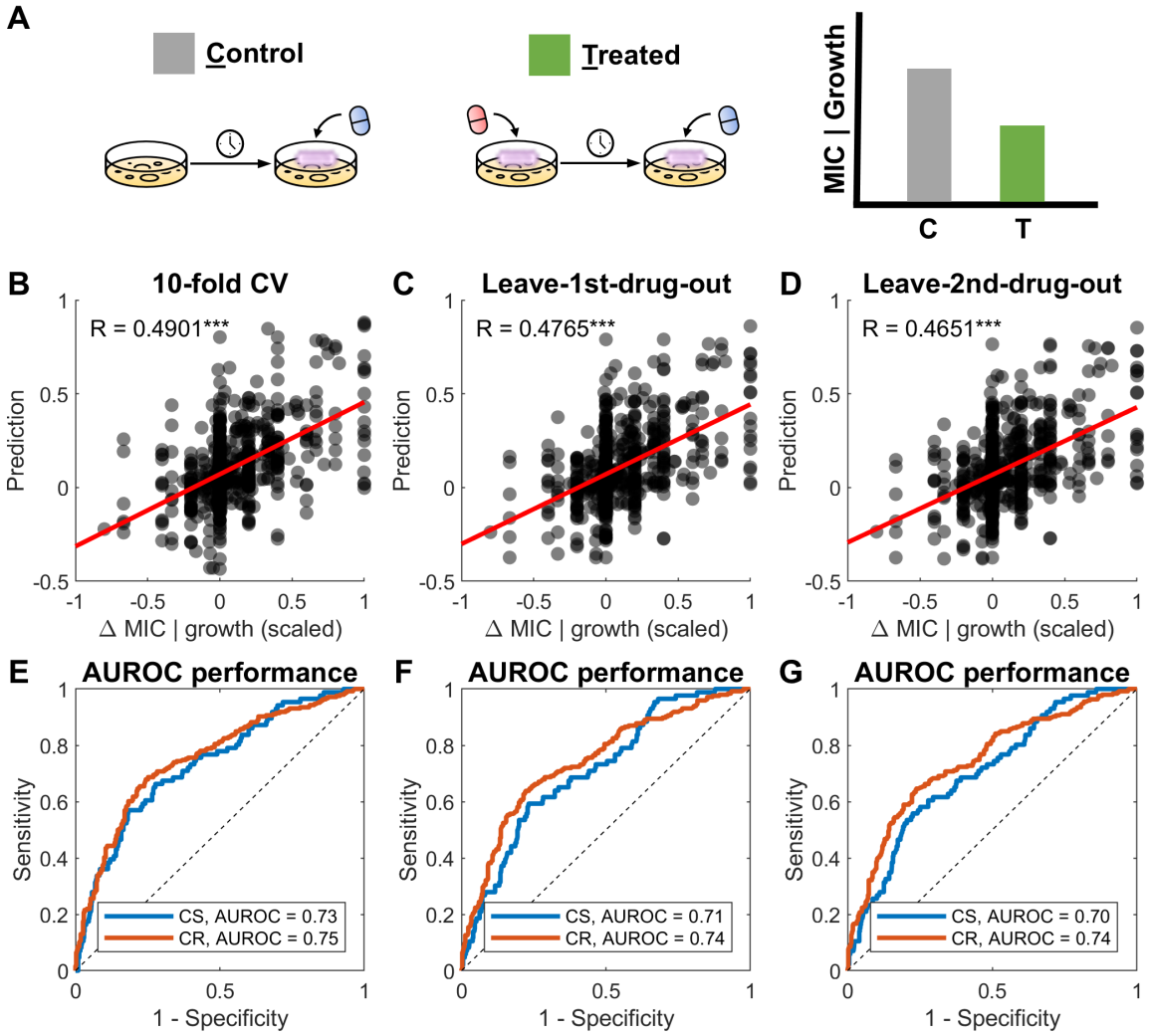

Figure 2-3 Model performance for sequential drug interactions. (**A**) The sequential treatment data used in this work measured outcomes based on the change in the minimal inhibitory concentration (MIC) or bacterial growth for a second antibiotic treatment given after exposure to a first antibiotic and compared to an untreated control (i.e., no pre-treatment with a first antibiotic). CARAMeL model performance using sequential data was evaluated based on 10-fold cross-validation (CV), leave-first-drug-out, and leave-second-drug-out analyses. Shown are the (**B-D**) scatter plots between experimentally measured outcomes (change in MIC or growth) vs. model predictions and (**E-G**) the AUROC performance for detecting collateral sensitivity (CS, outcome < 0) or cross-resistance (CR, outcome > 0). AUROC: area under the receiver operating curve. ***p-value < 10^{-3}.

To gain mechanistic insight into which factors influence combination therapy outcomes, we trained a CARAMeL model using all interaction data available for *E. coli*. We then ranked

features by their predictive importance based on how the model accuracy decreases when a feature is removed (see Methods for details). In total, we found that 580 features explained 95% of the variance in model predictions (**Dataset 2-1**). Of note, entropy features were amongst the top 20, implying that metabolic disarray due to antibiotic stress is indicative of treatment efficacy (**Figure S2-5**). For the GEM-derived features (i.e., sigma and delta scores), we determined that the differential flux through 167 metabolic reactions associated with the top features significantly distinguished between synergistic and antagonistic interactions (two-sample t-test, adjusted p-value < 0.05, **Dataset 2-2**). We then deduced that eight metabolic pathways were enriched by this set of 167 reactions (hypergeometric test, adjusted p-value < 0.05, **Table 2-1**). Differential activity through these pathways aligned with the expected metabolic response to antibiotic treatments. For example, increased flux through DNA repair systems (e.g., nucleotide salvage) is expected after exposure to quinolones, which target DNA gyrase (Fàbrega et al., 2009). Differential flux through transport reactions is also a common tactic that decreases drug concentrations within the bacterial cell, therefore minimizing their adverse effects (Levy, 2002).

Table 2-1 Metabolic pathways enriched amongst top predictors for the *E. coli* CARAMeL model. Pathway enrichment was determined based on 580 features explaining 95% of the variance in model predictions. These features mapped to 333 reactions in the *E. coli* GEM iJO1366, out of which 167 had differential flux that significantly distinguished between synergy and antagonism (two-sample t-test, adjusted p-value < 0.05). Based on this 167-reaction list, eight pathways were found to be significantly enriched (hypergeometric test, adjusted p-value < 0.05). N = number of reactions in pathway, Ratio = N / total reactions in pathway, P-value = hypergeometric test adjusted p-value.

Pathway	N	Ratio	P-value
Purine and Pyrimidine Biosynthesis	9	0.36	3E-05
Pyruvate Metabolism	5	0.50	1E-04
Inorganic Ion Transport and Metabolism	19	0.17	1E-04
Transport, Inner Membrane	37	0.11	1E-03
Glycine and Serine Metabolism	4	0.29	6E-03
Glycolysis/Gluconeogenesis	5	0.23	8E-03
Nucleotide Salvage Pathway	17	0.12	1E-02
Cell Envelope Biosynthesis	15	0.12	3E-02

2.4.4 CARAMeL simulates the impact of intrinsic and extrinsic metabolic heterogeneity on drug interactions

In vivo metabolic conditions span growth in diverse substrates such as sugars, nucleotides, glycerol, lipids, and hypoxic conditions (Eisenreich et al., 2010). In contrast to existing approaches for drug combination design, CARAMeL enables drug interaction predictions in a large array of metabolic conditions. This can help prioritize drug combinations for successful clinical translation considering that the predominant nutrient source can change depending on where bacteria reside inside the host (Brown et al., 2008). By screening different conditions that are representative of *in vivo* environments, we can identify drug combinations that target *E. coli* in diverse metabolic conditions. Moreover, evaluating drug combinations based on efficacy across a large compendium of metabolic network states will ensure robustness against heterogeneity.

To demonstrate the power of using CARAMeL in predicting condition-specific combination therapy outcomes, we applied it to predict pairwise drug interactions in multiple media conditions. For this task, we gathered experimental data for *E. coli* treated with four single drug treatments (Aztreonam (AZT), Cefoxitin (CEF), Tetracycline (TET), Tobramycin (TOB)) and two pairwise drug treatments (CEF + TET, CEF + TOB) (**Table S2-5**). Of note, this treatment panel evaluated the metabolic response in *E. coli* to bactericidal (i.e., death-inducing) and bacteriostatic (i.e., growth-inhibiting) drugs, both individually and in combination. Each drug treatment outcome was assessed in *E. coli* cultured in Biolog phenotype microarray (PM) (Bochner et al., 2001) plate-1, which measured metabolic respiration in 95 carbon sources and one negative control (**Figure 2-4A**). Out of these 95 media conditions, 57 could be simulated based on the metabolites annotated in the *E. coli* GEM (**Dataset 2-3**). As a result, ML model development and

all downstream analyses were conducted using the data subset pertaining to the 57 media conditions that were simulated.

We constructed a ML model using the following inputs: flux profiles for the four drug treatments as well as the 57 media conditions, and interaction outcomes for 228 (4 * 57) drug-media combinations. We then evaluated our model by predicting outcomes for 114 (2 * 57) drug-drug-media combinations (**Figure 2-4B**). Overall, we found that model predictions significantly correlated with experimental outcomes ($R = 0.68$, $p < 10\text{-}16$, **Figure 2-4C**). We also assessed correlations specific to each drug pair and found that model predictions still corresponded well with experimental data (CEF+TET: $R = 0.59$, $p \sim 10\text{-}6$, CEF+TOB: $R = 0.81$, $p < 10\text{-}16$). This large-scale inspection of combination therapy outcome in different growth environments was only possible with the CARAMeL approach, where flux profiles could be determined for 57 media conditions. A direct comparison of the same scale was not possible with the omic-based approach, as neither chemogenomic nor transcriptomic data was available for all these media conditions.

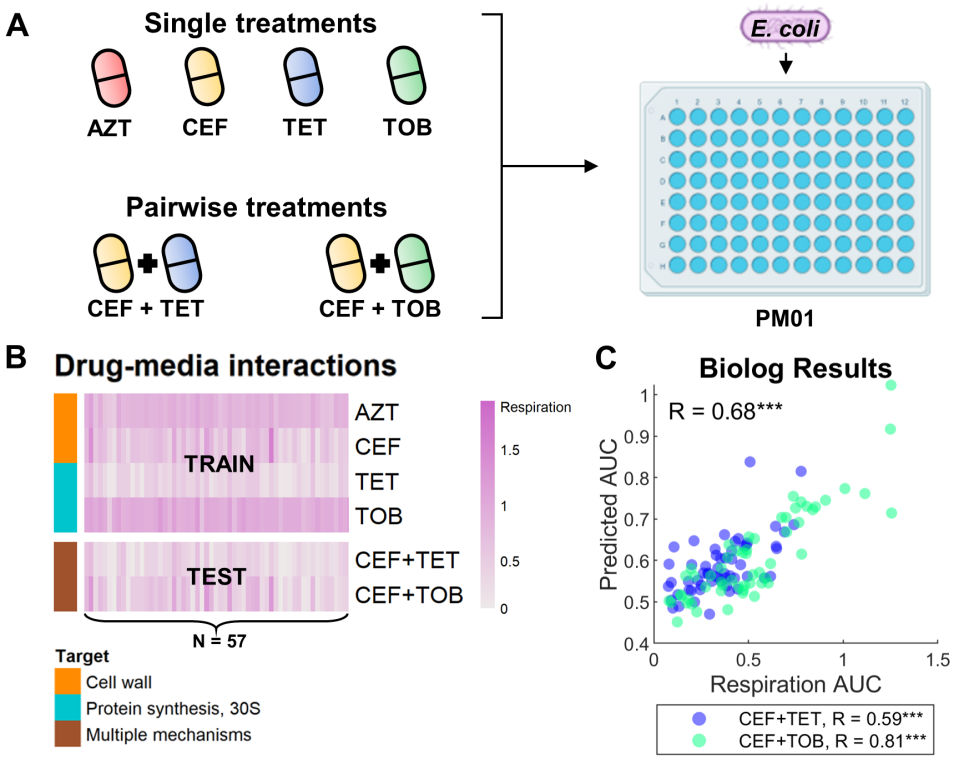

Figure 2-4 CARAMeL accurately predicted drug interaction outcomes in 57 carbon sources. (**A**) *E. coli* was cultured in 96 carbon sources (Biolog PM01 plate), then treated with four single drug treatments (AZTreonam, CEFoxitin, TETtracycline, TOBramycin) and two pairwise treatments (CEF + TET and CEF + TOB). (**B**) Heatmap of metabolic activity (measured based on the respiration ratio between treatment vs. control) in response to all experimental perturbations (data only shown for the 57 media conditions simulated using the *E. coli* GEM). (**C**) Spearman correlation between experimental outcome and model predictions for all combinations in the test set are shown. GEM: genome-scale metabolic model. *** p-value < 10^{-3}.

We next evaluated how cell-to-cell heterogeneity influenced combination therapy outcomes using population FBA (Labhsetwar et al., 2013), a modeling approach that simulates cell-specific metabolic heterogeneity based on single-cell proteomics data (Taniguchi et al., 2010). Specifically, information on the protein copy number levels measured for *E. coli* cultured in M9 glucose media is used to constrain the metabolic model. To simulate heterogeneity between cells, the single-cell proteomics data is randomly sampled based on the Gamma distribution for each cell and subsequently used to constrain the GEM to simulate cell-specific metabolic states (**Figure 2-5A**). We used population FBA to simulate 1,000 *E. coli* cells cultured in M9 glucose media (Methods). We then generated pairwise predictions between all drugs for which the *E. coli*

CARAMeL model was trained on (N = 33) against the 1,000 simulated cells (**Dataset 2-4**). For each drug pair, we evaluated three interaction cases: (a) simultaneous treatment (D1 + D2), (b) sequential treatment from D1 to D2, and (c) sequential treatment from D2 to D1. For sequential interactions, we set the duration for the first treatment to 14 days, based on the most commonly prescribed antibiotic treatment duration against bloodstream infection by *Enterobacteriaceae* (Tansarli et al., 2019), and one day for the second treatment.

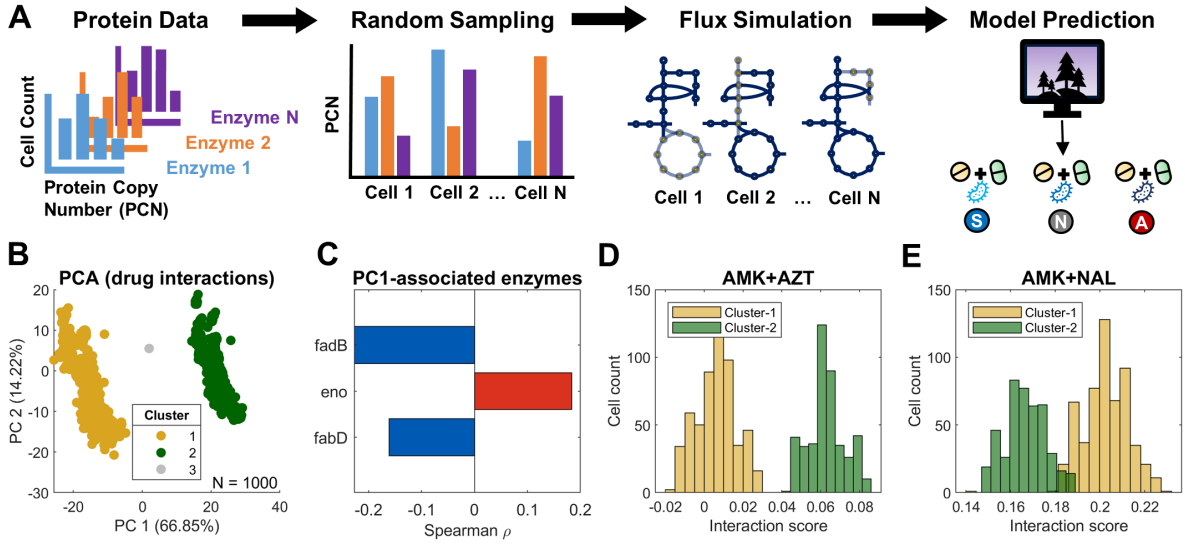

Figure 2-5 Single cell-specific combination therapy predictions. (**A**) Schematic showing how population FBA (Labhsetwar et al., 2013) was applied to simulate cell-specific metabolic heterogeneity. Specifically, single-cell proteomics data (Taniguchi et al., 2010) was randomly sampled (based on the Gamma distribution) and used to constrain the *E. coli* genome-scale metabolic model to simulate cell-specific fluxes, which were ultimately used to generate cell-specific drug interaction predictions. (**B**) Cells were found to cluster into two distinct groups after applying principal component analysis (PCA) onto the simultaneous prediction data (PC loadings for the first two dimensions reported in ***Data S6***). (**C**) The sampled level for three enzymes (eno, fadB, and fabD) were found to significantly correlate with cell-specific scores along principal component 1 (PC1) from panel B. (**D**) Cluster-1 cells were predicted to be more sensitive to most drug combinations (e.g., AMK + AZT) compared to cluster-2 cells. (**E**) For a smaller set of drug combinations (15%), primarily involving quinolones (e.g., AMK + NAL), cluster-2 cells were predicted to be more sensitive than cluster-1 cells. AMK: amikacin, AZT: aztreonam, NAL: nalidixic acid.

Using the prediction landscape for the 1,000 cells, we determined the extent of cell-to-cell variability for each unique drug pair (**Dataset 2-5**). Overall, sequential predictions varied more largely between cells (up to 14% change in standard deviation relative to the mean) while there was less than 5% change in standard deviation compared to the mean for the simultaneous case,

suggesting that simultaneous treatments may be more robust to heterogeneity (**Figure S2-6**). Interestingly, the variation among simultaneous predictions tended to follow a bimodal distribution (**Figure S2-7**). Applying principal component analysis (PCA) onto the simultaneous prediction landscape for all 1,000 cells confirmed that two distinct sub-populations can be determined via k-means clustering (**Figure 2-5B** and **Figure S2-8**, see Methods for details). We further confirmed that the cell clustering was not being driven by non-uniform sampling of the flux solution space by re-sampling single-cell fluxes using optGpSampler (Megchelenbrink et al., 2014) (**Figure S2-9**). Of note, this distinct cell grouping was not observed when PCA was applied to cell-specific proteomics data nor metabolic flux data (**Figure S2-10**).

We next sought to determine whether the clustering pattern seen in the drug interaction PCA plot was being driven by specific enzyme levels or metabolic activity. Thus, we evaluated the correlation between the cell-specific scores along principal component 1 (PC1) against corresponding enzyme levels and simulated flux profiles. We determined that sampled levels for three enzymes (eno, fadB, and fabD) significantly correlated with the cell mapping along PC1 (**Figure 2-5C**). These enzymes correspond to enolase (involved in glycolysis), a multi-functional enoyl-CoA hydratase (involved in lipid metabolism), and malonyl-CoA-acyl carrier protein transacylase (involved in lipid metabolism), respectively. A similar comparison of PC1 scores with the simulated flux data revealed more than 400 significantly associated reactions (**Dataset 2-7**), which altogether correspond to 16 pathways (hypergeometric test, adjusted p-value < 0.05, **Figure S2-11**). These findings confirm that cluster-1 cells differ from cluster-2 cells based on their metabolic activity through glycolysis (eno) and lipid metabolism (fadB and fabD).

Hence, fluctuations in the levels of these three proteins were predicted to drive the broad metabolic shift between the two sub-populations. To confirm the causality, we performed

knockouts of these three proteins. A similar PCA assessment for cells simulated to have single- and multi-gene knockout of eno, fadB, and fabD confirmed that the PCA-based cell clustering seen in **Figure 2-5B** is strongly driven by the metabolic states characterized by eno and fabD levels (**Figure S2-12**).

Based on the direction of the enzyme correlation with PC1 scores, we inferred that cluster-1 cells exhibit low glycolysis and high lipid metabolism, while cluster-2 cells exhibit the opposite behavior. For a large set of drug combinations (85%), we found that reduced glycolysis coupled with high lipid metabolism promoted more synergistic outcomes (**Figure 2-5D**, **Dataset 2-8**), while the same metabolic state was found to promote more antagonistic outcomes for a smaller set (15% of the combinations) (**Figure 2-5E**, **Dataset 2-8**). Of note, a small number of cells representing <1% of the total population (labeled as "cluster-3") did not cluster together with either dominant sub-population but instead fell near the center of the drug interaction PCA space (**Figures 2-5B** and **Figure S2-7**). Closer inspection of enzyme levels for eno, fadB, and fabD revealed that the sampled levels for eno were much lower for cluster-3 cells (~400 per cell) compared to cluster-1 and cluster-2 cells (~600 per cell, **Figure S2-13**). Considering that enolase is an essential enzyme for maintaining glycolysis and cell growth, an adequately high level for enolase (e.g., > 500 per cell) may be required to simulate stable flux solutions that lead to the patterns we observe in **Figure 2-5B**. These cells may represent an unstable transition state between cluster 1 and 2.

Interestingly, the smaller set of drug combinations with antagonistic outcomes in cluster 1 is overrepresented by combinations that include quinolones such as nalidixic acid (~12% among synergistic vs. ~86% of antagonistic combinations in cluster-1 involved quinolones, refer to **Dataset 2-8**). A prior study has found that quinolone efficacy is reduced in high-density bacterial

populations, likely due to depletion of metabolites that couple carbon metabolism to oxidative phosphorylation (Gutierrez et al., 2017). The same study subsequently shows that quinolone efficacy can be restored via supplementation with glucose and an electron acceptor, which stimulate respiratory metabolism. Our findings, coupled with the literary evidence described above, indicate that cluster-1 cells may represent a sub-population that is tolerant to treatments involving quinolones. Given the highly interconnected nature of cellular metabolism, stochastic changes in a small number of key metabolic enzymes can result in distinct phenotypes when treated with stressors. These two sub-populations may not be evident in an unperturbed system which shows fluctuations in numerous proteins; however, when exposed to antibiotics they may result in bifurcation into two stable sub-populations. Though experimental validation would be required to fortify these results, we confirmed that all the reported findings tied to the cell-specific predictions are robust to a wide range of modeling parameters (**Figure S2-8**).

2.4.5 Screening for robust combination therapies

Synergy observed in the lab may not result in synergy *in vivo* due to differences in growth conditions or drug pharmacokinetics, wherein drugs may reach the infection site at different times rather than simultaneously (Cicchese et al., 2021). Considering these factors, combination therapies that show synergy across growth conditions and time scales hold the best potential for successful clinical translation. To discover such therapies, we predicted pairwise and three-way regimen outcomes for all drugs for which the *E. coli* CARAMeL model was trained on (N = 33) across 57 carbon sources (from Biolog PM01). For sequential interaction predictions, treatment duration for pairwise treatments was set to 14 days followed by 1 day, while three-way treatments were set to a 14-14-1-day prescription. In total, we generated predictions for 90,288 pairwise combinations ($_{33}C_2$ pairs x 3 interaction cases x 57 PM01 conditions, **Dataset 2-9**) and 2,176,944

three-way combinations ($_{33}C_3$ combinations x 7 interaction cases x 57 PM01 conditions, **Dataset 2-10**).

Out of 528 unique drug pairs and 5,456 unique three-way interactions, none was predicted to be synergistic across all media conditions and interaction cases. In fact, sustained synergy across media conditions seems to occur for only a small subset (< 10%) of drug interactions (**Figure S2-14**). Specifically, 73 drug pairs and 165 three-way interactions were predicted to yield synergy both simultaneously and sequentially in at least one media condition (**Figure 2-6** and **Figure S2-15**). Of note, all 73 drug pairs showed less than 5% cell-to-cell variation based on population FBA for all interactions cases (i.e., simultaneous and sequential interactions). Upon closer inspection of both pairwise and three-way sets, synergy was not found to be retained across a majority of media conditions for three-way drug interactions. On the other hand, several pairwise interactions were found to retain synergy well; specifically, 24 drug pairs out of 73 were found to be synergistic in more than 50% of conditions in both simultaneous and sequential cases.

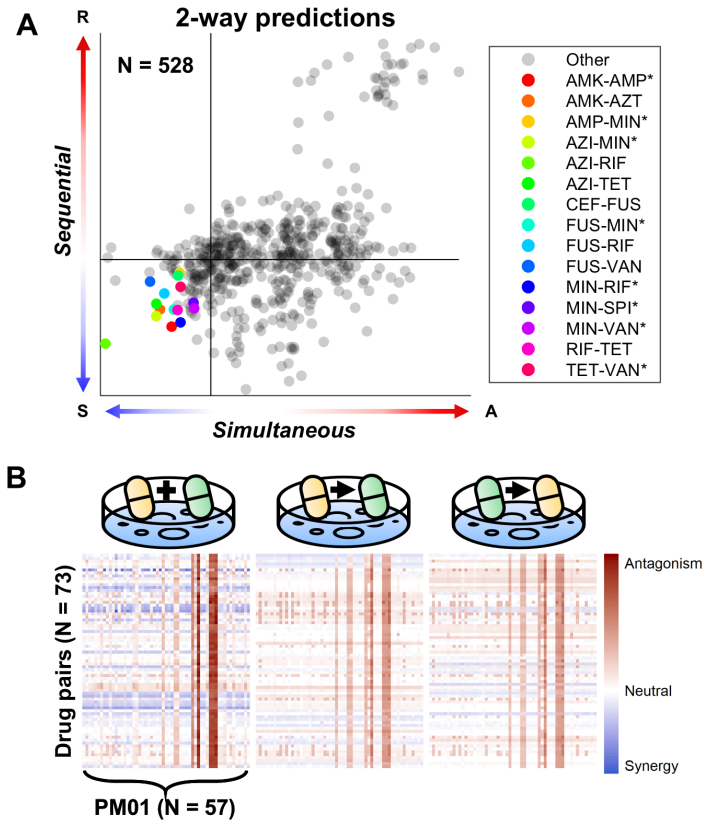

Figure 2-6 Pairwise combination therapy prediction across 57 media conditions. (**A**) Out of 528 drug pairs, 73 were predicted to yield synergy (IS < 0) in at least one media condition for both the simultaneous and sequential cases (the top 15 robustly synergistic drug pairs are listed in the legend). (**B**) Heatmap of the predicted interaction scores for the 73 drug pairs across 57 media conditions and three interaction types ($D_1 + D_2$, $D_1 \rightarrow D_2$, $D_2 \rightarrow D_1$). Refer to **Table S2-2** and **Table S2-4** for full descriptions on antibiotics used for *E. coli*.

Interestingly, several of these 24 drug pairs possess evidence for clinical use against bacterial infections. For example, amikacin-ampicillin treatment (AMK-AMP) has previously been shown to be clinically effective for a wide range of infections (American Thoracic Society, 2005; Dellinger et al., 2013; Krause et al., 2016) including treatment of bacteremia in neutropenic patients(Palmblad & Lönnqvist, 1982) and neonatal bacterial infections (Umaña et al., 1990). Other drug interactions of note include: azithromycin-rifampicin (AZI-RIF), which has demonstrated clinical efficacy in treating arthritis induced by pathogenic *Chlamydia* (Gram-negative) (Carter et al., 2010); fusidic acid-rifampicin (FUS-RIF), which has shown clinical efficacy against prosthetic joint infection caused by drug-resistant *Staphylococci* (Gram-positive)

(Zimmerli et al., 2004); and minocycline-rifampicin (MIN-RIF), which has been shown to prevent colonization by slime-producing staphylococci in catheters (Raad et al., 1995). Additionally, rifampicin combined with other drugs has been advised as treatment for Gram-negative and non-mycobacterial infections (Drapeau et al., 2010; Forrest & Tamura, 2010). Further investigation into the set of 24 drug pairs predicted to yield robust synergy may lead to the discovery of new combination therapies that could be put to clinical use.

2.5 Discussion

Here we introduced CARAMeL, a modeling approach to design condition-specific antibiotic regimens. CARAMeL offers multiple advantages over prior methods of similar nature. First, our approach enables use of diverse data types (e.g., chemogenomics, transcriptomics) individually or in combination, derived from a single source or in combination from multiple sources, therefore maximizing the number of drugs that are screened. For instance, our *E. coli* CARAMeL model leveraged use of both chemogenomics data (for defining drug flux profiles) and proteomics data (for simulating single cells), a feat that cannot be accomplished with prior methods of similar nature. Second, we extended our approach to simulate different interaction cases (simultaneous vs. sequential) when designing combination therapies. To our knowledge, no framework currently exists to incorporate these factors into drug discovery efforts against AMR. Third, the use of GEMs enables simulation of highly tunable metabolic conditions (as showcased with our analysis of the Biolog PM01 data), which may be leveraged to investigate combination therapy outcomes in the host environment. GEMs also enable the simulation of pathogen metabolic heterogeneity, due to both intrinsic stochasticity and the metabolic environment. Pathogen heterogeneity is a critical barrier in designing effective antibiotic therapies, and this must be factored into combination therapy design to mitigate the rise of resistant strains.

Additional advantages to the CARAMeL approach include its mechanistic model interpretability, its ability to simulate pathogen metabolic heterogeneity, and its use in generating predictions across numerous conditions in large-scale. Regarding model interpretation, the *E. coli* CARAMeL model revealed that entropy, or metabolic disarray, plays an important role in combination therapy outcome. The direct link between model features (i.e., sigma and delta scores) and GEM reactions also pinpointed pathways that are activate in response to drug treatment (**Table 2-1**), many of which align with the expected resistance mechanisms against antimicrobial stress (Fàbrega et al., 2009; Levy, 2002).

Using population FBA (Labhsetwar et al., 2013), we investigated how drug interaction outcomes may differ from cell-to-cell. Our findings potentially point to a connection between the metabolic state of a cell and its tolerance against combination treatments. Specifically, we found that sensitivity to a broad-range of drug combinations may be influenced by the variation in activity of glycolysis and lipid metabolism; these processes are directly related to antibiotic action and interaction such as uptake, respiration, and oxidative stress (Stokes et al., 2019). Our results also imply that drug interaction outcomes measured for a bulk cell population may not be representative for cell sub-populations. Surprisingly, very few cells show the "average" behavior of the population; in most cases, the average prediction may be defined by the outcome in two dominant sub-populations where one is more sensitive to treatment while the other is more tolerant. This investigation, along with our results with the Biolog data, demonstrate how pathogen metabolic heterogeneity may arise due to both intrinsic stochasticity and the local growth environment. Pathogen heterogeneity is a critical barrier in designing effective antibiotic therapies, and this must be factored into combination therapy design to mitigate the rise of resistant strains.

Finally, analysis of the drug interaction landscape suggests that only a small set of 24 out of ~6,000 combinations show robust synergy across growth conditions and interaction cases, with some possessing clinical evidence for efficacy (American Thoracic Society, 2005; Carter et al., 2010; Dellinger et al., 2013; Drapeau et al., 2010; Forrest & Tamura, 2010; Palmblad & Lönnqvist, 1982; Raad et al., 1995; Umaña et al., 1990; Zimmerli et al., 2004). Further investigation into this list of drug interactions may lead to the discovery of new combination therapies for clinical application.

Ultimately, CARAMeL serves as a proof-of-concept of how computational approaches, such as systems-level metabolic modeling and machine learning, can be combined to create hybrid models that provide mechanistic insight into various biological processes (Cantrell et al., 2022; Y. Kim et al., 2021; Zampieri et al., 2019), in this case antimicrobial efficacy and resistance. Although the use of GEMs in CARAMeL offers major advantages with data compatibility, condition tunability, and mechanistic insight, it also introduces some limitations. The level of accuracy and thoroughness in GEM annotation may influence CARAMeL model performance. Moreover, our current approach only provides a "snapshot" perspective of the metabolic response to a condition. This may be a potential reason for the diminished CARAMeL model performance in predicting sequential outcomes. Nevertheless, these are areas that can be addressed with continued curation of GEMs (Bernstein et al., 2021) and advances in dynamic metabolic modeling (Chung et al., 2021; Saa & Nielsen, 2017). Overall, the ability to simulate specific growth environments and pathogen metabolic heterogeneity offers the potential to evaluate treatment efficacy *in vivo* and advance clinical translation of novel antibiotic regimens. Moreover, these combination therapies could restore use of defunct antibiotics against resistant pathogens while mitigating further resistance (Baym et al., 2016; S. Kim et al., 2014). Beyond bacterial infections, CARAMeL has

the potential to design explainable combination therapies that are urgently needed to combat fungal infections (Livengood et al., 2020) and drug-resistant cancer cells (Mokhtari et al., 2017). Such broader applications can be achieved by leveraging the large volume and diversity of highly curated GEMs that exist and continue to be constructed (Fang et al., 2020). Our approach can further be used to understand the role of metabolic heterogeneity in cancer treatment, which plays a major role in tumor drug resistance (Jamal-Hanjani et al., 2015; Junttila & De Sauvage, 2013).

2.6 Methods

2.6.1 Experimental design (biolog phenotype microarray)

E. coli MG1655 was cultured in Biolog phenotype microarray (PM) 1, which screened bacterial growth in 95 carbon sources and a negative control (i.e., water) (Bochner et al., 2001). *E. coli* was subsequently treated with six distinct drug treatments in duplicate: aztreonam (0.03 ug/mL), cefoxitin (1.87 ug/mL), tetracycline (1.42 ug/mL), tobramycin (0.15 ug/mL), cefoxitin (1.87 ug/mL) + tetracycline (1.42 ug/mL), and cefoxitin (1.87 ug/mL) + tobramycin (1.42 ug/mL). Including a reference plate (*E. coli* growth in PM01 only), phenotype in each treatment was colorimetrically measured in duplicate using tetrazolium violet dye, which quantifies cellular respiration. All experimental procedures, data collection, and quality control were performed at Biolog, Inc. The area under the respiration curve was calculated using MATLAB and reported as the ratio of treatment to reference.

2.6.2 Simulating metabolic flux using GEMs

The *E. coli* GEM iJO1366 (Orth et al., 2011) and the *M. tb* GEM iEK1008 (Kavvas et al., 2018) were used to simulate metabolic fluxes at steady-state. To simulate drug flux profiles, chemogenomic data for *E. coli* (Nichols et al., 2011) and transcriptomic data for *M. tb* (Ma et al.,

2019) served as GEM constraints. Specifically, differential gene regulation in response to each drug treatment was inferred from each dataset. For chemogenomic data, which measured single-gene knockout (KO) fitness, genes KOs that promoted growth were assumed as dispensable while gene KOs that resulted in low fitness were assumed to be essential for growth in said condition. Based on these assumptions, genes corresponding with low ($z < -2$) and high ($z > 2$) fitness were inferred to be up- and down-regulated, respectively. Of note, the original source for the *E. coli* chemogenomic data used in this study was already processed and normalized into z-scores that accounted for both the gene KO and drug treatment effects. For transcriptomic data, which measured single-gene expression, up- and down-regulation were directly inferred based on high ($z > 2$) and low ($z < -2$) expression values, respectively. These processes yielded individual sets of differentially regulated genes that were integrated into corresponding GEMs using a linear optimization version of the integrative metabolic analysis tool (iMAT) (Shen, Boccuto, et al., 2019; Shlomi et al., 2008). To determine media flux profiles, metabolite availability was computationally defined by constraining exchange reactions annotated in iJO1366. For each carbon source of interest (e.g., glycerol), the lower bound (i.e., uptake rate) for the corresponding exchange reaction (e.g., glycerol exchange) was set to -10 g/mmol to allow cellular intake.

Of note, use of the linear iMAT algorithm required constraint-based modeling (CBM) parameter fine-tuning for three variables: kappa, rho, and epsilon (Campit & Chandrasekaran, 2020; Shen, Cheek, et al., 2019). Kappa and rho serve as relative weights for “off” and “on” reactions associated with the differentially expressed genes, respectively, in their contribution to the objective function. Epsilon represents the minimum flux through “on” reactions. For the purposes of this research, we varied all three parameter values from 10^{-3} to 1 and determined the optimal parameter set based on three criteria: (1) maximizing the Spearman correlation between

predicted and actual interaction scores after 10-fold cross-validation using a training dataset, (2) minimizing the number of conditions simulated to have no growth, and (3) ensuring non-zero variability in the simulated growth rates between conditions. **Table S2-6** provides results for all three assessments for all parameter sets of interest. The following optimal parameter values were obtained for each GEM using the training dataset: (1) iJO1366 – kappa =10-2, rho = 10-2, epsilon = 1, and (2) iEK1008 – kappa = 10-2, rho = 10-2, epsilon = 10-2. These parameter values were used for all results when benchmarking CARAMeL against previous approaches based on *E. coli* and *M. tb* drug interaction datasets (**Table S2-7**).

To simulate cell-specific flux data, we applied population FBA (Labhsetwar et al., 2013), an approach that models metabolic heterogeneity within a cell population using proteomics data. For the purposes of this study, we defined a population of 1,000 *E. coli* cells to simulate using the default parameters for population FBA. For the reproducibility analysis (related to **Figure S2-8**), we ran population FBA for 1,000 cells and subsequently used the simulated flux data to generate cell-specific drug interaction outcome predictions a total of 30 times. To retrieve uniform sampling of the cell-specific flux solution space (related to **Figure S2-9**), we applied optGpSampler (Megchelenbrink et al., 2014) to generate 100 flux solution samples for 10 unique cells derived from a population FBA simulation. See the populationFBA.mlx file in the GitHub repository for this study (https://github.com/sriram-lab/CARAMeL) for details on the exact implementation of population FBA and optGpSampler. Of note, the flux data for all conditions (i.e., drug, media, single-cell) used to define joint profiles was generated from a single run of the condition-appropriate CBM method (i.e., iMAT, FBA, population FBA). The exact flux data that was used to generate all results is stored as a data file in the GitHub repository associated with this study (https://github.com/sriram-lab/CARAMeL).

2.6.3 Data processing to determine joint profiles

Flux profiles were used to define joint profiles for each drug combination, which were comprised of four pieces of information: sigma scores, delta scores, cumulative entropy, and treatment time interval (**Figure S2-2**). Sigma and delta scores were representative of the combined and unique effect of drugs involved in a combination, respectively. Of note, joint profiles for the original omics-based approaches were only defined by sigma and delta scores (Chandrasekaran et al., 2016; Cokol et al., 2018; Ma et al., 2019). For CARAMeL, the general procedure for determining sigma and delta scores was retained from the original literature, with the input data (flux profiles) being the only difference. Both score types were determined after flux profiles were binarized based on differential flux activity (either positive or negative) in comparison to baseline, mathematically defined below:

$$v_{i,positive} = \begin{cases} 1 \; if \; \dfrac{v_{i,treatment}}{v_{i,baseline}} > 2 \\ 0 \qquad otherwise \end{cases}, v \in \mathbb{R}^m$$

Equation 2-2 Reaction flux binarization criterium for positive differential flux activity.

$$v_{i,negative} = \begin{cases} 1 \; if \; \dfrac{v_{i,treatment}}{v_{i,baseline}} < -2 \\ 0 \qquad otherwise \end{cases}, v \in \mathbb{R}^m$$

Equation 2-3 Reaction flux binarization criterium for negative differential flux activity.

where v = reaction flux and m = total number of GEM reactions. Sigma scores were mathematically defined for both simultaneous and sequential interactions using the following equation:

$$\sigma_i = \frac{2}{n} \sum_{j=1}^{n} v_{i,j}, v \in \mathbb{R}^{m \times n}$$

Equation 2-4 Sigma score definition for joint profiles.

where σ = sigma score, v = binarized flux profile, m = total number of GEM reactions, and n = total number of conditions in a combination. Delta scores were separately defined for simultaneous and sequential interactions based on Eq. 6a and Eq. 6b, respectively:

$$\delta_{i,simultaneous} = \begin{cases} 1 \; if \; \sum_{j=1}^{n} v_{i,j} = 1 \\ 0 \quad otherwise \end{cases}, v \in \mathbb{R}^{m \times n}$$

Equation 2-5 Delta score definition for joint profiles of simultaneous drug interactions.

$$\delta_{i,sequential} = t_n v_{i,n} - \frac{2}{n} \sum_{j=1}^{n-1} t_j v_{i,j}, t \in \mathbb{R}^n, v \in \mathbb{R}^{m \times n}$$

Equation 2-6 Delta score definition for joint profiles of sequential drug interactions.

where δ = delta score, t = treatment time interval, v = binarized flux profile, m = total number of GEM reactions, and n = total number of conditions in a combination. Cumulative entropy features were determined by processing non-binarized flux profiles in two steps. First, metabolic entropy for each condition was mathematically defined by the following equation:

$$H_j = ln(\sigma_j^2)$$

Equation 2-7 Entropy feature definition for joint profiles.

where H_j = metabolic entropy due to condition j and σ_j^2 = variance in the non-binarized flux profile for condition j. Of note, this formulation was adapted from Zhu et al., who quantified entropy of the bacterial stress response to antibiotics (Z. Zhu et al., 2020). Next, the mean and sum in entropy for all conditions involved in an interaction were used to define two distinct entropy features. Finally, the time feature was defined as the time interval between the first and last treatment for a combination. For simultaneous interactions, the time feature was set to zero.

2.6.4 ML model development using random forests

All CARAMeL models were built in MATLAB (Mathworks, Inc.) using the regression-based Random Forests (RF) algorithm (Breiman, 2001). Briefly, RF is an ensemble method comprised of decision trees that learn to associate feature information to a target variable. For the regression-based approach, the RF model returns the mean prediction from all decision trees. To develop CARAMeL models, joint profiles served as feature information while drug interaction scores were used as the target variable. Interaction scores were quantified using the Loewe additivity model (Loewe & Muischnek, 1926), which is based on drug concentrations (refer to the original sources of drug interaction datasets for further details in score calculation). Both joint profiles and interactions scores for drug combinations of interest were used as model inputs during training, while only joint profiles were provided as input during model testing. Default values for all other model parameters were used during both training and testing.

2.6.5 ML model performance assessment

Model performance was evaluated based on two metrics: (1) the Spearman correlation between actual and predicted interaction scores and (2) the area under the receiver operating curve (AUROC) for classifying interactions as synergistic or antagonistic. Of note, model predictions for TB regimens used in clinical trials were negative transformed before being compared to clinical outcomes. Since these clinical trials reported percentage of patients that were cured, we would expect to see a negative correlation between interaction scores and clinical efficacy, with synergistic regimens (negative IS) performing better than antagonistic regimens. The sign for the scores were hence flipped to maintain a positive correlation indicating good model performance. Classification of simultaneous drug interactions was based on score threshold values reported in the original literature for a dataset. For both sequential interactions and the CARAMeL model

trained on all interaction data for *E. coli*, interaction scores were first scaled by the maximum absolute value (**Equation 2-8**):

$$x_{scaled} = \frac{x}{max|x|}$$

Equation 2-8 Drug interaction score scaling function.

where x = reported drug interaction score and x_{scaled} is the value used to train the *E. coli* CARAMeL model.

Scaled interaction values below -0.1 and above 0.1 were then used to classify interactions as synergistic and antagonistic, respectively. For the 10-fold cross-validation analysis conducted for sequential interactions, the interaction data was randomly partitioned into ten subsets of similar size (N ~ 63). CARAMeL was then applied to predict each subset at a time, where the given subset was left out of the model training (i.e., the remaining 90% of the data was used to train the model). All model predictions were then compared to the sequential data as a whole to calculate the overall Spearman correlation and AUROC values.

2.6.6 CARAMeL top feature extraction

Top features were determined based on their ranked importance in generating accurate predictions. To calculate feature importance, each feature was first left out of model training and testing. The mean squared error (MSE) between predicted and true interaction scores was then calculated for each model. Finally, feature importance was measured as the increase in MSE for a model lacking a feature compared to the model trained on all features. After ranking features according to decreasing importance, the first set of features amounting to a cumulative importance of 0.95 (corresponding to 95% variance explained) were selected for downstream model interpretation and analysis. To determine overall importance, we trained a CARAMeL model using all interaction data available for *E. coli*. Broadly, this included three sets of simultaneous

combinations (Chandrasekaran et al., 2016; Cokol et al., 2018) (pairwise, three-way, and media-specific treatments) and three sets of sequential interactions (Imamovic & Sommer, 2013; Oz et al., 2014; Suzuki et al., 2014) (differing based on elapsed treatment time). To account for differing units of measurement between datasets, we scaled interaction scores according to **Equation 2-8**. This scaling constrained all interaction scores to range between ±1 while retaining the sign consensus for classifying interactions based on their score (negative IS → synergy, positive IS → antagonism). In total, we trained our model on 966 drug interactions and attained highly accurate predictions ($R = 0.45$, $p < 10\text{-}16$) for both synergistic (IS < -0.1, AUROC = 0.67) and antagonistic (IS > 0.1, AUROC = 0.71) interactions based on a 10-fold cross-validation.

2.6.7 PCA and k-means clustering to determine cell sub-populations

Principal component analysis (PCA) was applied onto three datasets pertaining to single-cell results: (1) the sampled enzyme levels (352 proteins x 1,000 cells), (2) the simulated metabolic reaction fluxes (2,583 reactions x 1,000 cells), and (3) the CARAMeL predictions for simultaneous drug interactions (528 drug pairs x 1,000 cells). PCA results were then visualized onto the 2-dimensional space defined by the first two principal components (PCs) for all three PCA applications. The cell sub-populations reported in the main text were determined via k-means clustering ($k = 2$) of the PCA data for drug interactions. The silhouette value (i.e., measure for evaluating cluster assignment) for each cell was subsequently calculated to determine the presence of any "outlier" cells (i.e., cluster-3, silhouette value < 0.5).

2.6.8 Statistical analysis

A one-way analysis of variance (ANOVA) test was used to compare both the entropy mean and entropy sum of drug interactions grouped by their classification (synergy, neutral,

antagonism). A multiple comparison test based on Tukey's honestly significant difference (HSD) was subsequently performed to identify statistically significant pairwise differences using a p-value threshold of 0.05. A two-sample Student's t-test with unequal variance was used to define which reactions distinguished between synergistic and antagonistic interactions based on differential flux activity. Lastly, a hypergeometric test was conducted to determine significantly enriched metabolic pathways based on GEM reactions associated with top CARAMeL predictors. For this test, the total number of reactions annotated in iJO1366 corresponded with the population size. Of note, the p-values determined from t-tests and hypergeometric tests were adjusted using the Benjamini-Hochberg approach (Benjamini & Hochberg, 1995).

2.7 Supplementary Materials

2.7.1 Figures

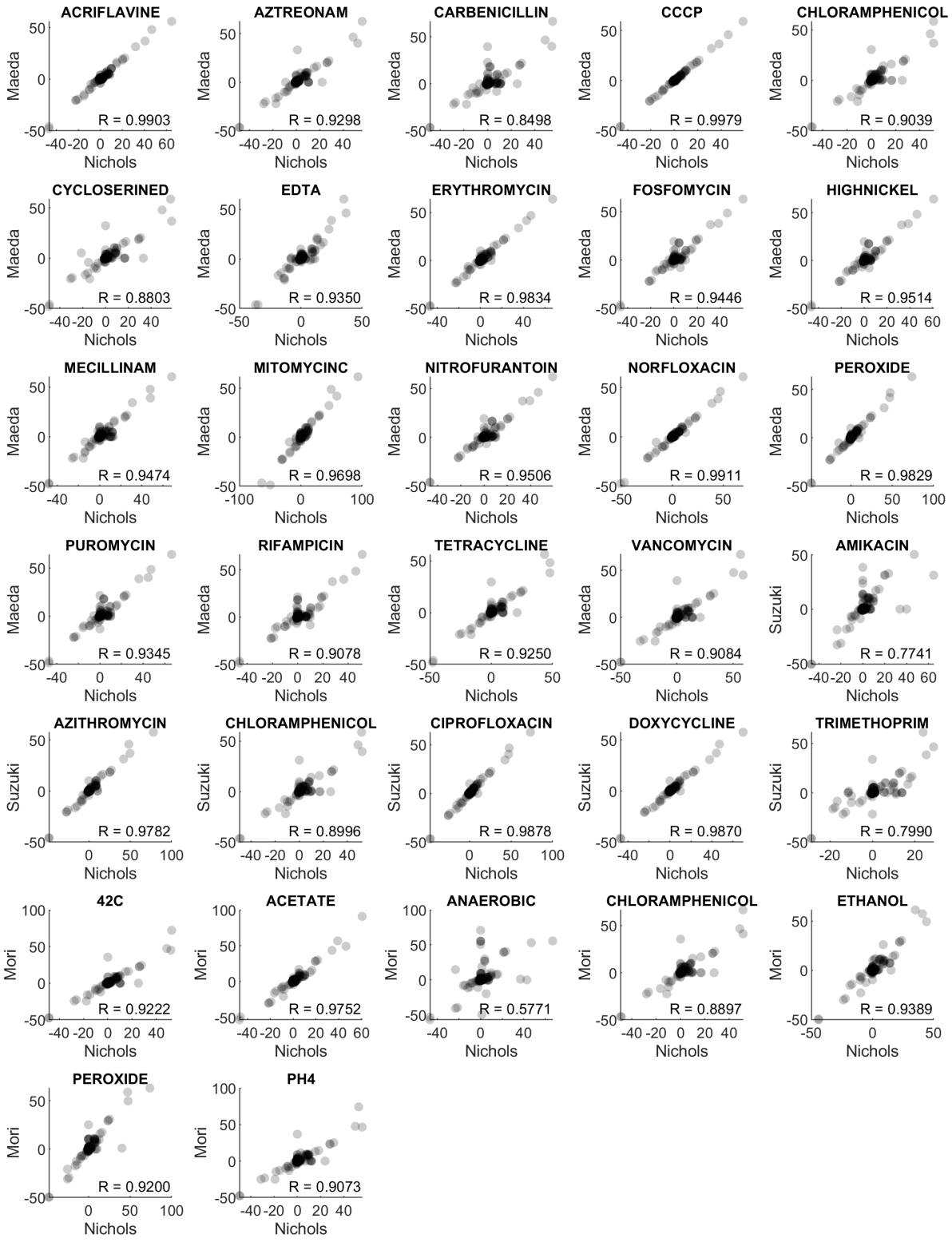

Figure S2-1 Flux profile comparison between different omic-based simulations. Correlations based on Pearson's method (all yielded $p << 10^{-3}$). All plots possess the same number of points (i.e., reactions, N = 2,583). Nichols: chemogenomic-based (Nichols et al., 2011), Maeda: transcriptomic-based (Maeda et al., 2020), Suzuki: transcriptomic-based (Suzuki et al., 2014), Mori: proteomic-based (Mori et al., 2021).

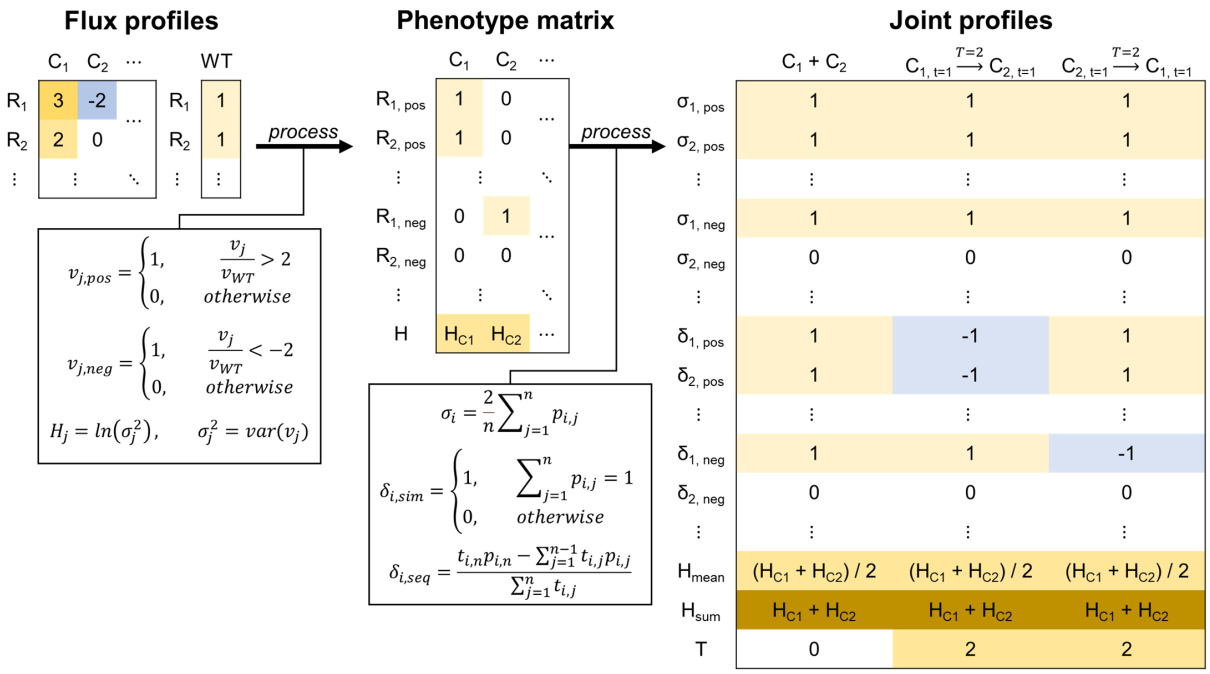

Figure S2-2 Schematic of flux data processing into joint profiles. Flux data (v) simulated from genome-scale metabolic models is binarized according to differential flux (either positive or negative) in comparison to wild type (WT, i.e., reference). These binarized flux profiles, along with the entropy (H) calculated for each condition (C), define the phenotype matrix which is subsequently processed into joint profiles. The sigma (σ) definition is the same between simultaneous (sim) and sequential (seq) interactions, while the delta (δ) definition differs depending on the interaction type. R = reaction, T = time interval, n = number of conditions in a combination.

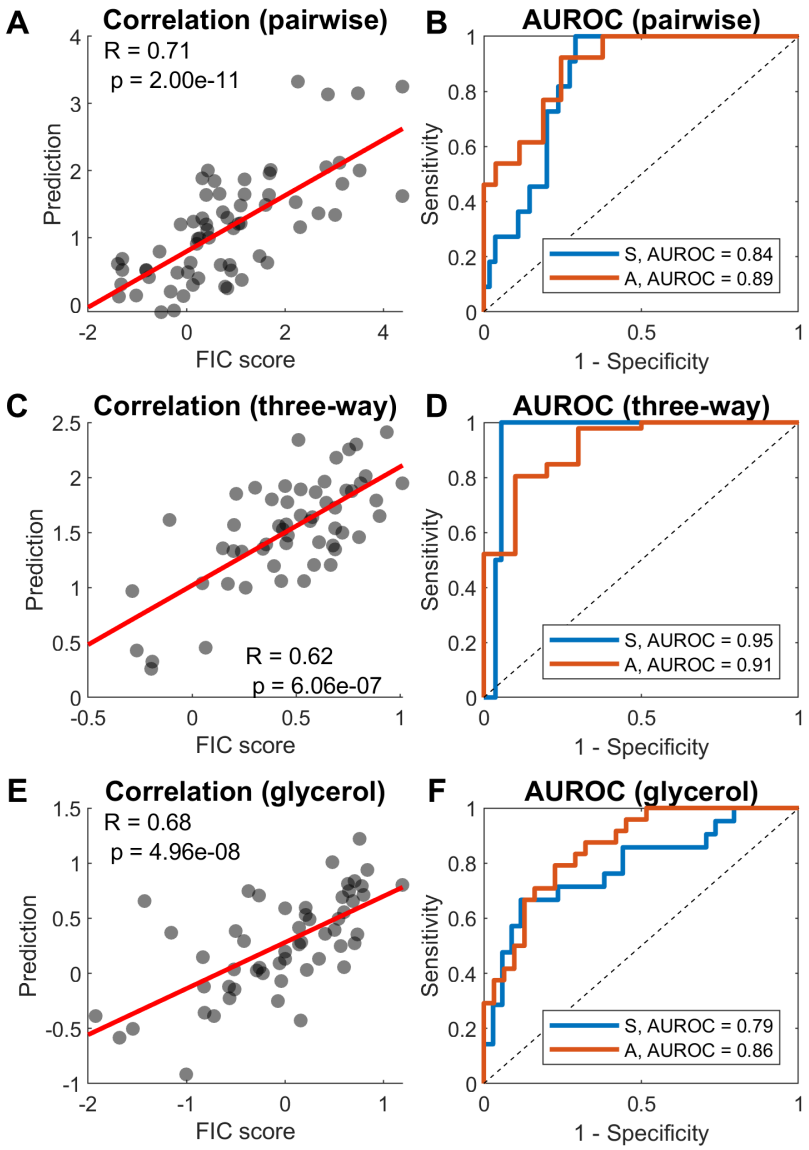

Figure S2-3 CARAMeL results for *E. coli* drug interaction data. Model performance results visualized as scatter and receiver operating curve (ROC) plots are shown for predicting (**A-B**) pairwise interactions, (**C-D**) three-way interactions, and (**E-F**) pairwise interactions in M9 glycerol. AUROC: area under the receiver operating curve. FIC: fractional inhibitory concentration, S: synergy, A: antagonism.

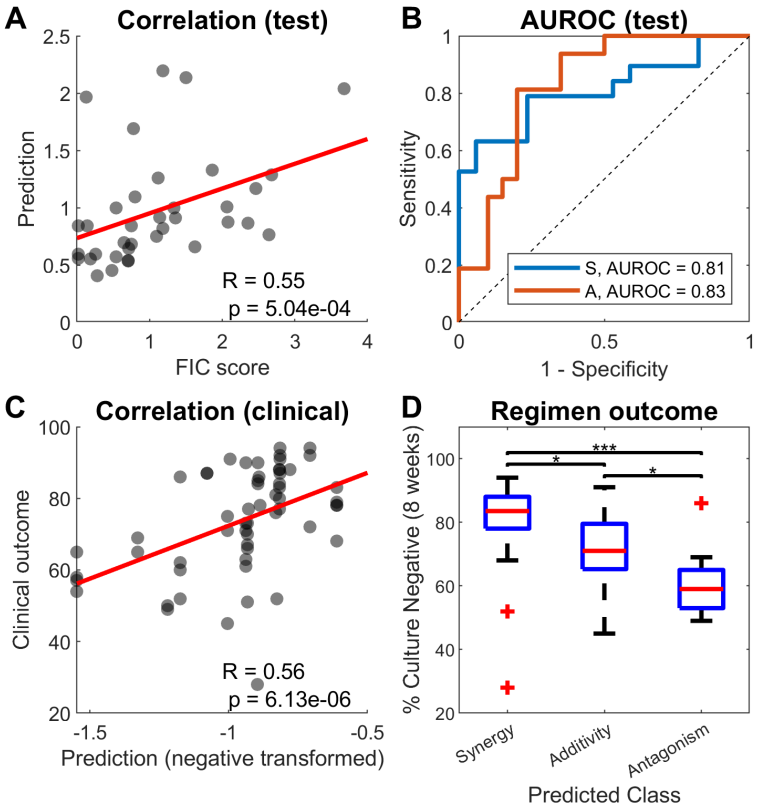

Figure S2-4 CARAMeL results for *M. tb* drug interaction data. (**A-B**) Model performance results visualized as scatter and receiver operating curve (ROC) plots are shown for predicting multi-drug interactions measured experimentally. (**C**) The model predictions for 57 TB regimens prescribed in clinical trials correlate with clinical efficacy. (**D**) Predictions classified as synergistic capture most of the efficacious treatments (sputum clearance > 80%). AUROC: area under the receiver operating curve, ** p-value < 0.01, *** p-value < 0.001 (unpaired t-test). FIC: fractional inhibitory concentration, AUROC: area under the receiver operating curve, S: synergy, A: antagonism.

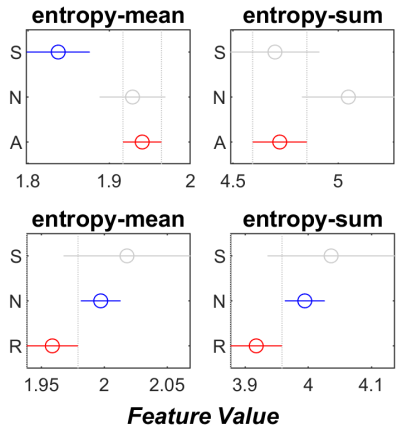

Figure S2-5 Metabolic entropy is predictive of combination therapy outcomes. The mean metabolic entropy induced by a drug combination is significantly lower for synergistic (S) interactions than antagonistic (A) interactions), while cross-resistant (R) interactions seem to induce lower metabolic entropy overall. Each line with a circle represents the 95% confidence interval of the entropy score for a particular group. Color difference indicates significant differences between intervals (ANOVA, p < 0.05).

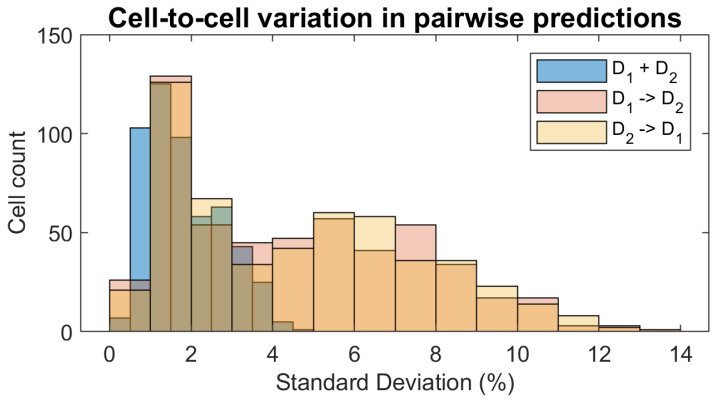

Figure S2-6 Cell-to-cell variation in pairwise drug interaction predictions. The cell-to-cell variation (represented as the percent change in standard deviation) in drug pair predictions is shown for three interaction cases: $D_1 + D_2$, $D_1 \rightarrow D_2$, $D_2 \rightarrow D_1$.

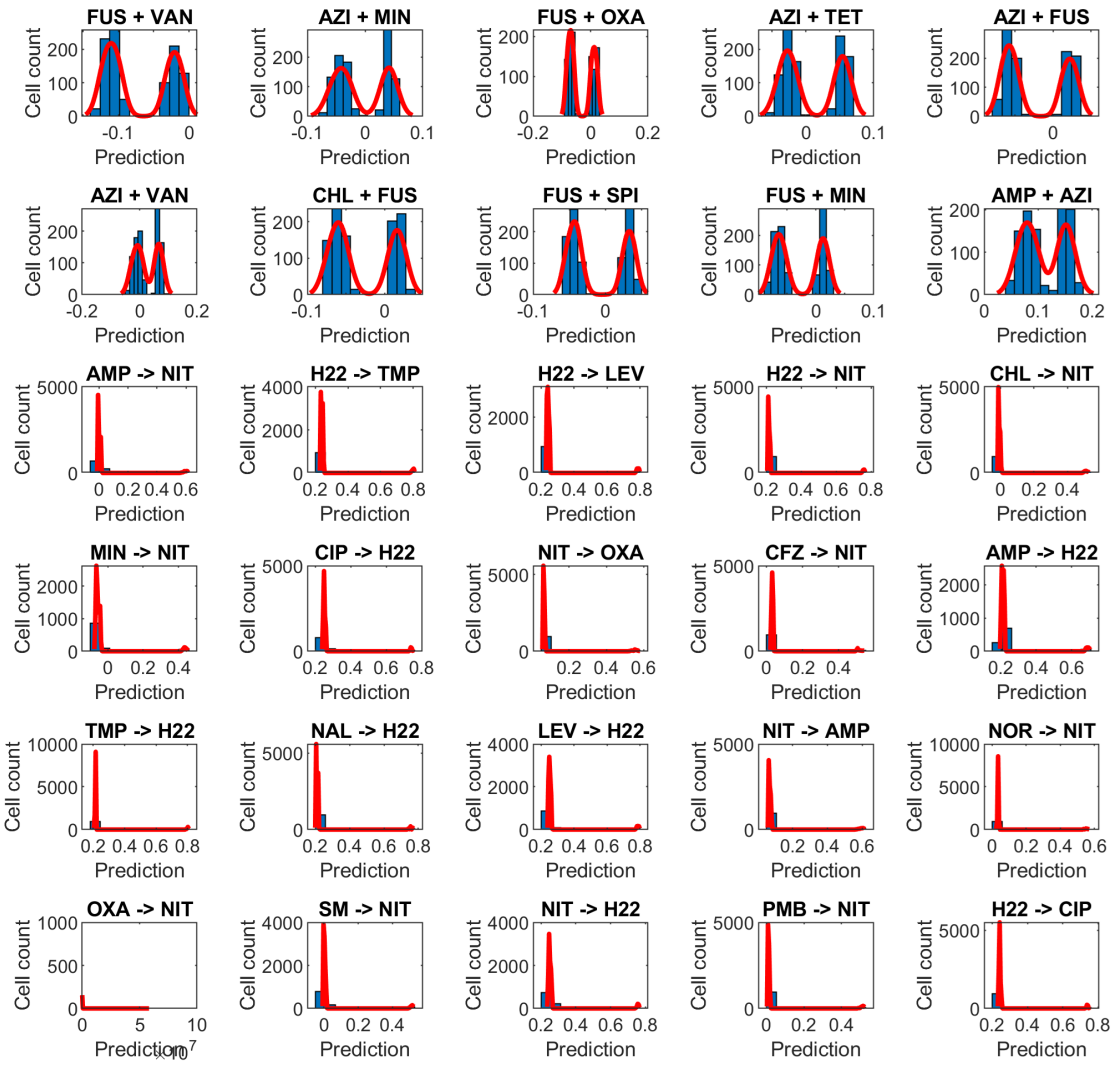

Figure S2-7 Distribution of cell-specific outcome predictions for select drug interactions. The distribution for the top ten drug interactions with the largest variation across cells are shown for all time cases ($D_1 + D_2$, $D_1 \rightarrow D_2$, $D_2 \rightarrow D_1$). Refer to **Table S2-2** and **Table S2-4** for full descriptions on antibiotics used for *E. coli*.

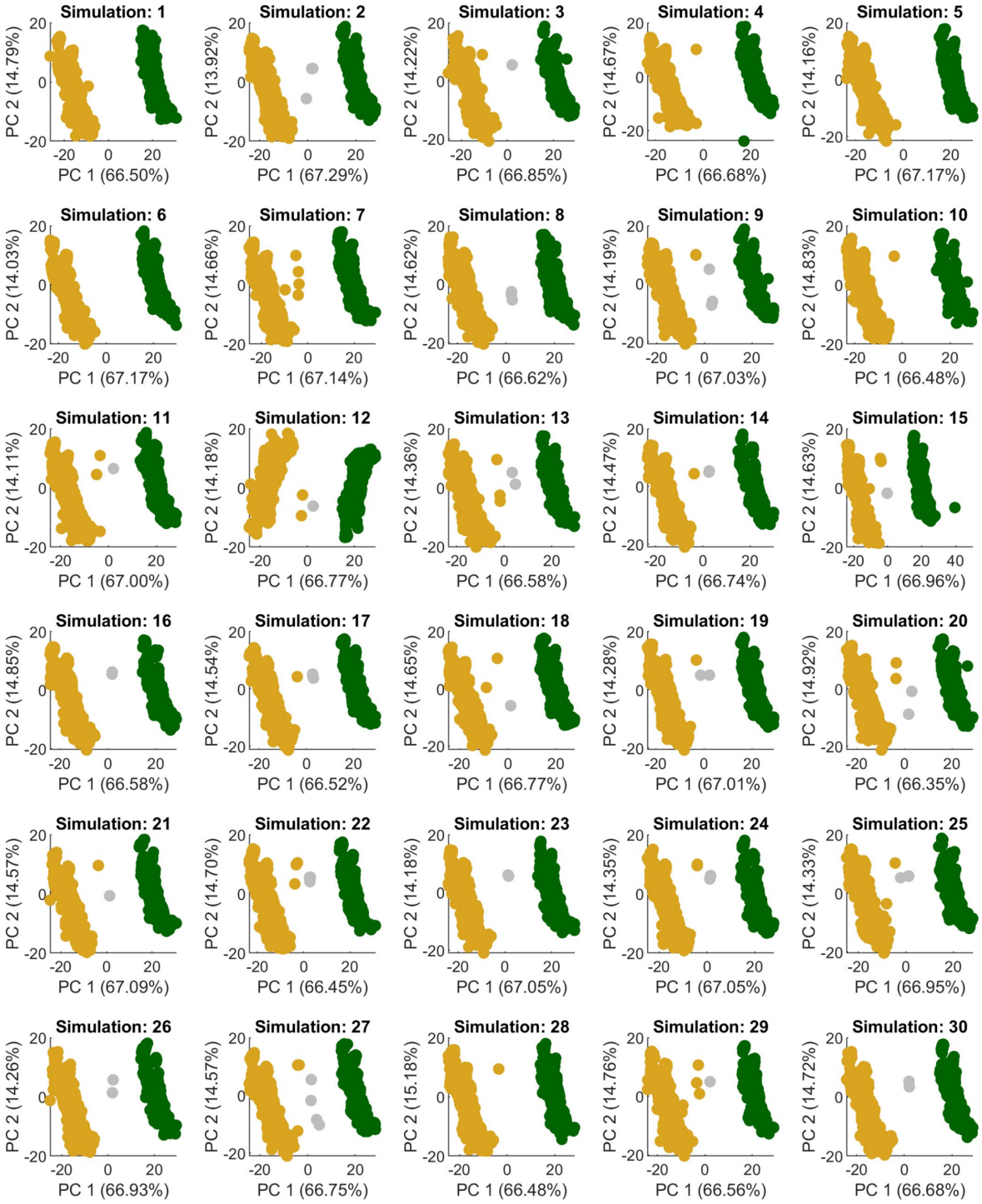

Figure S2-8 Cell clustering based on drug interaction data is reproducible. Repeated simulation (N = 30) of cell-specific fluxes (via population FBA) followed by CARAMeL prediction of cell-specific drug interaction outcomes reproducibly shows bimodal distribution of simultaneous prediction data, as seen in the 2-dimensional visualization of cell placement along the principal component (PC) space.

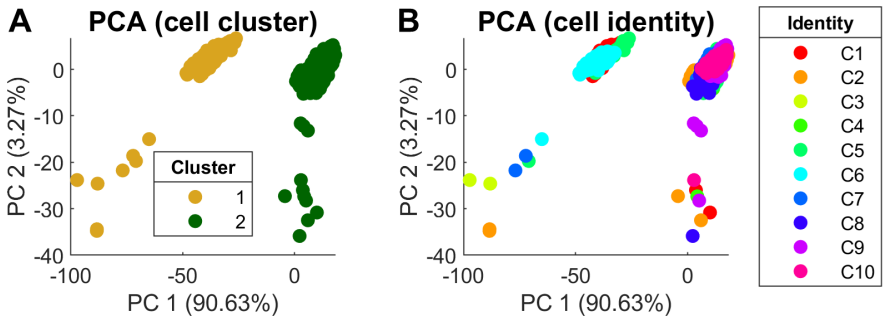

Figure S2-9 Cell clustering is not driven by non-uniform sampling of the flux solution space. Cell-specific drug interaction outcomes were repeatedly determined for a given cell based on uniform sampling of the flux solution space via optGpSampler. (**A**) The principal component analysis (PCA) visualization of the prediction data for simultaneous drug interactions shows similar clustering patterns as seen in Figs. 5B and S8. (**B**) The same PCA visualization grouped by cell identity shows that predictions belonging to the same original cell identity cluster together (except for a few outliers).

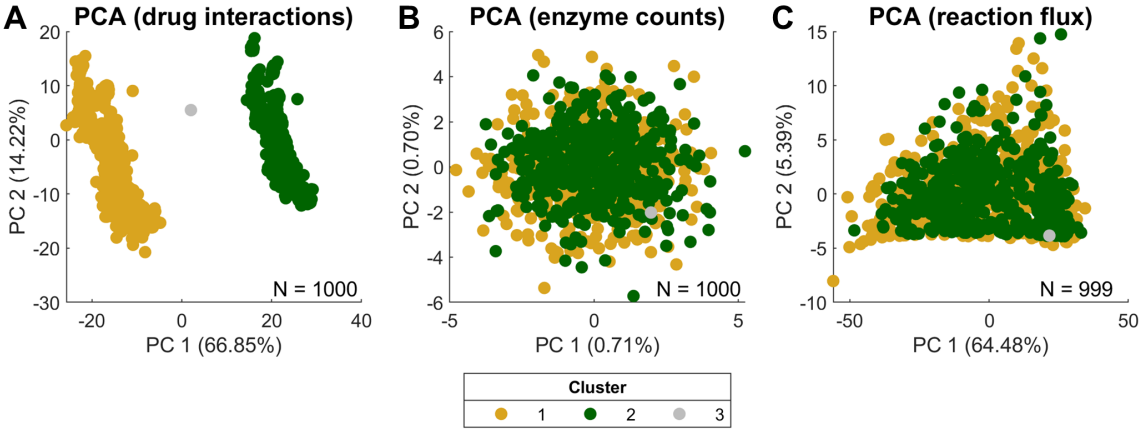

Figure S2-10 Distinct cell clustering only occurs in CARAMeL prediction data for cell-specific drug interaction outcomes. Cell clustering was investigated by applying principal component analysis (PCA) for cell-specific (**A**) drug interaction prediction data, (**B**) sampled enzyme count data, and (**C**) simulated metabolic flux data. The cluster groups shown in the legend were defined via k-means clustering of the PCA-transformed data for drug interactions. Of note, panel A is the same image shown in **Figure 2-5B** in the main text. Additionally, panel C only shows the placement of 999 cells in PCA space due to removal of one outlier point.

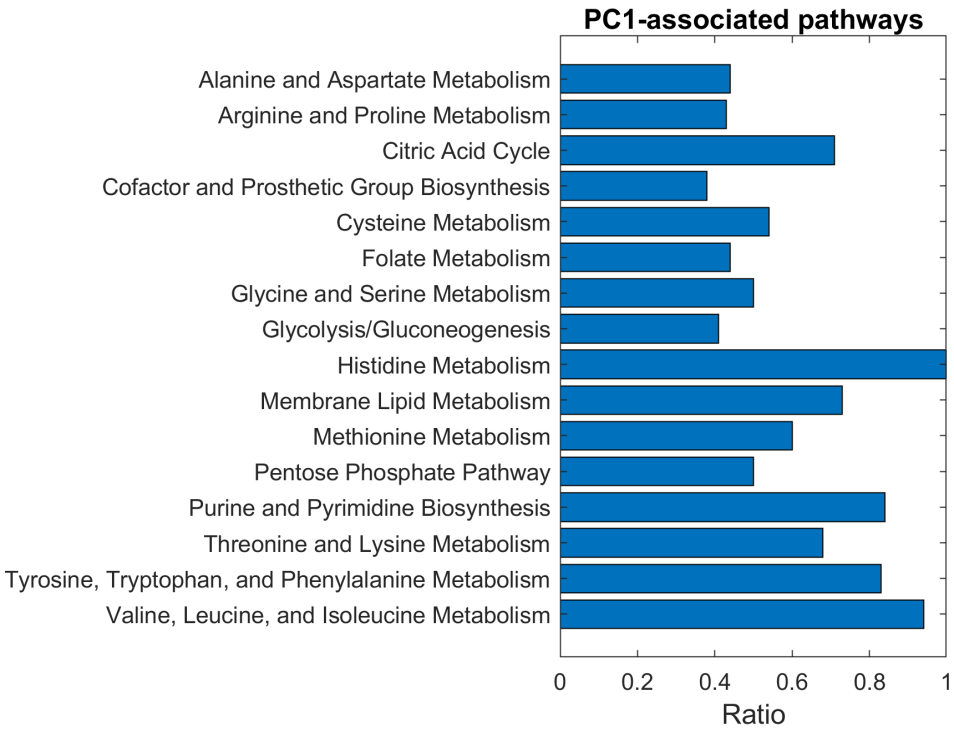

Figure S2-11 16 metabolic pathways are significantly associated with cell clustering. Over 400 metabolic reactions were found to robustly correlate in a significant manner with cell-specific scores along principal component 1 (PC1) shown in **Figure 2-5B** (**Dataset 2-7**). A total of 16 pathways were subsequently found to be enriched by this set of reactions (hypergeometric test, adjusted p-value < 0.05).

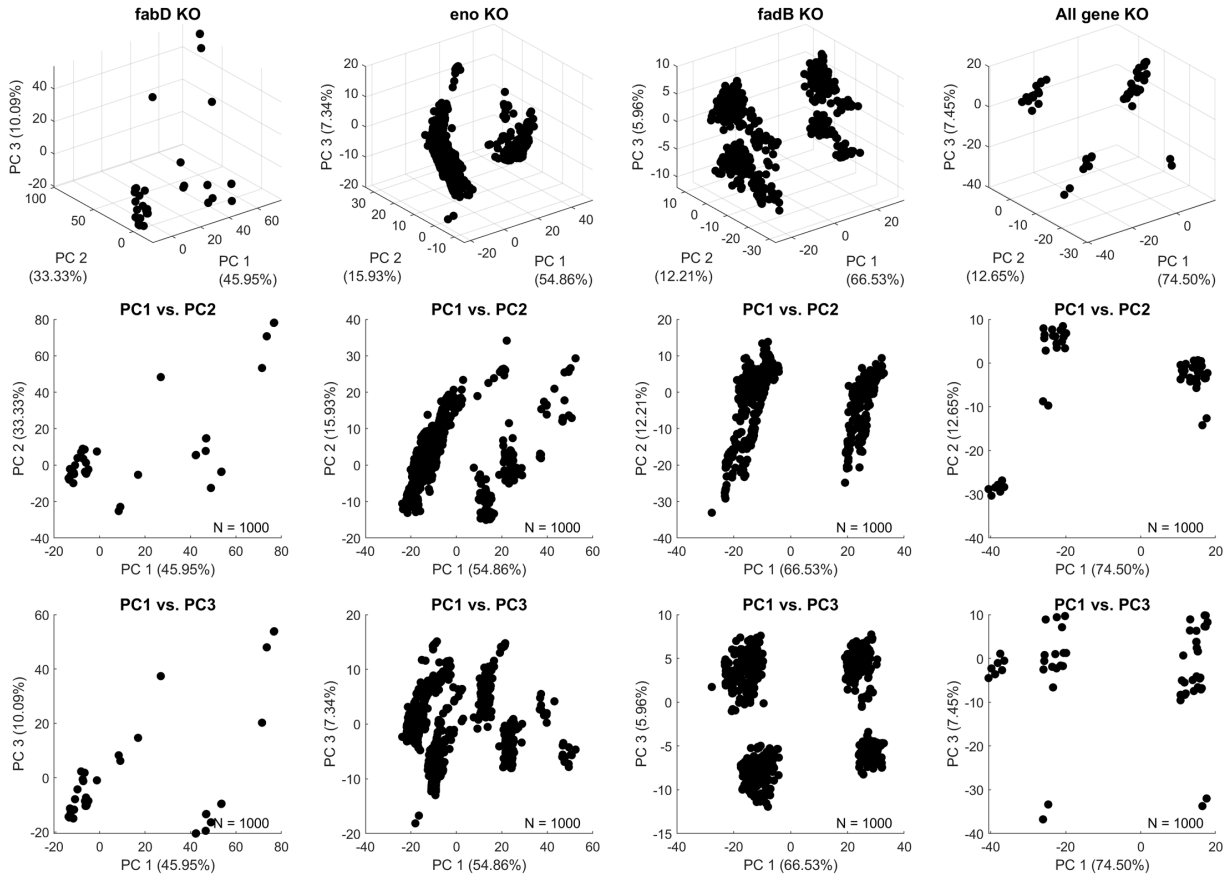

Figure S2-12 Cell clustering is driven by stochastic changes in eno and fabD levels. Single- and multi-gene knockout (KO) simulations for eno, fadB, and fabD reveal that the clustering pattern seen in Fig. 5B cannot be replicated in the absence of eno and fabD.

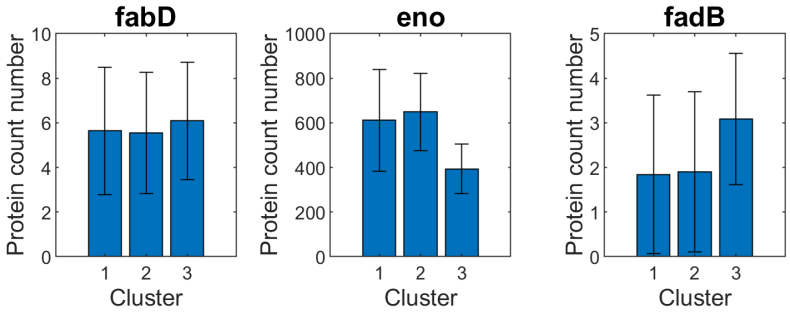

Figure S2-13 Cluster-3 cells are characterized by low eno levels. Cluster-3 cells, or those that do not cluster together with the dominant cell sub-populations seen in Fig. 5B, were found to possess much lower levels of eno (~400 per cell) compared to cluster-1 and cluster-2 cells (~600 per cell).

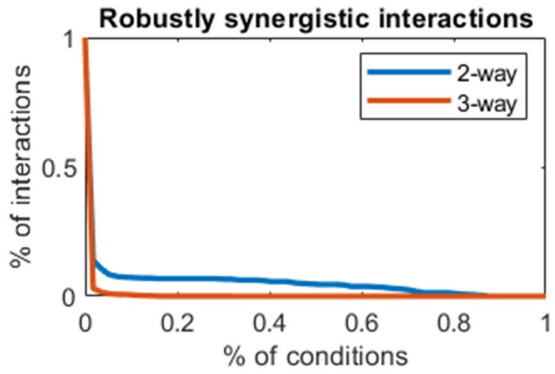

Figure S2-14 Distribution of cell-specific drug interaction predictions. The distribution for the top ten drug interactions with the largest variation across cells are shown for all time cases ($D_1 + D_2$, $D_1 \rightarrow D_2$, $D_2 \rightarrow D_1$). Refer to **Table S2-2** and **Table S2-4** for full descriptions on antibiotics used for *E. coli*.

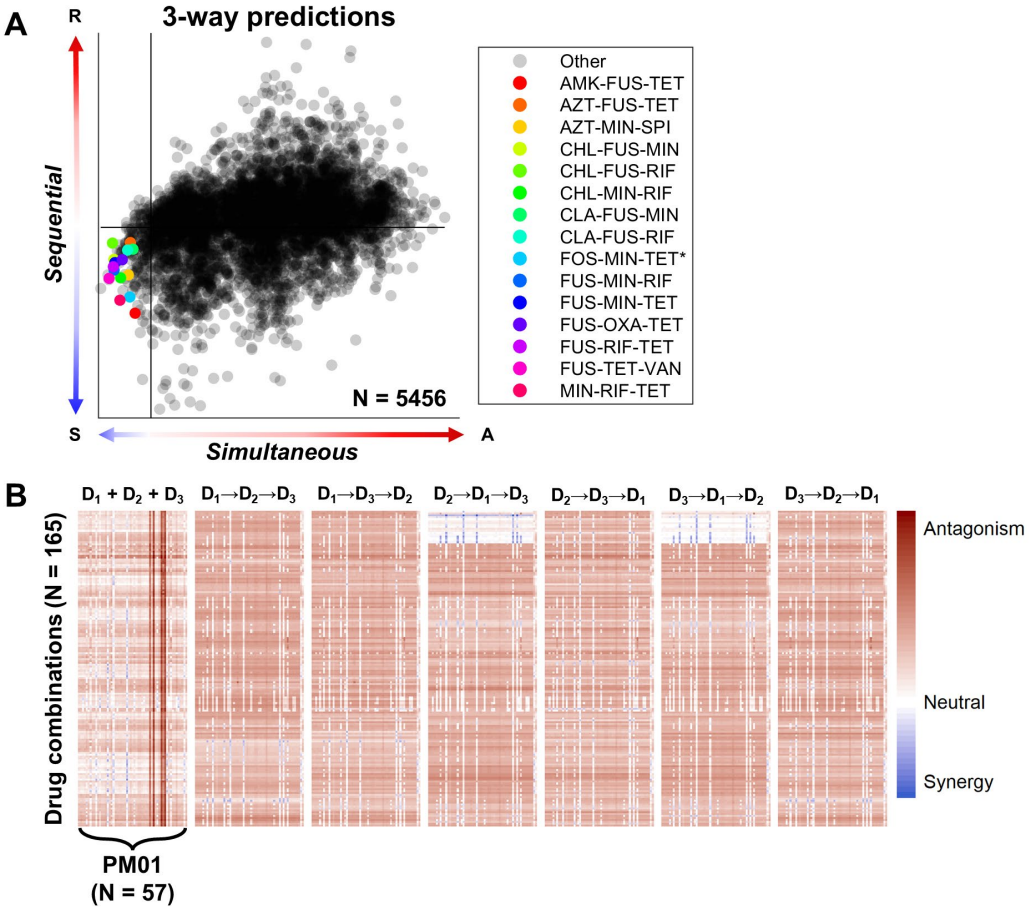

Figure S2-15 CARAMeL predictions for three-way combination therapy landscape. (**A**) Out of 5,456 unique three-way drug interactions, 165 were predicted to yield synergy (IS < 0) in at least one media condition for both the simultaneous and sequential cases (the top 15 robustly synergistic drug combinations are listed in the legend). (**B**) Heatmap of the predicted interaction scores for the 165 drug combinations across 57 media conditions and seven interaction types. Refer to **Table S2-2** and **Table S2-4** for full descriptions on antibiotics used for *E. coli*.

2.7.2 Tables

Table S2-1 Omics-based approach evaluation for different z-score thresholds. ***** Chosen parameters for *E. coli* and *M. tb*. R1: pairwise interactions (Chandrasekaran et al., 2016), R2: three-way interactions (Cokol et al., 2018), R3: glycerol interactions (Cokol et al., 2018), R4: pairwise and three-way interactions (Ma et al., 2019), R5: pairwise to five-way TB clinical regimens (Bonnett et al., 2017).

	Z-score	***E. coli* results**			***M. tb results***	
		R1	*R2*	*R3*	*R4*	*R5*
	0.25	0.1728	0.4548	0.5101	0.5604	0.4518
	0.50	0.3158	-0.0494	0.4004	0.5510	0.4870
	0.75	0.2558	0.4535	0.6616	0.5283	0.3555
	1.00	0.2780	0.3724	0.6781	0.5372	0.4802
	1.25	0.3541	0.4384	0.6566	0.5637	0.4102
	1.50	0.4269	0.5369	0.6501	0.5929	0.3889
	1.75	0.3494	0.3891	0.6460	0.5234	0.4580
*	2.00	0.6508	0.5201	0.7068	0.5537	0.4737
	2.25	0.4125	0.4671	0.6602	0.4489	0.4653
	2.50	0.3665	0.4159	0.6432	0.4064	0.3937
	2.75	0.3741	0.4621	0.6284	0.4139	0.4856
	3.00	0.4194	0.3473	0.6177	0.4969	0.5344

Table S2-2 List of antibiotics used in *E. coli* drug interaction datasets. Abb.: abbreviation.

				Dataset					
Compound	**Abb.**	**Target**	**Class**	**Pair (train)**	**Pair (test)**	**Three-way**	**LB**	**Glucose**	**Glycerol**
Amikacin	AMK	Protein synthesis, 30S	Aminoglycoside	✓	✓				✓
Gentamicin	GEN			✓	✓				
Spectinomycin	SPE				✓		✓	✓	✓
Tobramycin	TOB			✓	✓				
Minocycline	MIN		Tetracycline			✓			
Tetracycline	TET			✓	✓		✓	✓	✓
Azithromycin	AZI	Protein synthesis, 50S	Macrolide			✓	✓	✓	✓
Chlarythromycin	CLA			✓	✓				
Erythromycin	ERY			✓	✓				
Chloramphenicol	CHL		Phenylpropanoid	✓	✓	✓	✓	✓	✓
Ciprofloxacin	CIP	DNA gyrase	Quinolone	✓	✓	✓			
Levofloxacin	LEV			✓	✓				
Nalidixic acid	NAL			✓	✓	✓			✓
Ampicillin	AMP	Cell wall	Beta-lactam			✓	✓	✓	✓
Aztreonam	AZT						✓	✓	✓
Cefoxitin	CEF			✓	✓				✓
Oxacillin	OXA			✓	✓				
Vancomycin	VAN		Glycopeptide		✓				
Fusidic acid	FUS	Elongation factor	Fusidane		✓				
Trimethoprim	TMP	Folic acid biosynthesis	Pyrimidine	✓	✓				
Rifampicin	RIF	RNA synthesis	Rifampin		✓	✓	✓	✓	✓
Nitrofurantoin	NIT	Multiple mechanisms	Furan	✓	✓	✓			
Triclosan	TRI		Phenol				✓	✓	✓
Hydrogen peroxide	H22	Oxidative stress	Stress	✓	✓				

Table S2-3 List of antibiotics used in *M. tb* drug interaction datasets. Abb.: abbreviation, PTM: post-translational modification. * Putative mechanism.

				Dataset		
Compound	**Abb.**	**Target**	**Class**	**Train**	**Test**	**Clinical**
Sutezolid	SUTx	Protein synthesis, 23S	Oxazolidinone	✓		
Amikacin	AMK	Protein synthesis, 30S	Aminoglycoside	✓		
Kanamycin	KAN			✓		
Spectinomycin	SPE			✓	✓	
Streptomycin	SM			✓	✓	✓
Minocycline	MIN		Tetracycline	✓		
Tetracycline	TET			✓		
Azithromycin	AZI	Protein synthesis, 50S	Macrolide	✓		
Chlarythromycin	CLA			✓	✓	
Erythromycin	ERY			✓		
Roxithromycin	ROX			✓		
Linezolid	LZDx		Oxazolidinone	✓		
Chloramphenicol	CHL		Phenylpropanoid	✓		
Ciprofloxacin	CIP	DNA gyrase	Quinolone	✓	✓	
Levofloxacin	LEV			✓	✓	
Moxifloxacin	MOX			✓	✓	✓
Norfloxacin	NFX				✓	
Ofloxacin	OFX1			✓		✓
Novobiocin	NOV		Glycoside	✓		
Ampicillin	AMP	Cell wall	Beta-lactam	✓		
Oxacillin	OXA			✓		
Vancomycin	VAN		Glycopeptide	✓		
Cefaclor	CFL		Cephalosporin	✓		
SQ109	SQ109		Ethylenediamine	✓		
Isoniazid*	INH		Hydrazine	✓	✓	✓
Econazole	ECO		Imidazole	✓		
Pretomanid	PA824			✓		✓
Ethionamide*	ETH		Isonicotinic acid	✓		
Cycloserine D	CSD		Serine	✓		
PBTZ169	PBTZ169x		Thiazine	✓		
Capreomycin	CAP	Multiple mechanisms	Peptide	✓	✓	
Clofazimine*	CFZ		Phenazine	✓	✓	
Fusidic acid	FUS	Elongation factor	Fusidane	✓		
Ethambutol	EMBx	RNA synthesis	Ethylenediamine	✓		✓
Rifampicin	RIF		Rifampin	✓	✓	✓
Rifapentine	RIFP		Rifamycin			✓
Bedaquiline	BDQ	ATP synthase	Diarylquinoline	✓	✓	
Ethium bromide	EB	DNA structure	Phenanthridine	✓		

Pyrazinamide*	PZA	Fatty acid synthase	Pyrazine			✓
Menadione	MEN	PTM	Vitamin	✓		
Verapamil	VERx	Calcium channels	Phenethylamine	✓		
Thioridazine	THZ	Synaptic activity	Phenothiazine	✓		
Chlorpromazine	CPZ			✓	✓	

Table S2-4 List of antibiotics used in sequential drug interaction datasets for *E. coli*. Abb.: abbreviation.

				Time scale		
Compound	**Abb.**	**Target**	**Class**	*T = 10*	*T = 21*	*T = 90*
Amikacin	AMK	Protein synthesis, 30S	Aminoglycoside	✓	✓	✓
Gentamicin	GEN			✓		✓
Spectinomycin	SPE				✓	
Streptomycin	SM			✓	✓	✓
Tobramycin	TOB				✓	
Doxycycline	DOX		Tetracycline		✓	✓
Minocycline	MIN			✓		✓
Tetracycline	TET			✓	✓	✓
Azithromycin	AZI	Protein synthesis, 50S	Macrolide	✓		✓
Erythromycin	ERY				✓	
Spiramycin	SPI				✓	
Chloramphenicol	CHL		Phenylpropanoid	✓	✓	✓
Ciprofloxacin	CIP	DNA gyrase	Quinolone	✓	✓	✓
Levofloxacin	LEV			✓		✓
Nalidixic acid	NAL			✓	✓	✓
Norfloxacin	NOR					✓
Ampicillin	AMP	Cell wall	Beta-lactam	✓	✓	
Cefoxitin	CEF				✓	
Ceftazidime	CFZ					✓
Amoxicillin	AMX			✓		
Sulfamonomethoxine	SMM	Folic acid biosynthesis	Sulfonamide		✓	
Trimethoprim	TMP		Pyrimidine	✓	✓	✓
Nitrofurantoin	NIT	Multiple mechanisms	Furan	✓	✓	
Fosfomycin	FOS	Cell wall biogenesis	Phosphonic acid	✓		
Fusidic acid	FUS	Elongation factor	Fusidane		✓	
Polymyxin B	PMB	Lipopolysaccharide	Peptide	✓		
Rifampicin	RIF	RNA synthesis	Rifampin	✓		✓

Table S2-5 Drug information for Biolog experiment. Abb.: abbreviation, Conc.: drug concentration.

					Conc. (µg/mL)	
Compound	**Abb.**	**Target**	**Class**	**Type**	*Single*	*Pairwise*
Aztreonam	AZT	Cell wall	Beta-lactam	Bactericidal	0.03	-
Cefoxitin	CEF			Bactericidal	1.87	1.87
Tetracycline	TET	Protein synthesis, 30S	Tetracycline	Bacteriostatic	1.42	1.42
Tobramycin	TOB		Aminoglycoside	Bactericidal	0.15	0.15

Table S2-6 Constraint-based modeling (CBM) parameter optimization results. ***** Chosen parameters for *M. tb*, **+** chosen parameters for *E. coli*. CV-R: 10-fold cross-validation correlation in the training dataset, GR-V: variance in growth rate, NG-P: percentage of no growth (GR = 0) conditions.

	CBM parameters			***E. coli* results**			***M. tb* results**		
	Kappa	*Rho*	*Epsilon*	*CV-R*	*GR-V*	*NG-P*	*CV-R*	*GR-V*	*NG-P*
	0.001	0.001	0.001	0.4055	0	0	0.3640	0	0
	0.01	0.01	0.001	0.3260	0.0074	0	0.5024	0.0003	0.0233
	0.1	0.1	0.001	0.4077	0.0634	0	0.4858	0.0005	0.0698
	1	1	0.001	0.4313	0.2022	0.3636	0.4409	0.0005	0.0698
	0.001	0.001	0.01	0.4260	0	0	0.4124	0	0
*	**0.01**	**0.01**	**0.01**	0.3739	0.0091	0	0.5207	0.0003	0.1395
	0.1	0.1	0.01	0.389	0.0670	0	0.5149	0.0004	0.6977
	1	1	0.01	0.4189	0.1866	0.4848	0.5242	0.0003	0.7674
	0.001	0.001	0.1	0.6406	0	0	0.5231	0	0
	0.01	0.01	0.1	0.4090	0.0095	0	0.4959	0.0001	0.5581
	0.1	0.1	0.1	0.3978	0.1056	0.0606	0.4792	0.0001	0.7907
	1	1	0.1	0.3869	0.1294	0.5152	0.4471	0.0001	0.8837
	0.001	0.001	1	0.3860	0	0	0.4620	0	0
+	**0.01**	**0.01**	**1**	0.6512	0.0113	0	0.5131	0.0003	0.6047
	0.1	0.1	1	0.6150	0.0994	0.0909	0.5270	0	0.8140
	1	1	1	0.6294	0.0765	0.5758	0.5099	0	0.9070

Table S2-7 Benchmarking correlation results based on different constraint-based modeling (CBM) parameter choices. ***** Chosen parameters for *M. tb*, **+** chosen parameters for *E. coli*. R1: pairwise interactions (Chandrasekaran et al., 2016), R2: three-way interactions (Cokol et al., 2018), R3: glycerol interactions (Cokol et al., 2018), R4: pairwise and three-way interactions (Ma et al., 2019), R5: pairwise to five-way TB clinical regimens (Bonnett et al., 2017).

	CBM parameters			***E. coli* results**			***M. tb results***	
	Kappa	*Rho*	*Epsilon*	*R1*	*R2*	*R3*	*R4*	*R5*
	0.001	0.001	0.001	0.2884	0.4441	0.5781	0.6370	0.5535
	0.01	0.01	0.001	0.5032	0.3516	0.5092	0.5873	0.4369
	0.1	0.1	0.001	0.4676	0.3666	0.5715	0.4946	0.2304
	1	1	0.001	0.5115	0.4001	0.5421	0.4717	0.4135
	0.001	0.001	0.01	0.3726	0.3636	0.5544	0.4638	0.5361
*	**0.01**	**0.01**	**0.01**	0.4525	0.2447	0.5900	0.5256	0.5445
	0.1	0.1	0.01	0.5390	0.2599	0.5514	0.4858	0.2642
	1	1	0.01	0.3899	0.3460	0.5915	0.4730	0.4124
	0.001	0.001	0.1	0.5421	0.5809	0.5669	0.5382	0.4483
	0.01	0.01	0.1	0.5829	0.5023	0.6281	0.6335	0.4263
	0.1	0.1	0.1	0.3313	0.3762	0.6382	0.5942	0.5140
	1	1	0.1	0.1545	0.4375	0.6745	0.5560	0.4982
	0.001	0.001	1	0.1772	0.1372	0.2668	0.3253	0.5380
+	**0.01**	**0.01**	**1**	0.6445	0.6216	0.6641	0.4884	0.4870
	0.1	0.1	1	0.6057	0.6536	0.6650	0.4947	0.4788
	1	1	1	0.6352	0.6169	0.6101	0.4939	0.3726

2.7.3 Datasets

All supplementary data files from this chapter are available in the online version of the CARAMeL publication: https://doi.org/10.1093/pnasnexus/pgac132

Dataset 2-1 Top CARAMeL features explaining 95% of the variance in model predictions.

Dataset 2-2 iJO1366 reactions explaining 95% of the variance between actual and predicted interaction outcomes.

Dataset 2-3 Biolog phenotype microarray 1 (PM01) conditions.

Dataset 2-4 CARAMeL predictions for 2-way drug interactions for 1,000 individual cells and three treatment strategies (1 x simultaneous, 2 x sequential) (N = 1,584,000).

Dataset 2-5 Cell-to-cell variation in predictions for pairwise drug interaction outcomes (N = 528).

Dataset 2-6 Principal component (PC) loadings 1 and 2 for the principal component analysis (PCA) transformation of the drug interaction prediction data (simultaneous only).

Dataset 2-7 iJO1366 reactions that are robustly* associated with cell clustering. *Significant correlation with PC1 scores determined for all 30 replicated runs

Dataset 2-8 Cluster-based sensitivity and tolerance indication for the 528 unique drug pairs.

Dataset 2-9 CARAMeL predictions for 2-way drug interactions in 57 media conditions and three treatment strategies (1 x simultaneous, 2 x sequential) (N = 90,288).

Dataset 2-10 CARAMeL predictions for 2-way drug interactions in 57 media conditions and seven treatment strategies (1 x simultaneous, 6 x sequential) (N = 2,176,944).

Chapter 3 Microbial Crowdsourcing and Transfer Learning Model Predicts Strain-specific Drug Interactions

The material in this chapter was adapted from the following manuscript with minor adjustments:

Chang, D. C.*, **Chung, C. H.***, Rhoads, N. M., & Chandrasekaran, S. Microbial crowdsourcing and transfer learning model predicts strain-specific drug interactions. *In preparation*. * These authors contributed equally to this work

3.1 Abstract

Machine learning (ML) algorithms are necessary to efficiently identify potent drug combinations within a large candidate space to combat drug resistance. However, existing ML approaches cannot be applied to emerging and under-studied pathogens with limited training data. To address this, we developed a transfer learning and crowdsourcing framework (TACTIC) to train ML models on data from multiple bacteria. TACTIC was built using 2,965 drug interactions from 12 bacterial strains and generally outperformed traditional single-species ML models in predicting cross-species drug interaction outcomes. Upon evaluating the top gene-associated predictors for a TACTIC model trained on all 2,965 drug interactions, we uncovered that cross-species and species-specific drug interaction outcomes may be driven by metabolic and genetic drivers, respectively. Using the same TACTIC model, we identified small sets of drug interactions (N < 100) out of ~4,000 possible combinations that are predicted to be selectively synergistic against multiple groups of pathogenic bacteria including Gram-negative (e.g., *Acinetobacter baumannii*), Gram-positive (e.g., *Staphylococcus aureus*), and non-tuberculous mycobacteria (NTM) species.

Our implementation of TACTIC demonstrates how data from model organisms coupled with computational methods can be leveraged for drug discovery in context of less-studied organisms.

3.2 Introduction

Antibiotic resistance is becoming a global health crisis as growing resistance outpaces current antibiotic drug development. In the United States alone, more than 2.8 million antibiotic-resistant infections occur each year, with more than 35,000 cases resulting in death (Centers for Disease Control and Prevention, 2019). These infections are caused by a diverse set of bacterial pathogens that pose major health threats, especially if left unchecked. Some of the most concerning species include carbapenem-resistant *Acinetobacter baumannii*, multidrug-resistant *Pseudomonas aeruginosa*, and extremely drug-resistant *Mycobacterium tuberculosis* (henceforth *M. tb*) (Centers for Disease Control and Prevention, 2019; World Health Organization, 2014). At the same time, no new classes of antibiotics have been brought to market for decades (Hutchings et al., 2019).

One possible solution for overcoming antibiotic resistance is to design synergistic drug combination therapies (Tyers & Wright, 2019). Such combinations could engage multiple cellular targets to suppress growing resistance, which is difficult to achieve with a single active compound. A major drawback, however, is the challenge in exploring a vast combinatorial space that exponentially increases when considering new drugs or dosage levels. Due to the empirical nature of designing drug combination therapies, the discovery of new combined regimens has been slow. Most notably, the four-drug regimen course that is standard for treating tuberculosis (TB) has not changed in 50 years, which has led to growing resistance (Pai et al., 2016). Therefore, there is a dire need for alternative approaches that can efficiently screen and prioritize promising drug combinations.

Machine learning (ML) has recently been leveraged to design synergistic drug combinations for various complex diseases (Cantrell et al., 2022; Güvenç Paltun et al., 2021). In context of antibiotic resistance, an approach called INDIGO was developed to propose combination therapies effective against *Escherichia coli* and *M. tb* (Chandrasekaran et al., 2016; Ma et al., 2019). Specifically, omics data for *E. coli* and *M. tb* treated with individual drugs, along with corresponding drug combination assay data, were used to construct two separate models predictive of drug interaction outcomes (e.g., synergy) for each organism. The *E. coli* INDIGO model was further extended to predict drug interaction outcomes for *Staphylococcus aureus* by leveraging omics data for genes that are orthologous between the two species. Although INDIGO was shown to yield predictions that correlate with experimental data, the original models are biased towards *E. coli* and *M. tb*. In other words, the original models do not extend well for other organisms, especially species that are phylogenetically distant from *E. coli* and *M. tb* (e.g., *S. aureus*).

Within this study, we leverage transfer learning and crowdsourcing to construct predictive models for non-model yet clinically relevant bacterial pathogens. Transfer learning is a ML concept where a model trained on one task is re-applied to solve a different yet similar task, usually after some finetuning (Torrey & Learning, 2010). Crowdsourcing describes the process of amalgamating input from various information sources to complete a common task (Vaughan, 2018). We integrate these concepts onto a modeling foundation inspired by INDIGO to develop a new approach called TACTIC: *Transfer learning And Crowdsourcing to predict Therapeutic Interactions Cross-species*. We show that TACTIC generates more accurate predictions than INDIGO for 12 phylogenetically diverse bacterial strains. We then examine a fully trained TACTIC model to explain the genetic drivers for cross-species and species-specific drug

interaction outcomes. Finally, we apply TACTIC to predict drug combinations with narrow-spectrum synergy against pathogenic bacteria.

3.3 Results

3.3.1 Drug interaction data collection

To build and validate our framework, we compiled drug interaction data from 17 publications (Bhusal et al., 2005; Brochado et al., 2018; Chandramohan et al., 2019; Chandrasekaran et al., 2016; Coelho et al., 2015; Cokol et al., 2018; Gonzalo et al., 2015; Katzir et al., 2019; Ma et al., 2019; Ocampo et al., 2014; Rey-Jurado et al., 2012, 2013; Russ & Kishony, 2018; Silva et al., 2016; Yeh et al., 2006; Yilancioglu & Cokol, 2019; W. Zhao et al., 2016) (**Figure 3-1A**, **Table 3-1**). In total, we attained 2,965 drug interactions involving 88 drugs measured across 12 strains representative of six species: *A. baumannii*, *E. coli*, *M. tb*, *P. aeruginosa*, *S. aureus*, and *Salmonella enterica* Serovar Typhimurium (henceforth *S.* Typhimurium) (**Figure 3-1B**, **Dataset 3-1**, **Dataset 3-2**). Drug interactions were quantified based on the Loewe Additivity (Loewe & Muischnek, 1926)l or Bliss Independence (Bliss, 1939) model, and sometimes both depending on the study. Based on the drug interaction classification scheme defined for each study, our pooled data consists of 913 synergistic (31%), 826 neutral (28%), and 1,226 antagonistic (41%) interactions (**Figure 3-1C**). Our pooled data is representative of two- to ten-way drug combinations, although more than 85% (N = 2,522) represents pairwise interactions.

Out of the 1370 unique drug combinations represented in our data collection, 757 were measured more than once (**Dataset 3-3**). This could be attributed to data being pulled from different studies, drug combinations being measured in different strains, or quantification of drug interactions using different metrics (**Figure S3-1A**). An inspection of the standard deviation calculated for each replicated drug combination revealed that combinations with the largest

difference in interaction scores (IS) were pulled from independent studies (**Figure S3-1B**). An evaluation of the agreement between class labels assigned for a replicated drug combination further showed that class disagreement was more prevalent when a combination was pulled from different studies and/or was measured in different strains (**Figure S3-1C**).

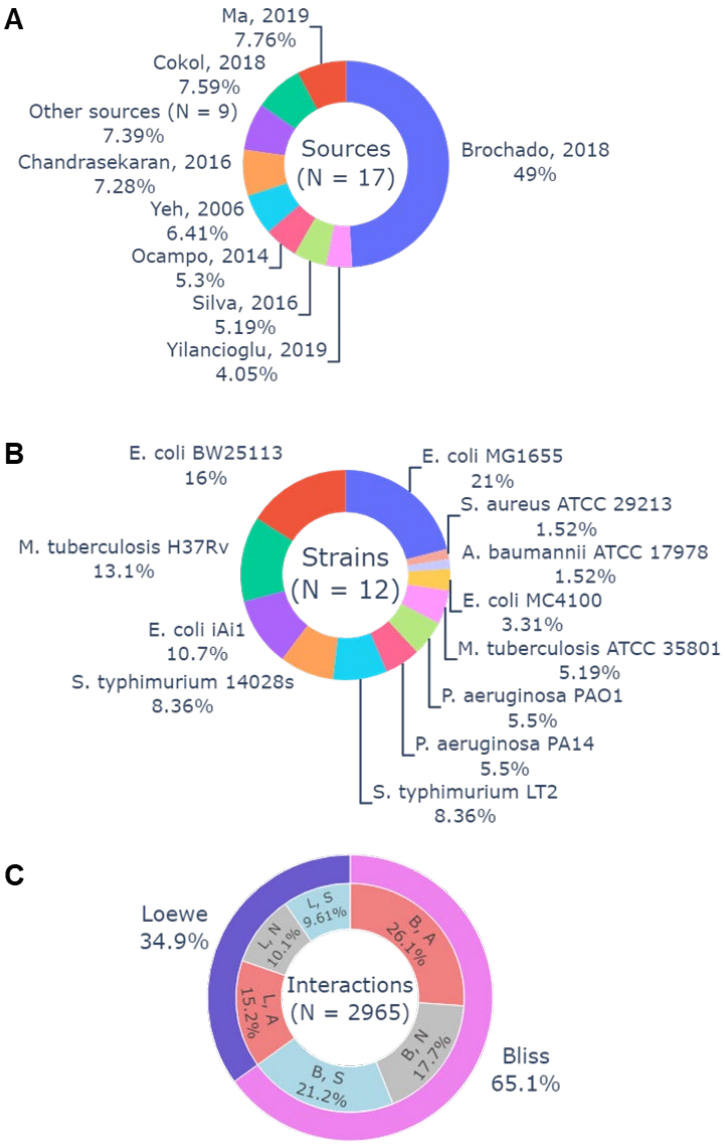

Figure 3-1 Drug interaction data collection for TACTIC. (**A**) Drug interaction data collected from 17 published sources was used to build TACTIC models. (**B**) This data collection measured outcomes in 12 bacterial strains representative of six organisms: *Acinetobacter baumannii*, *Escherichia coli*, *Mycobacterium tuberculosis*, *Pseudomonas aeruginosa*, *Salmonella enterica* serovar Typhimurium, and *Staphylococcus aureus*. (**C**) Drug interaction outcomes were measured using the Loewe Additivity and/or the Bliss Independence model, and data distribution was found to be relatively balanced between the three outcome classes: synergy (S), neutral (N), and antagonism (A).

Table 3-1 TACTIC drug interaction data collection. Drug interaction outcome measurements gathered from 17 independent studies. N_{total} = total number of interactions, N_{high} = number of high-order interactions.

Organism	Strain	N_{total}	N_{high}	Model	Interaction Outcome					
					Synergy		*Neutral*		*Antagonism*	
A. baumannii	ATCC 17978	45	30	Loewe	23	(0.51)	10	(0.22)	12	(0.27)
E. coli	BW25113	473	-	Both	117	(0.25)	155	(0.33)	201	(0.42)
	MC4100	98	26	Both	12	(0.12)	24	(0.25)	62	(0.63)
	MG1655	623	185	Both	123	(0.20)	218	(0.35)	282	(0.45)
	iAi1	316	-	Bliss	116	(0.37)	66	(0.21)	134	(0.42)
M. tuberculosis	ATCC 35801	154	134	Bliss	85	(0.55)	41	(0.27)	28	(0.18)
	H37Rv	389	68	Loewe	181	(0.47)	56	(0.14)	152	(0.39)
P. aeruginosa	PAO1	163	-	Bliss	44	(0.27)	47	(0.29)	72	(0.44)
	PA14	163	-	Bliss	51	(0.31)	54	(0.33)	58	(0.36)
S. aureus	ATCC 29213	45	-	Loewe	5	(0.11)	23	(0.51)	17	(0.38)
S. Typhimurium	14028s	248	-	Bliss	77	(0.31)	68	(0.27)	103	(0.42)
	LT2	248	-	Bliss	79	(0.32)	64	(0.26)	105	(0.42)

Of note, there was little consensus in the interaction outcome measured for the combination between isoniazid (INH) and rifampicin (RIF), despite being measured in only one strain (*M. tb* H37Rv) and being quantified based on a common mathematical model (Loewe Additivity). While one study defined this combination as synergistic based on a score of -0.089, another study found this combination to be antagonistic with a score of 0.982. Interestingly, a similar level of incongruence was also found for the combinations between INH and PA-824 (lowest score = -0.245, highest score = 0.176), bedaquiline (BDQ) and PA-824 (lowest score = -0.749, highest score = 0.155), and clarithromycin (CLA) and RIF (lowest score = -5.778, highest score = 0.111) (**Figure S3-2**). Though it is difficult to pinpoint the exact reason why these outcomes differ so greatly, these discrepancies in the interaction outcome are most likely due to differences in experimental conditions such as the growth media that was used, the drug concentration gradient evaluated for the combination, and/or the drug sensitivity profile of *M. tb* H37Rv.

On the other hand, a handful of drug combinations (N = 36) measured for the same strain of *E. coli* or *M. tb* by different studies agreed on the outcome class, even when the interaction was measured using different mathematical models (**Dataset 3-3**). For drug combinations repeatedly

measured in different strains (N = 664), the vast majority (>86%) either agreed on a single outcome class (N = 215) or disagreed between neighboring class labels (synergy vs. neutral, neutral vs. antagonism, N = 357). These drug interactions may indicate those with broad-spectrum activity, where broad-spectrum synergistic combinations may provide a therapeutic option to treat infections where the causative agent is unknown. In contrast, drug interactions measured to have diverging outcomes across different organisms (N = 92) may serve as narrow-spectrum therapies that selectively target a known pathogen.

3.3.2 Benchmarking TACTIC against INDIGO

TACTIC is an extension of INDIGO (Chandrasekaran et al., 2016), a computational approach for predicting drug interaction outcomes between antibacterial agents. Our approach specifically expands on the orthology aspect, which enables the application of a dataset measured for one organism (e.g., *E. coli*) to another (e.g., *S. aureus*). Unlike INDIGO models, which are trained on data for a single organism (i.e., *E. coli* or *M. tb)*, a TACTIC model is trained on omic and drug interaction data measured in multiple organisms (**Figure 3-2**). All other steps involved in developing a predictive model (e.g., defining ML model features, the ML algorithm used) were preserved from the original INDIGO publication and are reprised in the Methods section. The metric used for evaluating predictive model performance was also preserved. Specifically, model accuracy was measured based on the Spearman rank correlation between model predictions and experimentally measured drug IS, with high positive values indicating better performance.

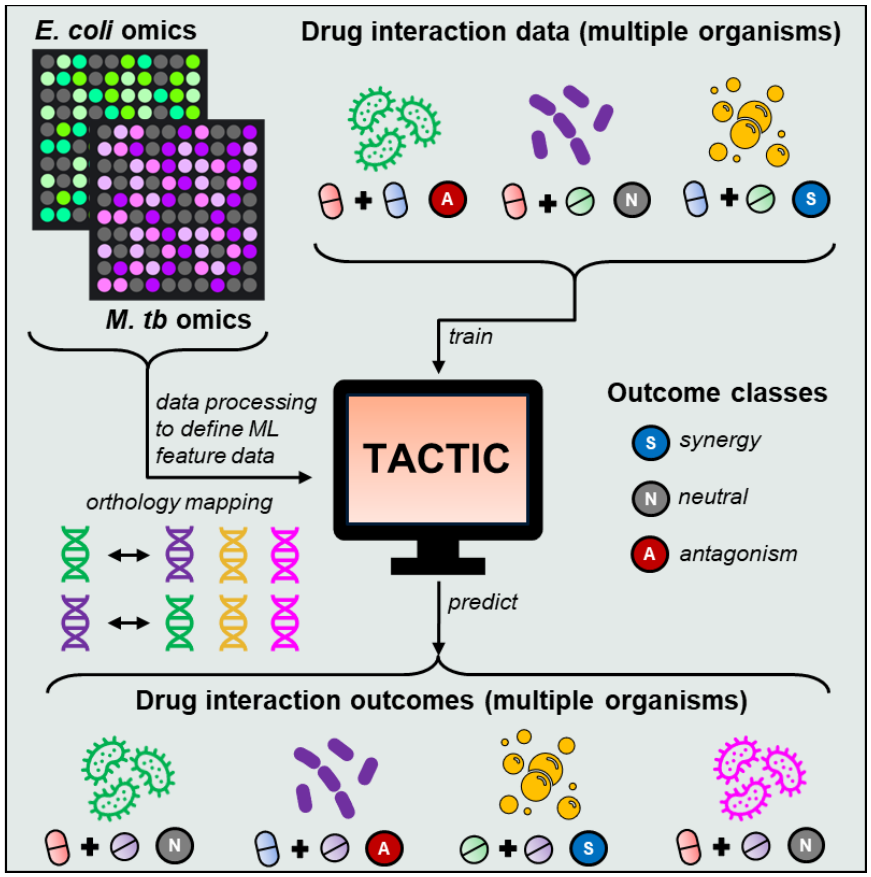

Figure 3-2 TACTIC approach schematic. The *Transfer learning And Crowdsourcing to predict Therapeutic Interactions Cross-species* (TACTIC) approach uses single drug response and drug interaction data to train a machine learning (ML) model that predicts drug interaction outcomes for multiple organisms. Single drug response data is processed to define ML features for a given set of drug combinations. Orthology mapping allows the transfer of drug response data measured in one organism to another by conserving data between orthologous genes.

We benchmarked TACTIC against INDIGO by evaluating their accuracy in predicting drug interaction outcomes for each of the 12 bacterial strains for which data was collected above. For INDIGO, we directly used the previously constructed *E. coli* (Chandrasekaran et al., 2016) and *M. tb* (Ma et al., 2019) models to generate predictions for all 2,965 drug interactions. For the TACTIC approach, we trained one model for each strain-specific dataset, where drug interactions measured for the strain of interest (N) were set aside for testing while the remaining drug interaction data (2,965-N) was used for training a model. We found that TACTIC models were considerably better at predicting drug interaction outcomes for *A. baumannii*, *P. aeruginosa*, *S.* Typhimurium, and most *E. coli* strains compared to INDIGO models (**Figure 3-3**). Unsurprisingly,

the INDIGO models for *E. coli* and *M. tb* yielded more accurate predictions for *E. coli* MC4100 and both *M. tb* strains, respectively; however, TACTIC models were still able to yield predictions comparable to those from the INDIGO models. Interestingly, all three models were less accurate in predicting drug interaction outcomes for *S. aureus*. This could potentially be due to the fact that *S. aureus* (Gram-positive) is phylogenetically distant from all other bacteria considered within this benchmarking analysis (Gram-negative strains).

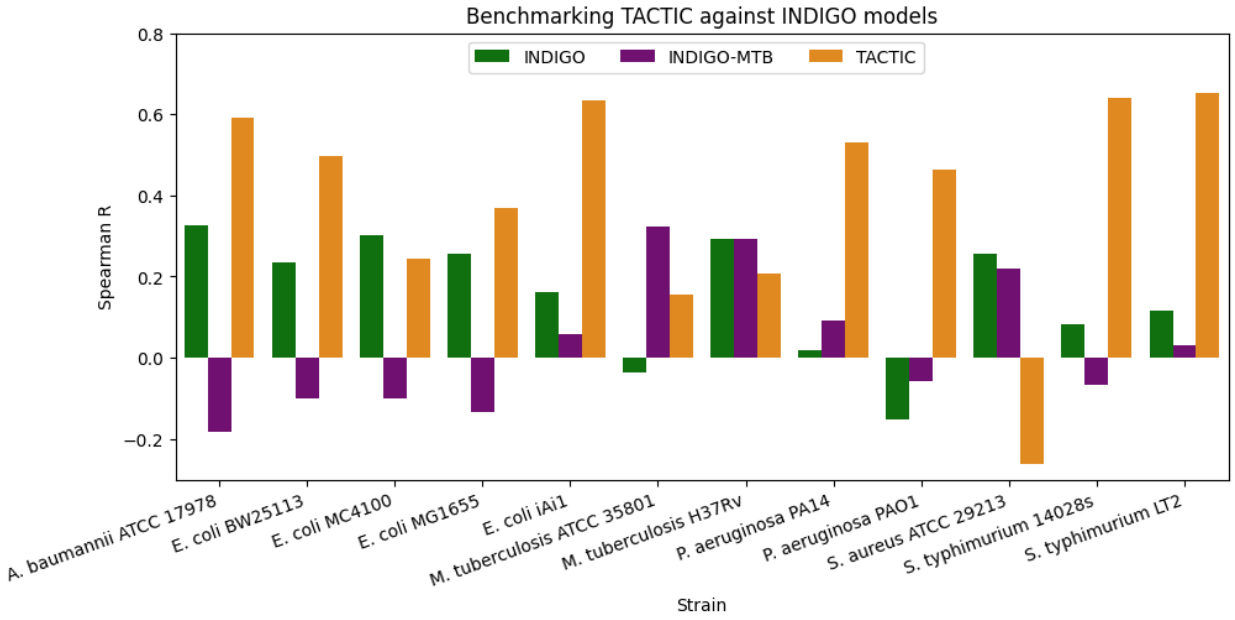

Figure 3-3 Benchmarking TACTIC against INDIGO. Strain-specific drug interaction outcome prediction accuracy was compared between TACTIC models and INDIGO models previously developed from *E. coli* (Chandrasekaran et al., 2016) or *M. tb* (Ma et al., 2019) data. Model performance was quantified based on the Spearman rank correlation between model predictions and experimentally measured drug interaction scores.

3.3.3 Genetic predictors of cross-species and species-specific drug interaction outcomes

Having confirmed that TACTIC provides an improvement over INDIGO in predicting drug interaction outcomes cross-species, we next trained a TACTIC model with the entire data collection on the 2,965 drug interactions measured across 12 bacterial strains. Using this fully trained TACTIC model, we sought to uncover which features the model most relied on for generating predictions and how changes in these feature values explained synergistic or

antagonistic outcomes. For this task, we first determined the set of ML features, ranked by decreasing importance score, that explained 95% of the variance in model predictions (see Methods for details). In total, ~2,500 features associated with 1,258 *E. coli* MG1655 genes and 411 *M. tb* H37Rv genes (both sets including 251 orthologous genes between the two organisms) met this criterium (**Dataset 3-4**). Although the most important genes (i.e., those with the highest cumulative importance score) did not show a biologically meaningful connection (**Figure 3-4A**), a gene set enrichment analysis of all top genes against the KEGG database (Kanehisa & Goto, 2000) revealed four pathways that are significantly enriched (**Figure 3-4B**, hypergeometric test, adjusted p-value < 0.05). Of note, all pathways relate to bacterial metabolism, with the biosynthesis of amino acids enriched by genes specific to both *E. coli* MG1655 and *M. tb* H37Rv.

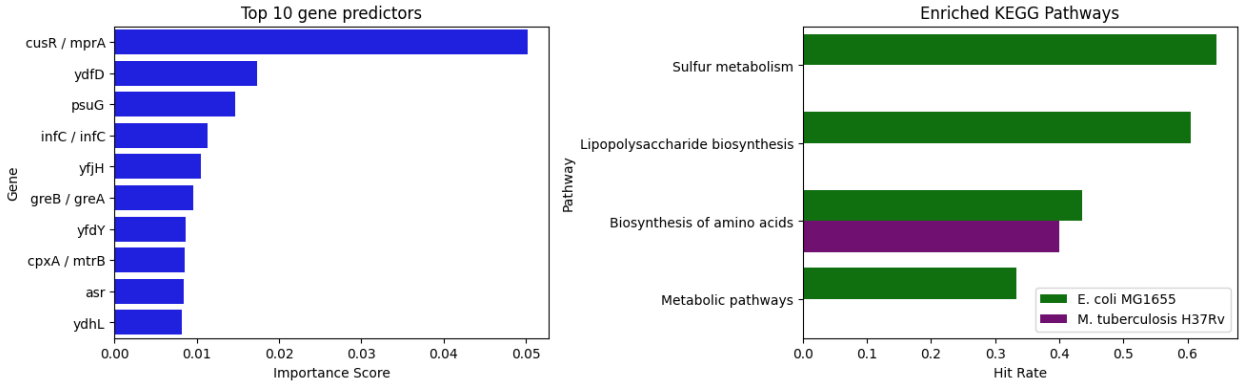

Figure 3-4 TACTIC model interpretation. (**A**) Based on importance scores determined for all 27,972 TACTIC model features, 2,499 were found to explain 95% of prediction variance (top 10 shown). (**B**) Four metabolic pathways were found to be significantly enriched (hypergeometric test, adjusted p-value < 0.05) by genes associated with top model features based on gene-pathway annotation in the KEGG database for *E. coli* str. K-12 substr. MG1655 and *M. tb* H37Rv genomes.

To gain a more fine-grained insight, we evaluated how the values for ML features associated with genes belonging to these pathways varied between synergistic and antagonistic interactions (see Methods for details). Using a stringent significance level (adjusted p-value < 1^{-6}) based on the adjusted p-value distribution for all feature-specific tests (**Figure S3-3**), we determined 79 sigma or delta features that differed based on the drug interaction outcome type

(**Dataset 3-5**). From this set, we visually pinpointed 11 genes for which both the sigma and delta feature values significantly differed between synergistic and antagonistic interactions along the same direction for gene-specific changes (**Table 3-2**, **Figure S3-4**). Interestingly, all 11 genes are unique to *E. coli* MG1655 and play a role in central metabolic pathways. Considering that information on these genes were derived from the *E. coli* chemogenomic dataset (Nichols et al., 2011), gene-specific values indicate changes in fitness for the knockout strain of a given gene in response to a particular condition. The trends for all 11 genes indicate that drug interactions involving at least one drug that perturbs central metabolic pathways generally result in antagonistic outcomes. These findings may align with a longstanding hypothesis that fully intact and active bacterial metabolism may potentiate drug efficacy (Kohanski et al., 2007; Martínez & Rojo, 2011); therefore, gene perturbations that attenuate metabolic activity may decrease combined antibiotic potency and lead to antagonistic interactions.

Table 3-2 *E. coli* MG1655 gene knockouts associated with antagonistic outcomes. KO: knockout.

Locus	Gene	Description	Primary Pathway	KO Fitness
b0115	aceF	pyruvate dehydrogenase, E2 subunit	Glycolysis / Gluconeogenesis	Positive
b0118	acnB	hypothetical protein	Citrate cycle (TCA cycle)	
b1136	icd	isocitrate dehydrogenase		
b3737	atpE	ATP synthase Fo complex subunit c	Oxidative phosphorylation	
b4042	dgkA	diacylglycerol kinase	Glycerolipid metabolism	
b3041	ribB	3,4-dihydroxy-2-butanone-4-phosphate synthase	Riboflavin metabolism	Positive
b0844	ybjI	5-amino-6-(5-phospho-D-ribitylamino) uracil phosphatase		Negative
b3620	waaF	ADP-heptose--LPS heptosyltransferase 2	Lipopolysaccharide biosynthesis	Positive
b3625	waaY	lipopolysaccharide core heptose (II) kinase		Negative
b3628	waaB	UDP-D-galactose: (glucosyl)lipopolysaccharide-1,6-D-galactosyltransferase		
b3632	waaQ	lipopolysaccharide core heptosyltransferase 3		

We next sought to investigate species-specific associations between ML feature patterns and drug interaction outcomes (synergy or antagonism). For this task, we assessed the relationship between IS and strain-specific drug impact for 24 drug combinations measured in six strains within the same study (Brochado et al., 2018). We defined strain-specific drug impact based on **Equation 3-1** below:

$$DI_{interaction} = \frac{\sqrt{\sum_{i=1}^{N_{features}} v_{interaction}}}{N_{orthologous}}$$

Equation 3-1 Quantification of strain-specific drug impact based on TACTIC model features.

where $DI_{interaction}$ is the drug impact for a given drug interaction, $v_{interaction}$ is the vector of ML features determined for the given drug interaction, $N_{features}$ is the total number of ML features, and $N_{orthologous}$ is the number of *E. coli* MG1655 and *M. tb* H37Rv genes that have corresponding orthologs annotated within the genome of the strain for which the drug interaction pertains to. Based on this metric, we found that the IS for two out of 24 drug combinations have a significantly negative correlation with strain-specific drug impact (**Figure S3-5**). Interestingly, these interactions (A22 + chloramphenicol and fosfomycin + novobiocin) are the only ones involving bacteriostatic-bacteriostatic interactions (**Dataset 3-2**). Given that the strain-specific drug impact metric is mainly driven by the number of orthologous genes between a given organism and the combined genomes of *E. coli* MG1655 and *M. tb* H37Rv, these findings imply that the deviation in cross-species drug interaction outcomes aligns with the phylogenetic distance for combinations that only involve bacteriostatic compounds. In turn, this may indicate that bacteriostatic drug effects are more dependent on the genetic state of a given organism, as opposed to bactericidal agents which are believed to be more dependent on the phenotypic (e.g., metabolic) state of a

bacterial cell (Dwyer et al., 2009; Kohanski et al., 2007; Lopatkin et al., 2019; J. H. Yang, Bening, et al., 2017).

3.3.4 Identifying narrow-spectrum drug synergies

Similar to single antibiotic treatments, combined drug therapies can be designed to impose broad- or narrow-spectrum potency against different bacteria. Given the increasing appreciation for commensal microbiomes that share a symbiotic relationship with human hosts (Y. Liu et al., 2021; Manor et al., 2020; Namasivayam et al., 2018; Sorbara & Pamer, 2022), we were interested in applying TACTIC to identify drug combinations that are selectively synergistic (i.e., show narrow-spectrum synergy) against different groups of pathogenic bacteria. For this task, we used the fully trained TACTIC model to generate drug interaction outcome predictions for all possible drug pairs out of 88 drugs (N = 3,828) across 18 bacterial strains (**Dataset 3-6**). This strain set included all of the 12 strains for which the TACTIC model was trained on as well as two non-tuberculous mycobacteria (NTM) species (*Mycobacterium abscessus* and *Mycobacterium smegmatis*) and four strains representative of gut microbiome commensals (*Bacteroides vugatus*, *Eubacterium eigens*, *Eubacterium rectale*, and *Lactobacillus rhammosus*). These new strains were selected based on growing concerns over NTM infections (Johansen et al., 2020) and studies that have deduced the species-level identities of commensal gut microbes (Forster et al., 2022; J. Yang et al., 2020).

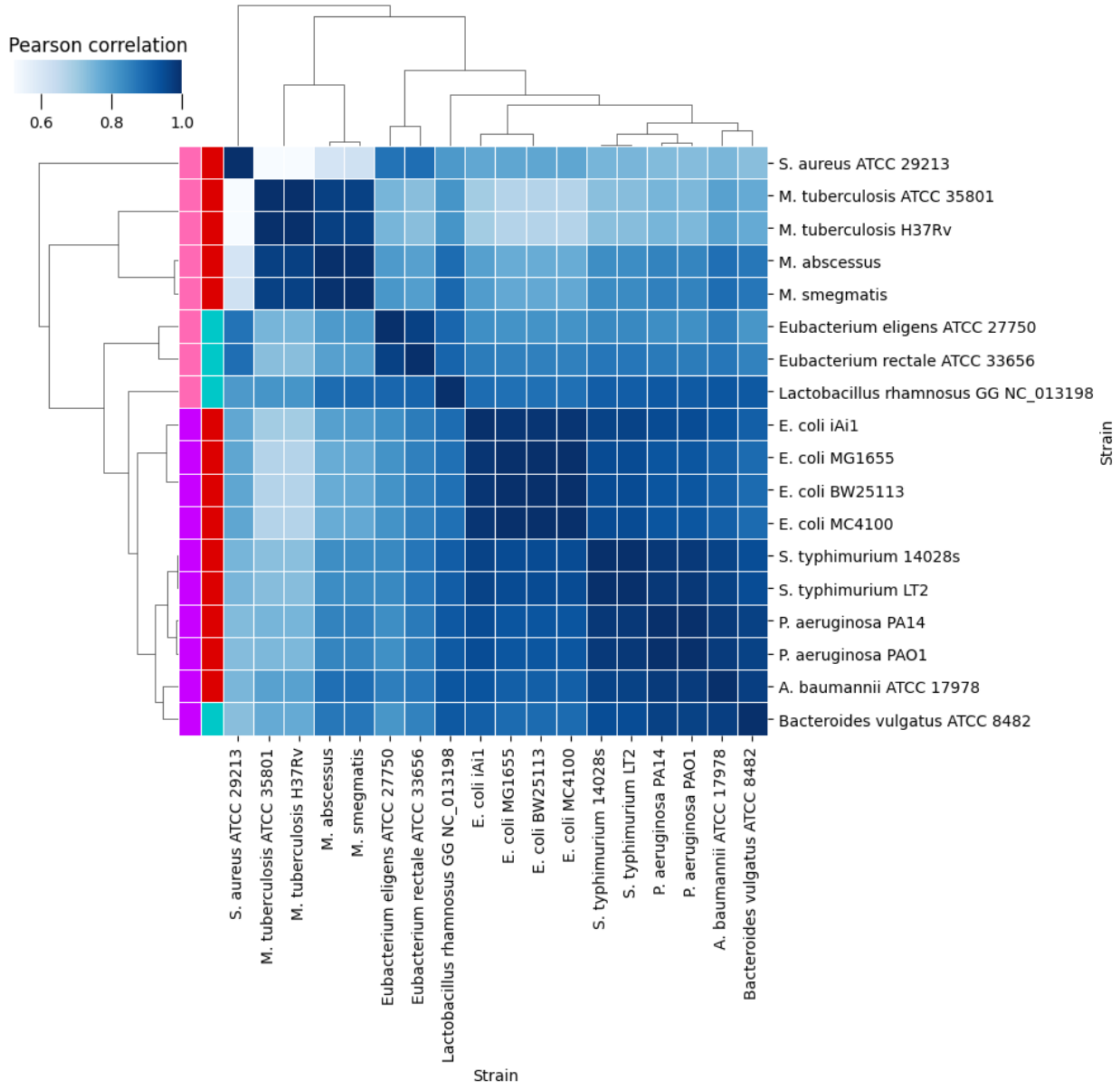

Figure 3-5 Correlation heatmap for strain-specific TACTIC model predictions. Drug interaction outcome predictions for all possible drug pairs between 88 drugs (N = 3,828) were generated across 18 bacterial strains by the full TACTIC model. The Pearson correlation for strain-to-strain predictions was calculated for all strain pairs and visualized as a clustered heatmap.

Based on our screen of 3,828 drug interaction outcomes across 18 bacterial strains, we first evaluated the similarity between strain-to-strain predictions. By defining similarity as the Pearson correlation between strain-specific predictions, we found that drug interaction outcome similarities are primarily based on the Gram stain of an organism (**Figure 3-5**). Of note, outcome predictions

for *S. aureus* were the most dissimilar from all other strain-specific predictions (lowest correlation < 0.6). Unsurprisingly, strain-specific predictions for the same species were most similar to one another, and Mycobacteria-specific predictions clustered amongst each other. Overall, we found that these trends based on the Gram stain and species identity agreed with our hypothesis that divergence in drug interaction outcomes between different bacteria is primarily driven by phylogenetic dissimilarity. Of note, strain-specific predictions seemed to cluster based on the strain-specific relationship with the host (i.e., pathogen vs. commensal) within Gram stain groups. This finding supported the potential of identifying drug combinations with selective synergy against pathogenic bacteria within our strain-specific prediction landscape.

To identify drug combinations with narrow-spectrum synergy, we compared TACTIC model predictions for four strain group comparisons: commensals vs. all pathogens, commensals vs. Gram-negative pathogens, commensals vs. NTM pathogens, and commensals vs. *S. aureus*. For these comparisons, we imposed two criteria to define narrow-spectrum synergy. The first was to select drug combinations that are predicted to be additive or antagonistic (predicted IS $\geq$ 0) across all commensal strains. The second criterium selected pathogen-specific synergies based on one of the four thresholds: strong comprehensive synergy (predicted IS < -0.2 for all pathogens), comprehensive synergy (predicted IS < 0 for all pathogens), strong average synergy (mean predicted IS < -0.2), and average synergy (mean predicted IS < 0). For the first comparison, only the average synergy threshold returned narrow-spectrum synergies against all pathogens (**Figure 3-6A**). A visual inspection of the top 20 narrow-spectrum synergies revealed that broad synergistic outcomes are hard to achieve for all pathogens, most likely because this group includes both Gram-negative and Gram-positive species. For the second comparison, 34 drug combinations were predicted to have comprehensive narrow-spectrum synergy against Gram-negative pathogens

(**Figure 3-6B**), with stronger synergies predicted against *E. coli* and *S.* Typhimurium strains compared to *A. baumannii* or *P. aeruginosa* strains. For the third comparison, 16 drug combinations were predicted to have strong comprehensive narrow-spectrum synergy against NTM pathogens (**Figure 3-6C**). Interestingly, most of these combinations (N = 14) include clarithromycin, which is known to have potent effect against NTM strains (Cowman et al., 2016). The last comparison revealed that 17 drug combinations are comprehensively synergistic against *S. aureus* (**Figure 3-6D**); however, most interaction predictions appear to be additive (IS ~ 0), with only two drug combinations predicted to be mildly synergistic (IS ~ -0.1). Although we have yet to experimentally validate whether TACTIC model predictions for narrow-spectrum synergy are observed *in vitro* and *in vivo*, the results from these four commensal vs. pathogen comparisons beg the exploration of precise drug combinations that could more effectively clear hard-to-treat infections caused by specific groups of pathogenic bacteria.

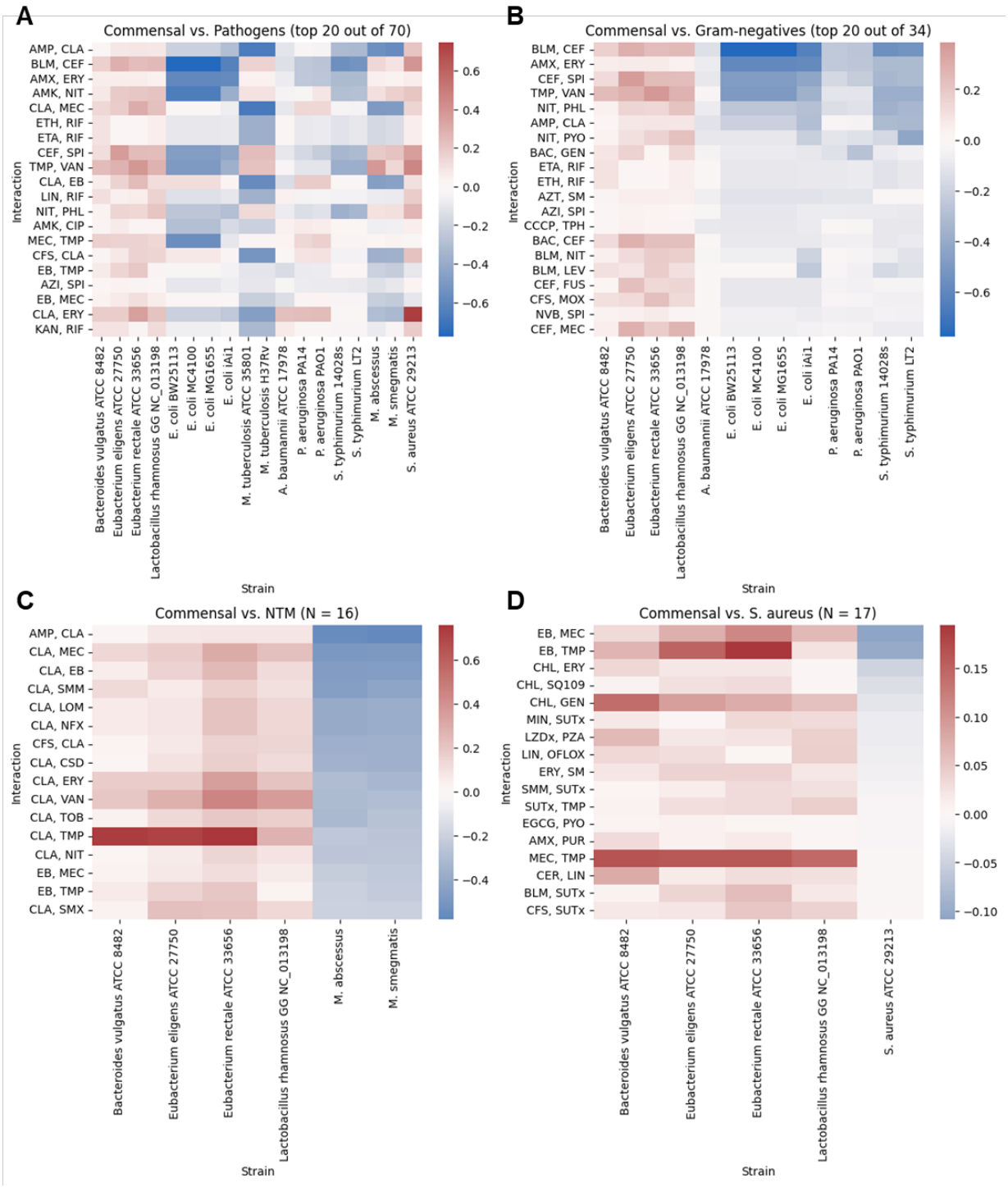

Figure 3-6 Narrow-spectrum synergy predictions against pathogenic bacteria. Narrow-spectrum synergy was defined by additive or antagonistic predictions (predicted IS ≥ 0) across all commensal strains and adjustable thresholds for synergistic predictions (predicted IS < 0) across pathogenic strains. In total, (**A**) 80 drug pairs are predicted to have general synergy (mean IS < 0) against all pathogenic strains, (**B**) 34 drug pairs are predicted to have comprehensive synergy (all IS < 0) against Gram-negative pathogens, (**C**) 16 drug pairs are predicted to have strong comprehensive synergy (all IS < -0.2) against non-tuberculous mycobacteria (NTM) pathogens, and (**D**) 17 drug pairs are predicted to have comprehensive synergy (all IS < 0) against *S. aureus*.

3.4 Discussion

Within this work we introduced TACTIC, a new computational approach that leverages transfer learning and crowdsourcing via orthology mapping to evaluate strain-specific drug interaction outcomes. Using a data collection of ~3,000 drug interactions measured across a phylogenetically diverse set of bacterial strains (**Dataset 3-1**), we showed that TACTIC models generated more accurate predictions cross-species compared to INDIGO (Chandrasekaran et al., 2016), a previous computational approach that served as the blueprint for the TACTIC approach. Using a complete TACTIC model trained on the entire drug interaction data collection, we further showed that this model could explain cross-species and species-specific drug interaction outcomes, which may be tied to the phenotypic (e.g., metabolic state) and genetic (e.g., Gram stain) nature of a given organism, respectively. Lastly, we used the full TACTIC model to generate a comprehensive prediction landscape of interaction outcomes for ~4,000 drug pairs across 18 bacterial strains. By comparing TACTIC model predictions for commensal strains against different groups of pathogenic bacteria, we identified a small set of drug interactions that are predicted to have narrow-spectrum synergy against the latter group. Although these predictions have yet to be validated by experimental data, they provide a manageable starting point for discovering combination therapies optimized to clear bacterial infections while minimizing detrimental effects on the commensal microflora of a human host.

The TACTIC approach provides a novel method to investigate strain-specific drug interaction outcomes; however, we underscore the fact that the prediction accuracy for TACTIC models may decrease for species that are phylogenetically distant (e.g., *S. aureus*) from organisms that are accounted for during model training (e.g., *E. coli* and *M. tb*). To address this limitation, omics data measuring the drug response in other organisms (e.g., *Staphylococcus spp*.) could be

integrated into TACTIC models to improve prediction accuracy and extended application to a diverse range of bacterial species. We also reiterate the issues of discrepancies in drug interaction outcome scores that may arise from differences in experimental procedures and calculation metrics used by independent research groups. Though not explicitly stated in the Results section, these discrepancies in outcome measurements reported by different studies may have impacted TACTIC model performance, especially for *M. tb* strains. A potential solution to this limitation could be the inclusion of information on the growth environment or the phenotypic state of an organism, which both play a major role in transient drug persistence and tolerance (K. Lewis, 2006), during TACTIC model development.

3.5 Methods

3.5.1 Data acquisition and curation

Two distinct data types were used to construct TACTIC models: drug response and drug interaction data. Drug response information was comprised of *E. coli* chemogenomic data (Nichols et al., 2011), where fitness of single-gene knockout strains was measured in response to individual stressors, and *M. tb* transcriptomic data (Ma et al., 2019), which measured differential gene expression in response to individual stressors. Each omic dataset was previously z-score normalized within its originating study; hence, the normalized omic data was directly used for defining TACTIC model features. The drug interaction data comprised of 2,965 combinations collected from 17 different literature sources covering 12 bacterial strains (**Table 3-1**, **Dataset 3-1**). Drug combinations ranged between two- to ten-way interactions and were quantified based on the Loewe Additivity (Loewe & Muischnek, 1926)l and/or the Bliss Independence (Bliss, 1939) model based on the originating study. Of note, the drug interaction data collection used in this study represents the subset for which the full set of ML features could be determined based on the

omics datasets from which drug response information was extracted. Each drug interaction was labeled into one of the three outcome classes (i.e., synergy, neutral, antagonism) based on the classification criteria specified in its originating publication.

3.5.2 Defining ML features for drug combinations

The method for defining ML features for a given drug combination are fully described in the INDIGO study (Chandrasekaran et al., 2016). Briefly, drug response data is first binarized to indicate substantial gene-level changes ($z > 2$ and $z < -2$) in cell response to a given stressor. The binarized vectors for all drugs involved in a given combination are then combined to define sigma and delta features for each gene, which mathematically represent the combined drug and drug-unique effect, respectively. Of note, a TACTIC model defines drug combination features based on two omic datasets that measure *E. coli* and *M. tb* drug response. To remove duplicated information captured within orthologous genes between these two organisms, a feature vector is defined by the sigma-delta transformation of the full set of *M. tb* genes and the sigma-delta transformation for genes unique to *E. coli*.

3.5.3 Orthology mapping for predictive modeling

The *E. coli* and *M. tb* omics datasets were directly used to define ML features for drug combinations measured against *E. coli* str. K-12 substr. MG1655 (henceforth *E. coli* MG1655) and *M. tb* H37Rv. For all other organisms, ML features were defined by first determining the sigma-delta feature vector for a given drug combination then filtering this vector based on the orthology mapping between *E. coli* MG1655, *M. tb* H37Rv, and the given strain. Gene orthology was determined by mapping the *E. coli* MG1655 and *M. tb* H37Rv genomes against the genomes for

all other strains based on genome annotation available in OrtholugeDB (Whiteside et al., 2013), a database that infers orthologs based on the reciprocal-best-BLAST hit (RBBH) rate.

3.5.4 TACTIC model construction using random forests

All TACTIC models were constructed in Python v3.10.8 (Python Software Foundation) using the regression-based Random Forests (RF) algorithm supplied through the scikit-learn package v1.2.0 (Pedregosa et al., 2011). Briefly, RF is an ensemble method comprised of multiple decision trees that independently learn to associate feature information (i.e., sigma-delta features for a given drug combination) to a target variable (i.e., the measured drug IS) during the training phase. Each decision tree is then tasked with estimating the target variable (i.e., drug interaction outcome) given feature information alone during the testing phase, and the average estimated value (i.e., the predicted drug IS) is returned by the RF algorithm. Randomization is factored into the model construction process via random sampling with replacement of the training dataset for each decision tree. This yields a diverse collection of decision trees that together reduce the variance between model predictions against true values for the target variable. Of note, all TACTIC models were constructed using the default parameter values for the RandomForestRegressor method in scikit-learn.

3.5.5 TACTIC model interpretation via feature importance

Feature importance for the full TACTIC model was determined by using the built-in computation for the scikit-learn RF algorithm, which defines importance as the mean decrease in variance for a regression task. Based on this definition, the importance score for each feature is calculated by first constructing a model without the given feature then comparing its prediction accuracy against that of the model trained on all features. Specifically, importance is quantified as the difference in

the mean squared error between model predictions and true values for the target variable. TACTIC model interpretation was completed by using the set of features ranked by decreasing importance score with a cumulative sum of 0.95, or the set of the most important features that explain 95% of the mean decrease in variance.

3.5.6 Statistical analysis

Three statistical tests were used for downstream model interpretation based on the set of sigma-delta features explaining 95% of model importance. First, the two-sample Student's t-test with equal variance was used to determine sigma features that statistically differ in mean value between synergistic or antagonistic drug interaction outcomes. For delta features, the chi-square test with Yates' correction was applied to determine any associations between synergistic or antagonistic drug interaction outcomes and drug-unique effects on a single gene. Finally, a hypergeometric test was performed to determine KEGG pathways that were significantly represented by genes associated with the top model features (those explaining 95% of the variance). This test was conducted for KEGG pathways annotated from both the *E. coli* MG1655 genome (organism code: eco) and the *M. tb* H37Rv genome (organism code: mtu). Of note, the number of pathways annotated for each genome served as the population size specified in the hypergeometric test. Importantly, p-values from all three statistical tests were adjusted using the Benjamini-Hochberg correction (Benjamini & Hochberg, 1995) to minimize the false discovery rate.

3.6 Supplementary Materials

3.6.1 Figures

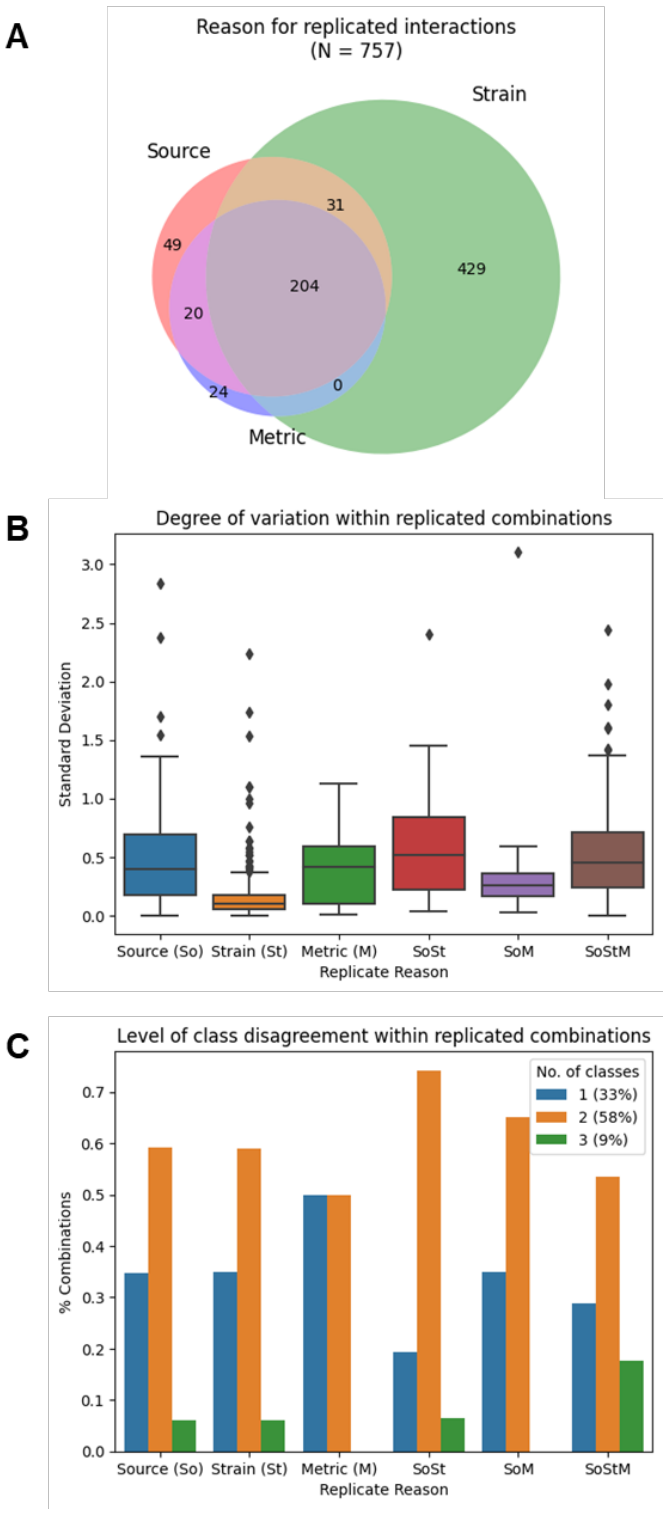

Figure S3-1 Replicated drug interactions in TACTIC data collection. (**A**) Replicated drug interactions occur due to data collected from different sources, measured in different strains, or quantified using different metrics. (**B**) Distribution of standard deviations calculated for each replicated drug interaction, grouped by the source for replicated data. (**C**) Number of outcome classes reported for each replicated drug interaction, grouped by the source for replicated data.

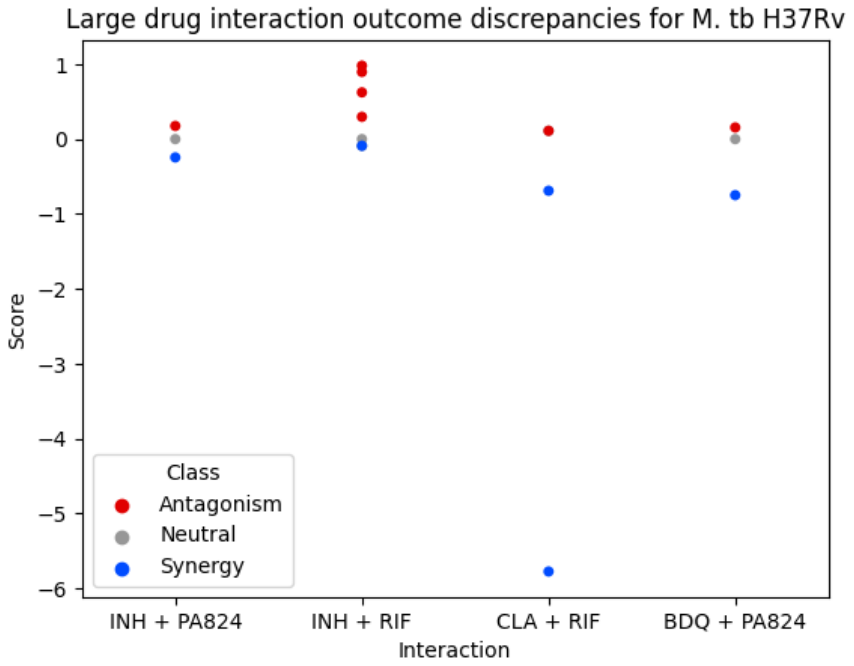

Figure S3-2 Anti-tuberculosis drug interactions with large discrepancy in reported outcomes. Four drug interactions common for treating tuberculosis were reported to have inconsistent combined treatment outcomes against *M. tb* H37Rv across different studies. BDQ: bedaquiline, CLA: clarithromycin, INH: isoniazid, PA824: PA-824, RIF: rifampicin.

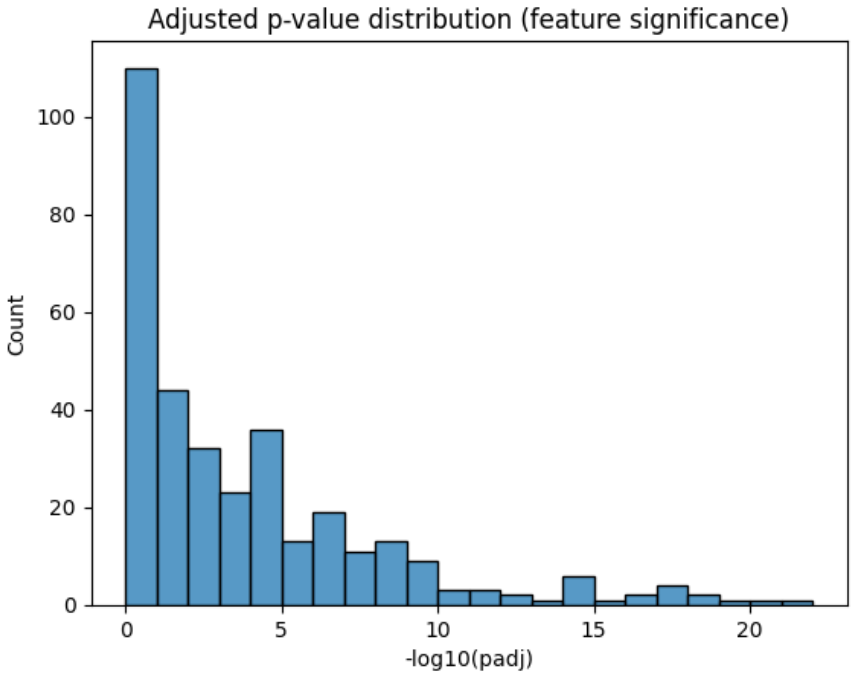

Figure S3-3 Adjusted p-value distribution for feature significance tests. The two-sample Student's t-test with unequal variance and the chi-square test with Yates' correction evaluated sigma and delta feature value association with drug interaction outcomes, respectively. All p-values were adjusted based on the Benjamini-Hochberg correction.

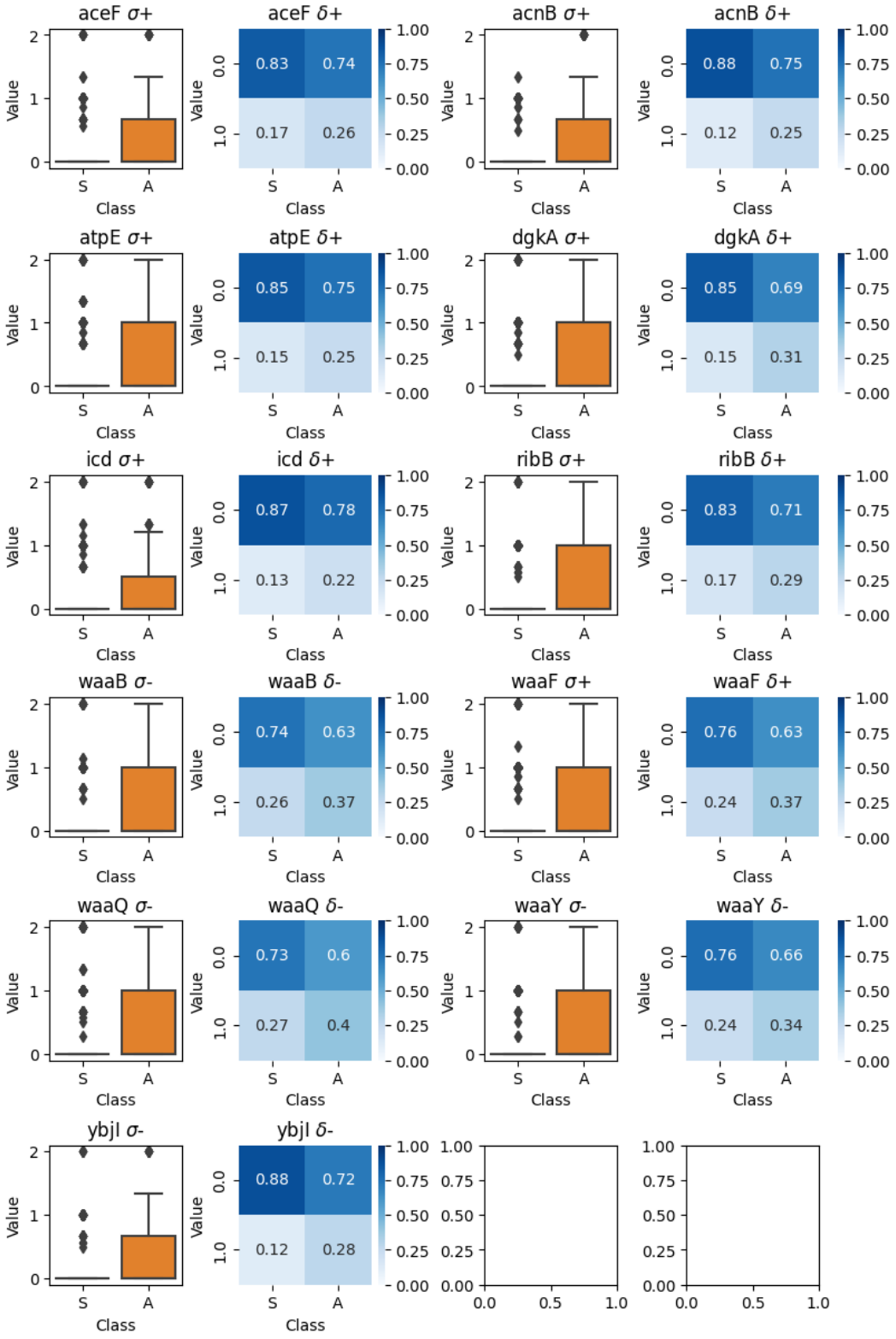

Figure S3-4 Difference in feature values between synergistic (S) and antagonistic (A) interactions for 11 metabolic genes. All 11 genes are associated with metabolic pathways that were determined to be enriched by top predictive features for the full TACTIC model.

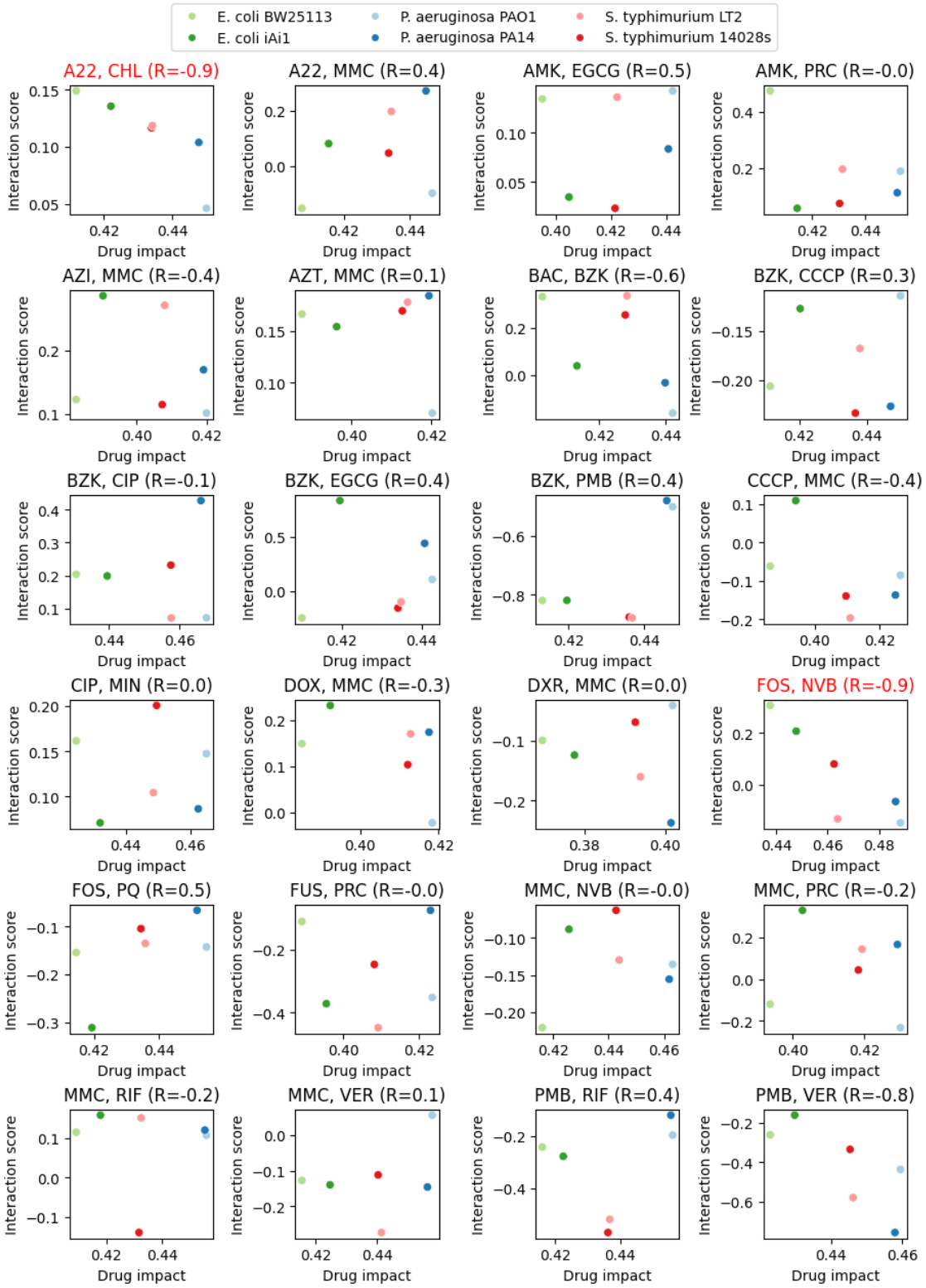

Figure S3-5 Relationship between strain-specific drug interaction scores against strain-specific drug impact. Drug impact was determined based on TACTIC model features determined for strain-specific drug interactions. See **Dataset 3-2** for drug code information.

3.6.2 Datasets

All supplementary data files from this chapter are available in the following external location:

https://www.dropbox.com/s/m8zwd7297ho5yh8/Chung_Carolina_Dissertation_Data.xlsx?dl=0

Dataset 3-1 TACTIC drug interaction dataset (N = 2,965).

Dataset 3-2 Description of compounds represented in TACTIC drug interaction dataset (N = 88).

Dataset 3-3 Unique drug interactions from the TACTIC drug interaction dataset (N = 1,370).

Dataset 3-4 Importance scores for all TACTIC model features (N = 27,972).

Dataset 3-5 Significance test results for ML model features derived from genes in enriched pathways (N = 337).

Dataset 3-6 Prediction landscape for 3828 pairwise drug interaction outcomes across 18 bacterial species.

.

Chapter 4 Case Studies on How Computational Methods Can Enhance Clinical Translation of Antibiotic Combination Therapies

This chapter discusses two collaborative projects that leverage CARAMeL (**Chapter 2**) and TACTIC (**Chapter 3**) to determine synergistic drug combinations in a clinically relevant context. For the first project, I collaborated with the Sherman Lab at the University of Washington (UW) to generate strain- and media-specific drug interaction outcomes predictions against *Mycobacterium tuberculosis* using CARAMeL. Our objective was to understand how predicted outcomes may change depending on these two factors. For the second project, I collaborated with Dr. Karthik Srinivasan at the U-M Kellogg Eye Center in using TACTIC to determine drug combinations predicted to be selectively synergistic against causative agents of endophthalmitis, a serious type of eye infection. For both projects, my direct contribution was to generate drug interaction outcome predictions that could be validated in the lab or clinic with the help of my collaborator. In describing my role in these two projects, I demonstrate how computational approaches like CARAMeL and TACTIC can effectively guide combination therapy design to maximize the odds of observing synergistic interactions at the clinical stage.

4.1 Applying CARAMeL to Assess Changes in Drug Interaction Outcomes for Tuberculosis during Disease Progression

4.1.1 Background

Tuberculosis (TB) is an airborne infectious disease caused by *Mycobacterium tuberculosis* (*M. tb*), which primarily resides and causes disease within the lung but is also capable of causing

extrapulmonary infections (Sharma et al., 2021). According to the World Health Organization (WHO), TB is the second leading cause of death due to an infection (after COVID-19), causing ~1.6 million deaths in 2021 alone (World Health Organization, 2015). Individuals infected with *M. tb* experience one of two disease states: latent, where *M. tb* cells reside in a dormant state of no growth, or active, where *M. tb* becomes virulent and transmissible to others. TB is one of the most widespread infectious diseases, though its incidence is disproportionately higher within underdeveloped regions in Africa and Asia (World Health Organization, 2015). Due to scarce availability of thorough medical interventions in such TB-concentrated regions, active TB cases often go undetected or improperly treated. Lack of treatment can lead to further growth and spread of *M. tb*, while improper care allows *M. tb* to develop various levels of drug resistance.

Two classes of drug-resistant *M. tb* are clinically recognized based on which anti-TB agents are rendered ineffective (Seung et al., 2015). The first is multidrug-resistant (MDR) *M. tb*, which is resistant to isoniazid (INH) and rifampin (RIF, a.k.a. rifampicin) (the two most potent first-line agents). The second class is extensively drug-resistant (XDR) *M. tb*, which is resistant to INH, RIF, a fluoroquinolone (the primary group of second-line treatments), and a second-line injectable agent. Though not classified as a drug-resistant class, dormant *M. tb* cells that form during latent TB play a key role in maintaining their persistent survival within a host (Gomez & McKinney, 2004). Hence, complete clearance of M. tb cells can be nearly impossible to achieve and the host may carry the risk of TB reactivation over the course of their lifetime.

From a macroscopic perspective, classifying TB as being in an active or latent phase can sufficiently capture the spectrum of TB progression; however, current TB research is focused on elucidating a microscopic-level view of how *M. tb* cells interact with host immune cells (Pai et al., 2016). From this point of view, TB infection is broken down into the following events. First, *M.*

tb cells enter the human host via the respiratory tract and travel down to the lung where they encounter alveolar macrophages (AMs). As the first-line defense, AMs engulf *M. tb* cells and encapsulate them within phagosomes to eliminate *M. tb* via phagocytosis. *M. tb* cells that evade death are able to hijack AMs, which may then allow *M. tb* to gain access into the lung interstitium. Within this new environment, other immune cells (i.e., T and B cells) act as a second-line defense to contain the infection by forming multicellular structures called granulomas. These structures serve two conflicting roles, depending on the perspective: for the host, granulomas act as barriers that prevent *M. tb* cells from migrating to other regions; for *M. tb*, granulomas provide a protected environment where they can continue to survive and replicate (i.e., latent TB). If the bacterial load within the granuloma becomes too great, the granuloma may burst and *M. tb* cells may escape to cause further infection (i.e., active TB). Given that the state of granuloma structures directly drives active or latent TB, and hence which therapy is most appropriate for a TB-infected patient, TB research is heavily focused on understanding these structures (Ramakrishnan, 2012). Importantly, the core region is comprised of caseum, a necrotic formation of infected foamy macrophages that provide a high-lipid, low-oxygen, and mildly acidic growth environment. Such conditions allow *M. tb* to persist beyond antibiotic exposure, thus allowing *M. tb* to enhance its drug resistance profile (Sarathy & Dartois, 2020).

Due to *M. tb* heterogeneity in its geographic distribution, resistance profile, and degree of infection, TB is a notoriously difficult disease to treat. Hence, the anti-TB regimen that is prescribed to a given patient must carefully consider these facets of heterogeneity in order to achieve successful *M. tb* clearance. Within this work, I leverage genome-scale metabolic modeling to understand *M. tb* metabolism for strain- and growth media-specific phenotypes. I also employ metabolic modeling to investigate any genetic vulnerabilities for *M. tb* growing within caseum

conditions, which are believed to harbor drug-tolerant or dormant *M. tb* cells. Finally, I incorporate simulated metabolic response data into CARAMeL (described in **Chapter 2**) to predict strain- and growth media-specific drug interaction outcomes. Upon validating that model predictions align with the expected outcomes for standard anti-TB regimens, I inspect the prediction landscape to determine how drug interaction outcome predictions vary across strain and growth media axes.

4.1.2 Methodology

4.1.2.1 Transcriptomics data collection

Transcriptomics (i.e., bulk gene expression) data was collected from six published sources and one unpublished dataset provided by the Sherman Lab at the University of Washington (UW) (**Figure 4-1A**). Gene expression data measured for 43 drugs was retrieved from the INDIGO-MTB study (Ma et al., 2019), which is the same data that was used in the CARAMeL publication (Chung & Chandrasekaran, 2022). Strain-specific data was collected from two publications which collectively characterized four phenotypic strains of *M. tb*. The first study, conducted by Colangeli et al. (Colangeli et al., 2018), measured gene expression changes in clinical *M. tb* isolates from patients who either were completely cured of TB or experienced TB relapse following first- and/or short-line therapy. Of note, higher MIC values for INH and RIF below the standard resistance breakpoints were associated with isolates from patients who experienced disease relapse; this may indicate a shift towards drug tolerance in the relapsed strains. The second study, led by Verma et al. (Verma et al., 2019), measured gene expression changes for *M. tb* isolates collected from TB-infected households with either low or high transmission rates. Of note, the authors found that transmission phenotypes were associated with distinct lung pathologies and granuloma composition.

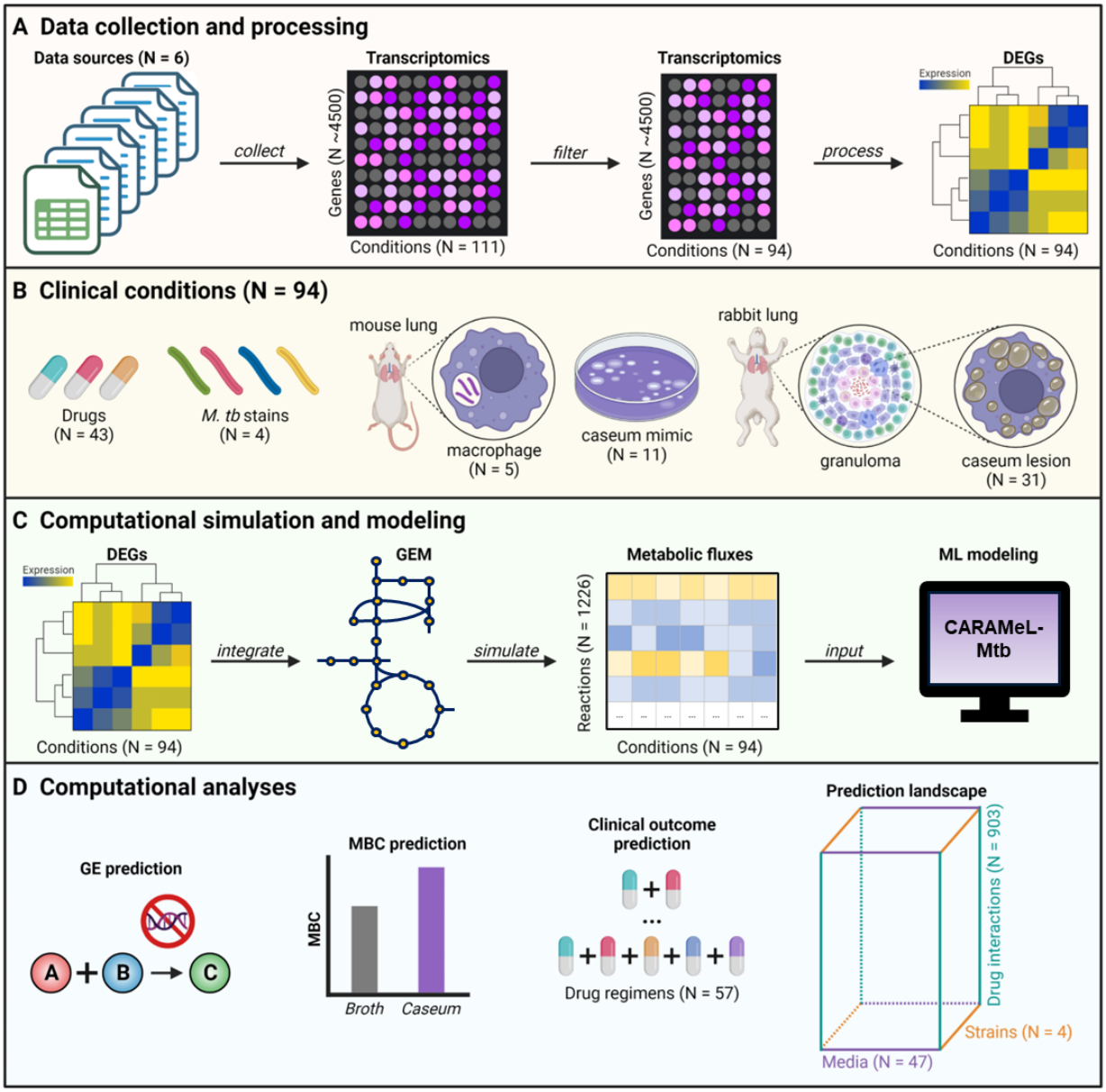

Figure 4-1 CARAMeL-Mtb approach schematic. (**A**) Data measuring bulk *M. tb* gene expression (i.e., transcriptomics) across 111 clinically relevant conditions was collected from six individual data sources. This data collection was filtered to remove low-quality reads (N = 17) then processed to determine differentially expressed genes (DEGs). (**B**) The curated dataset included DEG information on 94 drug-, strain-, and media-specific conditions. (**C**) DEG information was integrated into the *M. tb* genome-scale metabolic model (GEM) iEK1008 (Kavvas et al., 2018), which returned simulations of condition-specific metabolic responses. This data was then fed into a machine learning model predictive of drug interaction outcomes for *M. tb* (CARAMeL-Mtb). (**D**) Using both iEK1008 and CARAMeL-Mtb, four computational analyses were conducted: (1) gene essentiality (GE) prediction in caseum-mimicking media, (2) prediction of the minimum bactericidal concentration (MBC) in caseum compared to broth media, (3) clinical outcome prediction for 57 multi-drug regimens, and (4) prediction of pairwise drug interaction outcomes in strain- and media-specific conditions.

The remaining four transcriptomic data sources characterized *M. tb* growing in two types of environments: macrophages derived from TB-infected mouse lungs and within caseum conditions. Data from two published sources used distinct methodologies to measure gene expression for *M. tb* growing within alveolar or interstitial macrophages (AMs or IMs) of TB-infected mice. The first source (GEO accession: GSE116394) collected samples from AMs at 24 hours post-infection and employed Path-seq to measure enrichment of intracellular *M. tb* transcripts (Peterson et al., 2019). The second source (GEO accession: GSE132354) collected samples from both AMs and IMs at 14 days post-infection and applied dual RNA-seq to measure changes in *M. tb* gene expression (Pisu et al., 2020). Of note, the second source defined the *in vivo M. tb* transcriptome based on two references: differential gene expression compared to *M. tb* cultured in 7H9 broth or bone marrow-derived macrophages (BMDM).

Data on *M. tb* growth within caseum conditions was collected from two sources, which together measured gene expression changes for *M. tb* cultured in caseum-like growth media or rabbit-derived caseum samples. The published study, led by Sarathy et al. (Sarathy et al., 2023), introduced caseum-mimicking media conditions that aimed to reproduce the host lipid profile of *ex vivo* rabbit caseum. This study evaluated three inducers of foamy macrophage cells that characterize natural caseum conditions, namely: irradiated M. tb (iMTB), stearic acid (SA), and oleic acid (OA). *M. tb* gene expression was measured in each of these three caseum mimics at four timepoints: day 0 (shortly after infection induction), day 14, day 28, and day 42 (2-, 4-, and 6-weeks post-infection, respectively). Of note, the authors found that iMTB and SA most adequately resembled the properties and phenotypic behavior of *M. tb* cultured in rabbit caseum over time. The last data source, which comes from the Sherman Lab at UW, recapitulated *M. tb* growth in the SA-based caseum mimicking growth media at the same later timepoints but a different initial

timepoint (days 7, 14, 28, and 42). This dataset also provides gene expression measurements for *M. tb* within caseum samples collected from lung lesions (N = 43) of different TB-infected rabbits housed at the National Institutes of Health (NIH).

4.1.2.2 Inferring differential gene expression from bulk transcriptomics data

In total, the transcriptomics data collection is representative of 111 individual *M. tb* phenotypes: growth in response to 43 drug treatments, 4 clinical strains (cured, relapsed, low, high), growth in 5 mouse lung references (AM-H24, AM-D14-7H9, AM-D14-BMDM, IM-D14-7H9, IM-D14-BMDM), growth in 4 caseum mimics at 4 timepoints each (iMTB, SA, OA at days 0, 14, 28, 42 and HN878 at days 7, 14, 28, 42), and growth in 43 rabbit caseum extracts. Prior to data processing, 17 samples from the caseum set were removed due to low quality or low transcript coverage. These included all OA-based caseum mimic timepoints, the iMTB-based caseum mimic at day 14, and 12 rabbit caseum extracts. The remaining 94 *M. tb* transcriptomic profiles (**Figure 4-1B**) were then analyzed for differentially expressed genes (DEGs) as 5 independent datasets. The first dataset was derived from the INDIGO-MTB study, which provided z-score normalized gene expression values; hence, DEGs were determined based on z-score thresholds of +/- 2 for up- and down-regulated genes, respectively. Considering that the two studies that measured strain-specific *M. tb* transcriptomics were conducted by overlapping research groups (Colangeli et al., 2018; Verma et al., 2019), strain-specific DEGs were determined from a combined dataset including the following: 10 samples collected from patients cured of TB, 8 samples collected from patients who experienced TB relapse, 5 samples collected from TB-infected households with low transmission, 8 samples collected from high transmission households, and reference transcripts for *M. tb* H37Rv measured in triplicate. DEGs were determined by calculating the log2 fold-change (log2FC) in average gene expression for the four strains (cured, relapsed, low, high) compared to the average

for the reference (H37Rv). The third and fourth datasets provided the log2FC in gene expression along with the adjusted p-values for *M. tb* transcripts collected from mouse AMs at 24 hours and both AMs and IMs 14 days post-infection, respectively. This information was directly interpreted to determine DEGs for *M. tb* growing within TB-infected mouse lungs. Of note, the fourth dataset provided log2FC and adjusted p-value data based on two reference points: *M. tb* cultured in 7H9 broth or BMDM media. The fifth dataset included all samples relating to caseum conditions, and DEGs were determined by calculating the log2FC in gene expression within caseum mimics or rabbit caseum compared to a 7H9 broth control. For all log2FC-based DEG data, up- and down-regulated genes were inferred as those having values above 1 or less than -1 (indicative of 2-fold or larger changes), respectively.

4.1.2.3 Simulating condition-specific M. tb metabolism

The *M. tb* genome-scale metabolic model (GEM) known as iEK1008 (Kavvas et al., 2018) was used to simulate condition-specific metabolic responses. Of note, the objective function was set as the ATP maintenance reaction (i.e., ATPM) and not biomass based on the assumption that *M. tb* does not prioritize growth but instead, strategically modulates its metabolic activity to fluctuate between active and dormant states. The constrain-flux-regulation (CFR) algorithm (Campit & Chandrasekaran, 2020; Shen, Cheek, et al., 2019) was used to integrate curated *M. tb* transcriptomics data into iEK1008 to simulate condition-specific reaction fluxes at steady-state (**Dataset 4-1**, **Figure 4-1C**). In general terms, the CFR algorithm applies additional GEM constraints that maximize fluxes through reactions associated with up-regulated genes ("on" reactions) while minimizing fluxes through reactions controlled by down-regulated genes ("off" reactions). Of note, this method requires parameter fine tuning for the following three variables: kappa, which sets the relative weights for "off" reactions; rho, which sets the relative weights for

"on" reactions; and epsilon, which specifies the minimum flux through "on" reactions. The optimal set of CFR parameter values was determined by balancing the following three criteria: (1) minimizing the number of phenotypes simulated to have zero flux through the objective function, (2) maximizing the variability in the objective function solution across all phenotypes, and (3) maximizing the Spearman rank correlation between CARAMeL predictions against experimentally measured drug interaction scores for *M. tb* (refer to **Chapter 2** for further details). Upon inspecting all CFR parameter set permutations by varying each variable from 10^{-3} to 1 (**Table 4-1**), the following set yielded the best results and was used for all downstream analyses: kappa = 10^{-1}, rho = 10^{-1}, epsilon = 10^{-3}.

Table 4-1 Results for constrain-flux-regulation (CFR) parameter optimization. * Chosen parameters for CARAMeL-Mtb. P_{zero} = percentage of conditions with zero flux through the objective function, Var(obj) = variance in the objective function flux across conditions, R: Spearman rank correlation between model predictions and experimentally measured drug interaction data for *M. tb*.

	Kappa	Rho	Epsilon	P_{zero}	Var(obj)	R
	0.001	0.001	0.001	0.265	0	0
	0.01	0.01	0.001	0.546	0.002	0
*	0.1	0.1	0.001	0.591	0.017	0
	1	1	0.001	0.483	8.147	0
	0.001	0.001	0.01	0.524	0	0
	0.01	0.01	0.01	0.271	6E-04	0
	0.1	0.1	0.01	0.553	0.153	0
	1	1	0.01	0.554	5.721	0
	0.001	0.001	0.1	0.316	0	0
	0.01	0.01	0.1	0.355	0	0
	0.1	0.1	0.1	0.354	0.06	0
	1	1	0.1	0.577	1.629	0
	0.001	0.001	1	0.322	0	0
	0.01	0.01	1	0.371	0	0
	0.1	0.1	1	0.298	0.002	0
	1	1	1	0.51	7.781	0

4.1.3 Results

Using both the *M. tb* GEM (iEK1008) and a CARAMeL model trained on *M. tb* drug interaction data (CARAMeL-Mtb), we conducted the following four computational analyses (**Figure 4-1D**):

1. Gene essentiality (GE) prediction in caseum-mimicking media (N = 11) compared to a broth reference
2. Minimal bactericidal concentration (MBC) prediction for 12 anti-TB drugs in all caseum conditions (N = 42)
3. Clinical outcome prediction for 57 multi-drug regimens in all clinically relevant media (N = 47) compared to a no media reference
4. Drug interaction outcome prediction for all possible pairwise interactions between 43 drugs (N = 903) across all clinical strains (N = 4) and clinically relevant media (N = 47)

The purpose, implementation, and findings for each of these four analyses is further elaborated below.

The first analysis (GE prediction) aimed to pinpoint caseum-specific genetic vulnerabilities that could be experimentally validated. For this analysis, two constraints were applied onto iEK1008: single-gene deletion across all annotated genes (N = 1008) and media-specific growth inferred from transcriptomic data integration for all caseum-mimicking conditions (N = 11). GE was quantified as the relative change in the flux through the objective function (ATPM) for a gene knockout model compared to the media-corresponding gene-intact model (**Dataset 4-2**). GE for the broth reference was determined by carrying out single-gene deletion simulations without the media-specific constraint. Genes with differential essentiality in caseum-mimicking conditions compared to the broth reference were defined as those yielding more than 5% difference in the relative change in ATPM flux for at least one caseum mimic. Based on this criterium, four genes

were found to have differential essentiality between broth vs. caseum mimics (**Figure 4-2**): sucC (succinyl-CoA ligase subunit beta), sucD (succinyl-CoA ligase subunit alpha), acn (iron-regulated aconitate hydratase), and dctA (a probable C4-dicarboxylate-transport transmembrane protein). Of note, deletion of any ATP synthase subunit (N = 8) unsurprisingly yielded infeasible objective function solutions and were omitted from this analysis considering that ATPM flux is reliant on ATP synthase. The first three genes (sucC, sucD, acn) are primarily involved in the tricarboxylic acid (TCA) cycle, which is one of the three pathways directly involved in ATP production (Bonora et al., 2012). The fourth gene (dctA) is involved in the two-component system for the transport of TCA cycle intermediates (e.g., succinate) (Janausch et al., 2002). Upon inspecting the relative change in ATPM flux due to knockout of these four genes, the initial and last timepoints for *M. tb* growth in caseum mimics (days 0 and 42) are generally similar to the broth reference. This implies that metabolic adaptation to growth within a caseum-like media is a slow process, and that *M. tb* may fully adapt to this new environment within six weeks. Interestingly, the GE predictions indicate that ATP maintenance is relatively lower in *M. tb* growing within caseum-mimicking media at intermediate timepoints. Lower ATP production and/or usage may indicate that the cell is less metabolically active, thus perhaps entering a dormant state that is associated with persistent survival (Sarathy & Dartois, 2020).

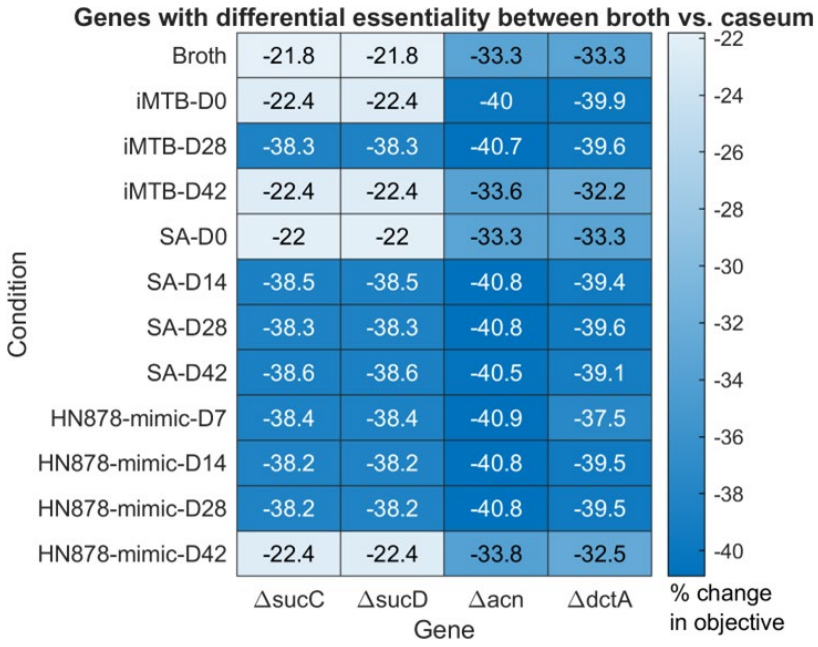

Figure 4-2 Differential gene essentiality prediction in caseum-mimicking conditions. The flux through the ATP maintenance (ATPM) reaction (set as the objective function for iEK1008) was simulated for 1008 single-gene knockout *M. tb* strains across 11 caseum-mimicking conditions (iMTB, SA, HN878) and a reference broth condition. Gene essentiality was quantified based on the relative change in the flux through the ATPM reaction due to the single-gene deletion compared to gene-intact *M. tb* simulated in the corresponding condition. Four genes (sucC, sucD, acn, and dctA) were found to have differential essentiality (>5% change in ATPM flux) in at least one caseum-mimicking condition compared to the broth reference.

The second analysis (MBC prediction) tested how well CARAMeL-Mtb could predict caseum-specific MBC by comparing experimental data against model predictions for drug-media interaction outcomes. The experimental data specifically measured the MBC_{90} (drug concentration to achieve 90% cell killing) for 12 drug treatments against *M. tb* cultured in both broth and caseum media (**Dataset 4-3**). The log2FC of the MBC_{90} in caseum compared to broth was used to validate model predictions. CARAMeL-Mtb was used to predict drug-media interaction outcomes between 12 drugs and all caseum conditions (N = 42). Model predictions, which are returned as interaction scores (IS) based on the Loewe Additivity Model (Loewe & Muischnek, 1926), were then translated into synergy ($IS < 0$) or antagonism ($IS \geq 0$) labels and compared against the equivalent translation of the experimental data ($log2FC(MBC_{90}) > 1$ indicating antagonism, $log2FC(MBC_{90}) \leq 1$ indicating synergy). The agreement (i.e., accuracy) between experimental data and model

predictions for all caseum conditions returned discrete results (**Figure 4-3**), with most conditions (N = 30) yielding high performance (accuracy > 0.9). Of note, predictions based on rabbit caseum conditions generally agreed better with experimental data compared to caseum-mimicking conditions. Within caseum mimics, the iMTB mimic timepoints yielded the most accurate predictions (accuracy > 0.9) while the HN878 mimic timepoints returned accuracies less than 0.6 (**Dataset 4-4**). These results provide one indication that the iMTB-based caseum mimic may best resemble *ex vivo* caseum lesions; however, the MBC prediction results are taken with caution due to the low sample size (N = 12).

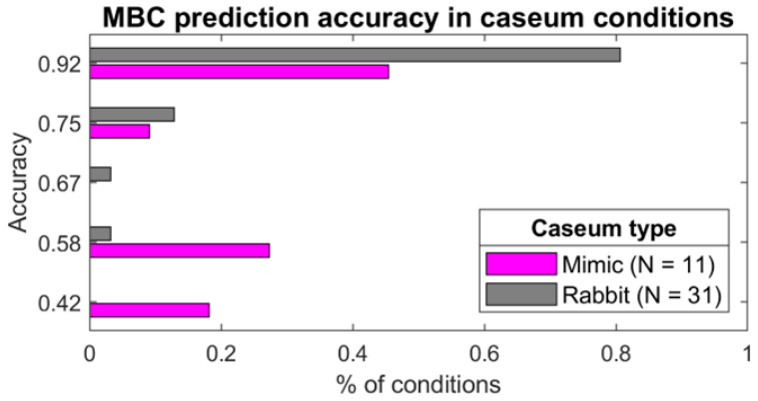

Figure 4-3 Minimal bactericidal concentration prediction in caseum conditions. The CARAMeL-Mtb model was used to predict the outcome for 12 drug-media pairs across 42 caseum conditions. Model predictions were compared against the minimal bactericidal concentration required for 90% cell killing (MBC_{90}) that was measured for the 12 drugs (see **Dataset 4-3**). Prediction agreement with experimental data was quantified as the classification accuracy, where synergy was defined by $MBC_{90} \leq 1$ and predicted interaction score (IS) < 0, while antagonism was defined by $MBC_{90} > 1$ and predicted IS ≥ 0.

The third analysis (clinical outcome prediction) evaluated whether media-specific drug interaction predictions aligned better with clinical outcomes compared to standard (i.e., drug-only) predictions. For this analysis, CARAMeL-Mtb was used to predict drug interaction outcomes for 57 multi-drug regimens for which clinical outcomes (i.e., % culture clearance after 8 weeks) were measured (Bonnett et al., 2017). Media-specific outcome predictions were generated across all clinically relevant media conditions (mouse-derived macrophage samples, caseum-mimicking media, rabbit caseum samples, N = 47), and the no media reference predictions were determined

based on ML features defined by the drug interactions alone (**Dataset 4-5**). Agreement between model predictions and actual clinical outcomes was quantified by the inverse Spearman rank correlation and a two-sample t-test of clinical outcome values grouped by the predicted class (synergy defined by IS < 0 and antagonism defined by IS >= 0). Based on these two metrics, predictions based on a rabbit caseum sample (R002-12-S4) were found to best align with clinical outcomes and outperformed the standard predictions. Specifically, both prediction sets significantly agreed with clinical outcomes based on the inverse correlation (**Figure 4-4A and Figure 4-4B**) but only predictions determined within the R002-12-S4 condition significantly differentiated clinical outcomes based on the predicted class (**Figure 4-4C and Figure 4-4D**). These findings highlight the importance of predicting drug interaction outcomes in condition-specific cases, which may better reflect combination therapy outcomes observed in the clinic.

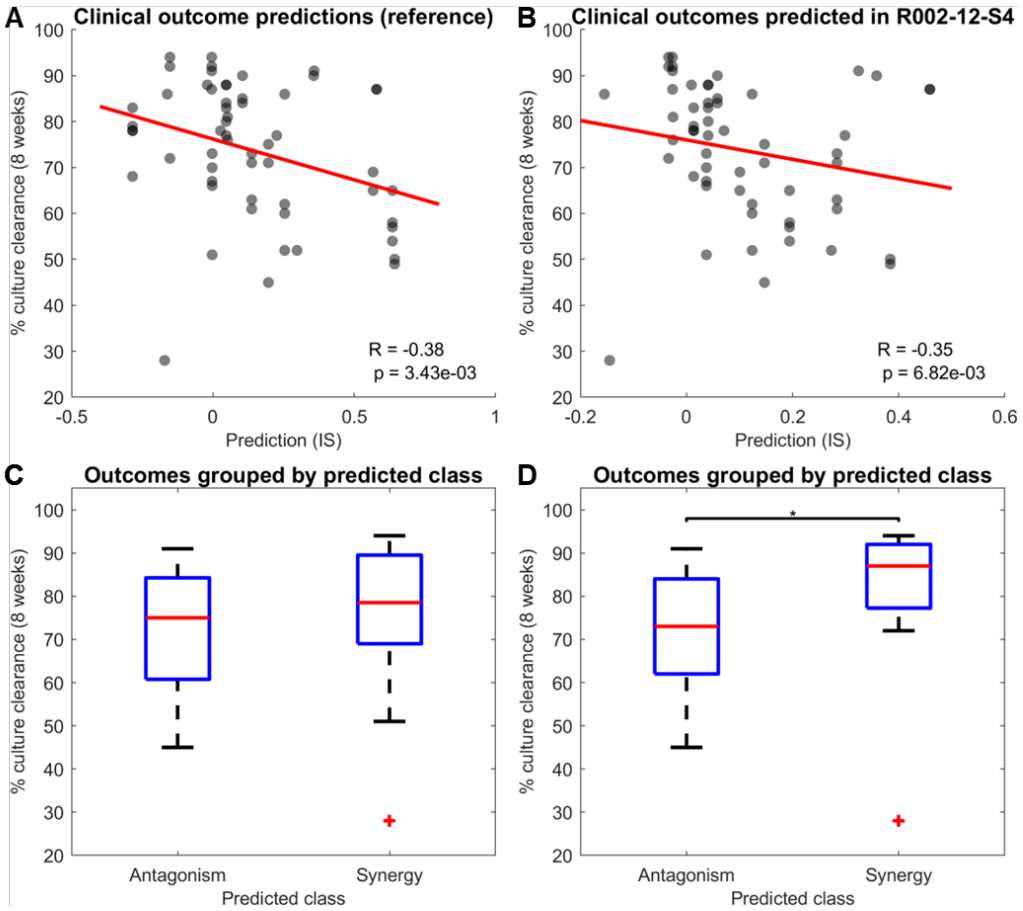

Figure 4-4 Clinical outcome predictions across 47 clinically relevant growth media conditions. Predictions for 57 multi-drug regimens were determined across 47 conditions representative of growth within macrophage cells, caseum-mimicking media, or rabbit caseum lesions. Prediction agreement with actual regimen outcomes (measured as the % culture clearance) was evaluated based on (**A-B**) the inverse Spearman rank correlation between actual and predicted outcomes and (**C-D**) a two-sample t-test measuring the difference in clinical outcomes between predicted synergy and antagonism labels. Predictions determined within a rabbit caseum condition (R002-12-S4) yielded the most accurate results (**B, D**) and are visually compared against predictions generated without a media-specific context (**A, C**).

The last analysis (prediction landscape for pairwise drug interactions across strain and media axes) aimed to explore how drug interaction outcomes differ between strain- and media-specific conditions. For this analysis, CARAMeL-Mtb was used to generate ~170,000 outcome predictions for all possible pairwise drug combinations between 43 drugs (N = 903) across four clinical *M. tb* strains (cured, relapsed, low, high) and 47 clinically relevant media conditions (**Dataset 4-6**). This prediction landscape was then inspected to carry out two main tasks: (1) evaluate how the predicted interaction outcome for INH + RIF (a central first-line treatment for

TB) changes across clinical *M. tb* strains and media conditions, and (2) identify drug combinations with significantly different predicted outcomes based on the clinical *M. tb* strain and/or the media type (defined as three groups: macrophage, caseum mimic, and rabbit caseum). For the first task, INH + RIF predictions were visualized as a strain-by-media clustered heatmap, with negative IS values indicating synergy and positive IS values indicating antagonism (**Figure 4-5**). Interestingly, this combination was predicted to be more antagonistic against the relapsed strain compared to all others, with strong antagonistic outcomes predicted in several rabbit caseum samples. These predictions align with the expected outcome for INH + RIF in the relapsed strain, considering that higher MIC values for INH and RIF were determined for clinical isolates from patients who experienced TB relapse in the originating study (Colangeli et al., 2018). Another notable finding is that INH + RIF is predicted to be synergistic against all strains when *M. tb* is simulated to reside within the macrophage and the HN878 (i.e., second SA-based) caseum mimic condition. On the other hand, this combination is predicted to be antagonistic in most rabbit caseum samples as well as the iMTB and SA caseum mimics. These prediction trends indicate that the iMTB and SA mimics may better resemble *ex vivo* caseum lesion conditions, and that *M. tb* may be more tolerant against INH + RIF within caseum compared to when it is encapsulated within macrophages.

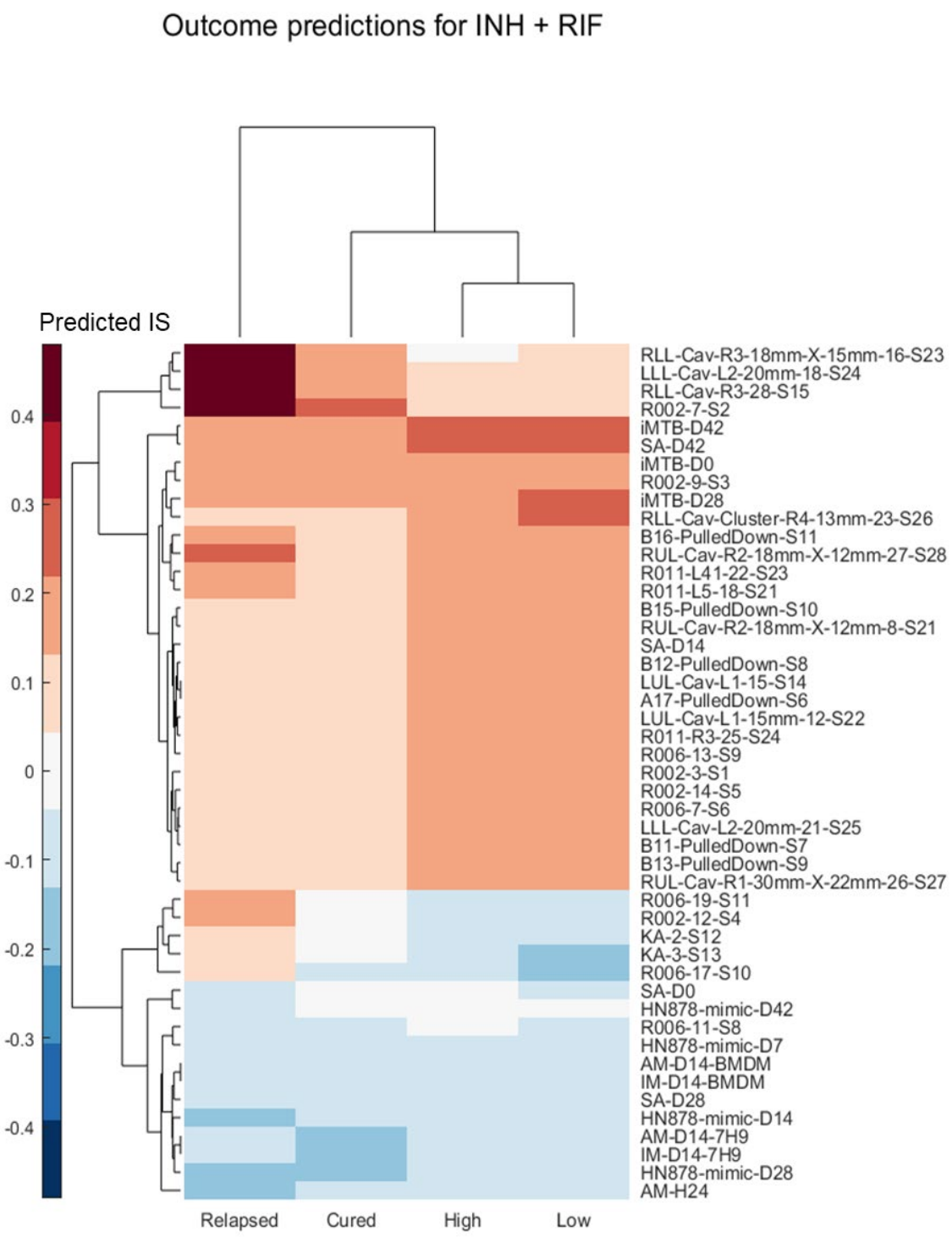

Figure 4-5 Predicted outcomes for INH + RIF across four *M. tb* strains and 47 media conditions. Strain- and media-specific outcome predictions for isoniazid (INH) combined with rifampicin (RIF) are shown as a clustered heatmap, where negative predictions for the interaction score (IS) correspond with synergy and positive prediction values correspond with antagonism.

For the second task, a two-way analysis of variance (2-way ANOVA) test was conducted for each drug combination to determine whether the predicted outcome significantly differs between clinical *M. tb* strains and/or the media condition type (macrophage vs. caseum mimics vs. rabbit caseum). Based on this analysis, 79 drug combinations were found to have a significant difference (adjusted p-value < 0.05) in the predicted outcome according to the strain type (**Figure 4-6A**). Overall, the predicted outcomes for this drug interaction subset did not reveal any variations that clearly distinguish between the simulated *M. tb* strain types (**Figure 4-6D**); however, drug interaction outcomes for the relapsed strain in several rabbit caseum conditions (N = 9, PC2 > 0.5) were predicted to be more strongly antagonistic compared to all other strain- and media-specific conditions. The 2-way ANOVA results evaluating the media effect revealed that outcome predictions for nearly all drug combinations (898 out of 903) significantly differ based on the media type (**Figure 4-6B**). Interestingly, the predicted values for this subset can differentiate media conditions into three distinct clusters (**Figure 4-6E**). The smallest cluster (N = 9, PC2 > 3) captures the relapsed strain simulated in the nine rabbit caseum conditions that were previously identified in the strain-specific analysis. The other two clusters (separated at the PC1 = 0 line) were found to have opposite drug interaction outcomes for 749 drug combinations (**Data S6**). Specifically, synergy was generally predicted for *M. tb* strains simulated within all macrophage conditions, all HN878 caseum mimics, most SA caseum mimics, and several rabbit caseum samples. On the other hand, antagonistic outcomes were predominantly predicted for all drug combinations within the remaining media conditions (all iMTB caseum mimics and most rabbit caseum samples). Based on the 2-way ANOVA test, the prediction landscape was also inspected for drug combinations for which the predicted outcome is significantly influenced by both the simulated strain and media type. This analysis revealed 37 drug combinations for which outcome predictions are significantly

impacted by both factors (**Figure 4-6C**). Interestingly, all combinations involved at least one of three fluoroquinolones (which target DNA gyrase), namely: levofloxacin (LEV), moxifloxacin (MOX), and ofloxacin (OFX1) (**Data S6**). Similar to the findings from the strain- and media-specific analyses, outcome predictions for the relapsed strain in nine rabbit caseum samples are strongly antagonistic and can distinguish these conditions from all others (**Figure 4-6F**, PC1 > 0.5 and PC2 < -0.1).

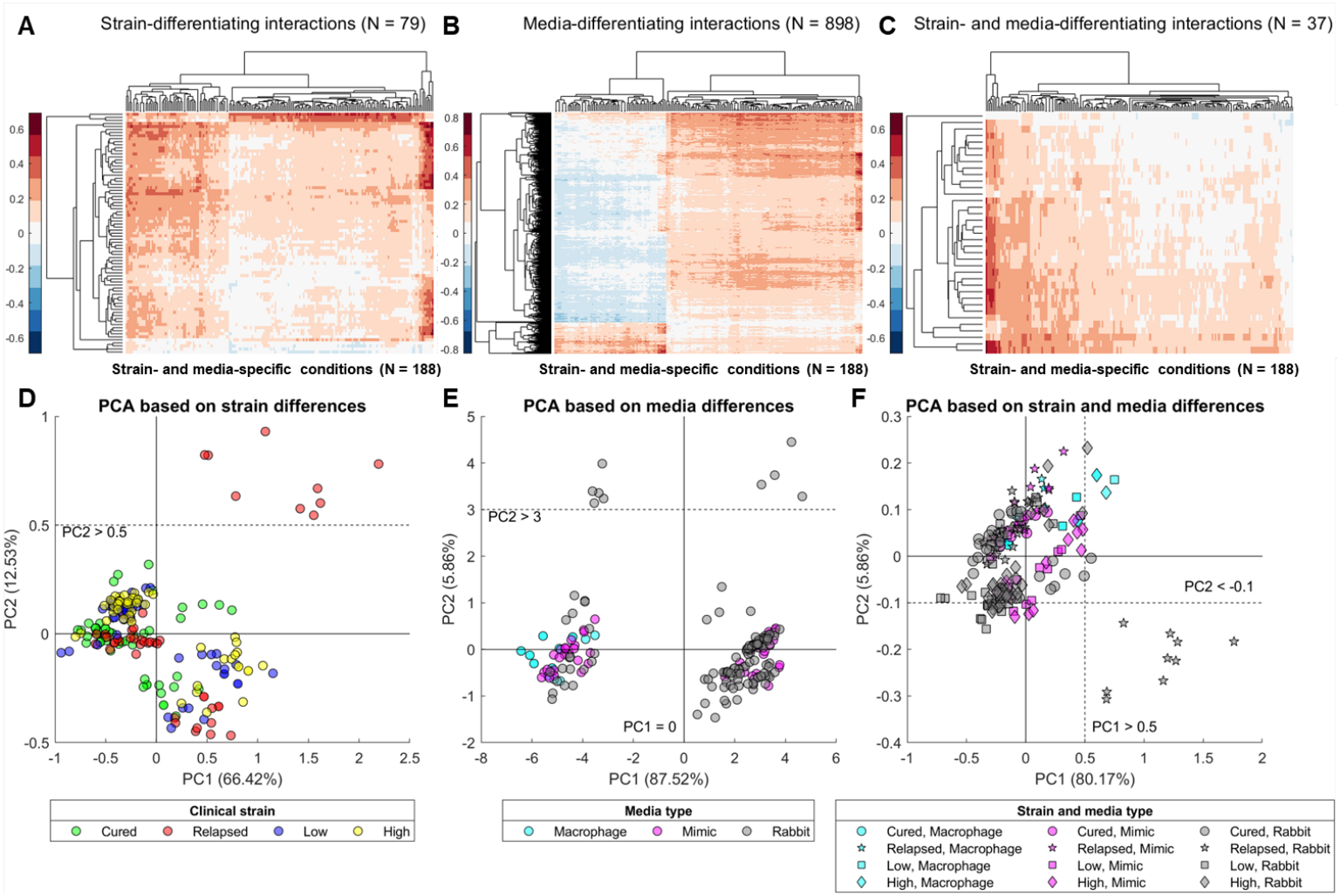

Figure 4-6 Strain- and media-differentiating drug interactions. The outcome for 903 pairwise drug combinations was predicted across four clinical *M. tb* strains and 47 clinically relevant media conditions. Strain- and/or media-differentiating drug interactions were determined based on a 2-way analysis of variance (ANOVA) test. Collectively, predicted outcomes are significantly (adjusted p-value < 0.05) differentiated based on (**A**) the *M. tb* strain for 79 drug combinations, (**B**) the media type for 898 drug combinations, and (**C**) both strain and media factors for 37 drug combinations. (**D-F**) Principal component analysis (PCA) visualization for each subset of differentiated drug interactions reveal that the media type has a stronger effect on the predicted outcome, where drug pair interactions are suggested to be predominantly antagonistic in most caseum conditions.

4.1.4 Discussion

Within this work, I sought to investigate how clinically relevant phenotypes related to *M. tb* drug resistance or tolerance levels and growth during different stages of TB progression may influence drug interaction outcomes. For this purpose, I compiled a collection of bulk *M. tb* transcriptomics data measuring gene expression changes across 94 conditions categorized into four types: response to single drug treatments, the clinical strain type, growth within mouse-derived AMs or IMs (representative of early TB infection), and growth within caseum (central structure within granulomas, indicative of later TB disease progression). By integrating this data collection into the *M. tb* GEM iEK1008, I simulated condition-specific metabolic signatures and subsequently fed this information into a CARAMeL model to develop CARAMeL-Mtb, a predictive model of strain- and media-specific drug interaction outcomes against *M. tb*.

Using both iEK1008 and CARAMeL-Mtb, I completed four computational analyses. First, I used iEK1008 to predict gene essentiality in caseum-mimicking media and determined that deletion of four genes involved in the TCA cycle (sucC, sucD, acn, and dctA) result in much lower ATP activity in caseum mimic conditions compared to *M. tb* growth in broth. This confirmed that most caseum-mimicking conditions work as expected by inducing a more dormant state for *M. tb*. Second, I applied CARAMeL-Mtb to predict drug-media interaction outcomes across all caseum conditions and found that most rabbit caseum conditions yielded predictions that best aligned with experimentally measured MBCs for 12 anti-TB drugs. Of note, predictions based on the iMTB-based caseum mimic were comparable to those determined in context of these rabbit caseum samples. Third, I employed CARAMeL-Mtb to predict multi-drug interaction outcomes across all media conditions (both AM/IM and caseum types) and determined that predictions within a rabbit caseum sample (R002-12-S4) most accurately agreed with data measuring clinical outcomes (i.e.,

% culture clearance after 8 weeks of treatment). Of note, these condition-specific predictions aligned better with clinical data compared to predictions made without media-specific context. For the fourth analysis, I generated outcome predictions for 903 drug pairs across four strain- and 47 media-specific conditions. After inspecting how this prediction landscape varies across strain- and media-specific axes, I found that the media condition more strongly influenced drug interaction outcomes. Specifically, nearly all drug interactions were predicted to be more synergistic against *M. tb* residing within macrophages and SA-based caseum-mimicking conditions compared to most rabbit caseum and iMTB-based caseum-mimicking conditions.

Overall, two main conclusions can be drawn based on the findings from the four computational analyses described above. First, combined drug treatments may be more effective during the early stages of TB disease, before the development of granulomas and casea within which *M. tb* can persist. This trend may align with a previous study which found that *M. tb* drug tolerance in caseum increases by 3- to 400-fold compared to broth culture depending on the drug (Sarathy et al., 2018). The second conclusion is that the iMTB-based caseum-mimicking media may best reflect the growth conditions within actual caseum. This is based on the fact that all iMTB caseum mimic conditions matched most rabbit caseum conditions for MBC predictions (**Data S3**) and patterns observed across the strain- and media-specific prediction landscape (**Figure 6**). However, these conclusions are currently hypothetical and require experimental or clinical validation to ascertain that they reflect actual *M. tb* behavior. Nonetheless, this work showcases how CARAMeL can be used to understand how drug interaction outcomes can be modulated in condition-specific cases.

4.2 Leveraging TACTIC to Determine Narrow-spectrum Combination Therapies for Treating Bacterial Cases of Endophthalmitis

4.2.1 Background

Endophthalmitis is one form of eye infection that is characterized by bacterial or fungal colonization of the fluidic region within the eyeball (Simakurthy & Tripathy, 2023). Compared to other types of eye infection, endophthalmitis has low incidence (Watson et al., 2018); however, this disease is considered to be a time-sensitive ophthalmic emergency as untimely or improper treatment may lead to blindness. Endophthalmitis can be classified based on the causative agent, mode of entry, and time between agent entry and infection onset. The causative agent can be bacterial or fungal in nature, and a bacterial agent can be further narrowed down based on different staining techniques (e.g., Gram stain, acid-fast stain). Endophthalmitis results from one of two modes of entry: exogeneous, which may be due to a traumatic injury or surgical operation (Fabiani et al., 2022), or endogenous, which occurs due to an underlying systemic complication such as diabetes or immunosuppression (Sadiq et al., 2015). Exogenous endophthalmitis that occurs after a surgical procedure is further classified based on time of onset post-surgery as fulminant (within four days), acute (within six weeks), or chronic (after six weeks). All these factors are critical to quickly pinpoint for an individual patient in order to prescribe the most effective treatment regimen.

Based on a retrospective study that identified the primary pathogen for more than 900 cases of endophthalmitis (Gentile et al., 2014), most infections (~85%) are caused by Gram-positive bacteria (e.g., *Staphylococcus spp*.) followed by Gram-negative bacteria (~10%, e.g., *Pseudomonas aeruginosa*) and fungal pathogens (~5%, e.g., *Candida albicans*). Depending on the causative agent, antifungal or antibacterial therapies are prescribed to clear or neutralize the

infection. For bacterial cases, two antibiotics, one broadly targeting Gram-positive pathogens (e.g., vancomycin) and the other having broad-spectrum activity against Gram-negative species (e.g., ceftazidime), are commonly given as initial treatments (Simakurthy & Tripathy, 2023). Once the causative agent is identified at the species-level, antibiotics with more narrow-spectrum activity are prescribed. Of note, the use of narrow-spectrum therapies is generally preferred to avoid any development of antibiotic resistance due to overexposure to unnecessary treatments (T. Das, 2020). Narrow-spectrum therapies are also ideal for minimizing any detrimental effects on commensal bacteria of the ocular microbiome such as *Corynebacterium* spp., which was recently shown to heighten host immunity against eye infections (St. Leger et al., 2017).

Within this study, I collaborated with Dr. Karthik Srinivasan (a visiting scholar at the U-M Kellogg Eye Center) to identify narrow-spectrum drug synergies against pathogens identified for internal cases of endophthalmitis. Specifically, I applied the TACTIC model (described in **Chapter 3**) to identify combination therapies predicted to have synergistic effect against pathogenic bacteria yet additive or antagonistic effect on commensal species. Upon validating TACTIC model predictions against expected drug interaction outcomes based on clinical and literature-based evidence, I propose a set of 48 drug pairs (out of 2,628 combinations) for further experimental and clinical investigation.

4.2.2 Methodology

Based on culture tests for internal endophthalmitis cases at the U-M Kellogg Eye Center (KEC), the following six species were identified as the primary pathogens: *P. aeruginosa*, *Pseudomonas mendocina*, *Pseudomonas putida*, *Pseudomonas stutzeri*, *Neisseria spp*., and *Gemella haemolysans*. For this set of pathogens, 15 antibiotics are typically used to clear bacterial infections (**Table 4-2**), with the combination of gatifloxacin (GAT) and moxifloxacin (MOX) used as the

first-line treatment. According to literature evidence on the ocular microbiome (Doan et al., 2016; Ozkan et al., 2017), species belonging to the *Corynebacterium*, *Propionibacterium*, and *Staphylococcus* genera are predominantly found on the eye surface of healthy individuals. Based on the combined information above, the full TACTIC model was employed to predict drug interaction outcomes for all possible pairwise combinations between 73 drugs against 12 bacterial strains (**Dataset 4-7**). The drug selection included 12 out of the 15 antibiotics used at the U-M KEC that could be accounted for by the omics data used in the TACTIC model; all other compounds were those represented within the drug interaction data that was used to train the TACTIC model. The strain selection was based on the genomes that were available in OrtholugeDB (Whiteside et al., 2013) for both pathogenic and commensal bacteria. Altogether, the 12 strains represent the following eight species: *P. aeruginosa*, *P. mendocina*, *P. putida*, *P. stutzeri*, *Neisseria gonorrhoeae*, *Neisseria meningitidis*, *Corynebacterium kroppenstedtii*, and *Propionibacterium propionicum* (**Table 4-3**). Of note, no genomes were available for species belonging to the *Gemella* genus, and the *Staphylococcus* genus was not included in the commensal set due to evidence of staphylococci commonly being the causative agent for Gram-positive endophthalmitis cases (Gentile et al., 2014).

Table 4-2 Antibiotics for treating internal cases of endophthalmitis. * used for first-line treatment. Abb.: abbreviation.

Abb.	Compound	Target	Class	Included	
AMK	Amikacin	Protein synthesis, 30S	Aminoglycoside	Yes	
GEN	Gentamicin				
CHL	Chloramphenicol		Phenylpropanoid		
CIP	Ciprofloxacin	DNA gyrase	Quinolone		*
GAT	Gatifloxacin				
LEV	Levofloxacin				*
MOX	Moxifloxacin				
OFL	Ofloxacin				
CET	Cefotaxime	Cell wall	Cephalosporin		
CFX	Cefuroxime				
CFZ	Ceftazidime				
VAN	Vancomycin		Glycopeptide		
IMI	Imipenem		Carbapenem	No	
PIP	Piperacillin		Penicillin		
TAZ	Tazobactam	Beta-lactamase	Beta-lactamase inhibitor		

Table 4-3 Bacterial strains included in TACTIC application against endophthalmitis. Ten strains belonging to the *Pseudomonas* and *Neisseria* genera were designated as pathogenic agents while the remaining two strains were representative of commensal species that naturally reside in the ocular microbiome.

Organism	Strain	Gram Stain	Group
Pseudomonas aeruginosa	DK2	Negative	Pathogen
	NCGM2.S1		
	PA7		
	UCBPP-PA14		
Pseudomonas mendocina	ymp		
Pseudomonas putida	KT2440		
	S16		
Pseudomonas stutzeri	DSM 10701		
Neisseria gonorrhoeae	FA 1090		
Neisseria meningitidis	MC58		
Corynebacterium kroppenstedtii	DSM 44385	Positive	Commensal
Propionibacterium propionicum	F0230a		

4.2.3 Results

In total, the TACTIC model generated more than 30,000 predictions that account for 2,628 unique drug pairs across 12 strains. Before inspecting this prediction landscape for interactions with

narrow-spectrum synergy, model predictions for the first-line treatment (GAT + MOX) as well as drug combinations experimentally tested against *P. aeruginosa* based on literature were evaluated. Experimental data was collected from two studies that measured the efficacy of antibiotic combinations against clinical or drug-resistant strains of *P. aeruginosa*. The first study, led by Kapoor & Murphy (P. Kapoor & Murphy, 2018), quantified the fractional inhibitory concentration (FIC) for five drug pairs, out of which three could be compared against TACTIC model predictions. The second study, conducted by Olsson et al. (Olsson et al., 2020), reported the class-based interaction outcome (i.e., synergy or antagonism) for polymyxin B (PMB) combined with 13 other antibiotics; out of 13 combinations, nine could be compared against TACTIC model predictions. **Figure 4-7** shows the predicted interaction scores across all strains for the 13 drug combinations that could be compared against clinical or literature-based evidence. Three conclusions were drawn from these results:

1. GAT + MOX is predicted to be mildly synergistic against all *P. aeruginosa* and *Neisseria* strains, but antagonistic for the other *Pseudomonas* species. For the commensal strains (*C. kroppenstedtii* and *P. propionicum*), this combination is predicted to be additive (i.e., neutral). These predictions indicate that GAT + MOX may be an effective first-line therapy for cases of endophthalmitis primarily caused by *P. aeruginosa* or *Neisseria spp*. but not for other cases. If these species-specific outcomes are shown to be true in the clinic, GAT + MOX may not be the optimal first-line treatment due to its incomplete and weak coverage against all identified pathogenic strains.
2. The three combinations from the Kapoor & Murphy study that could be compared against TACTIC predictions are ceftazidime (CFZ) + ciprofloxacin (CIP), CFZ + tobramycin (TOB), and CIP + TOB. Amongst these three, CFZ + TOB was the only combination to

experimentally show synergy for two out of four clinical strains of *P. aeruginosa*. TACTIC model predictions indicate that CFZ + TOB is relatively more synergistic than CFZ + CIP or CIP + TOB, thus aligning with literature-based trends.

3. Out of the 13 drug combinations involving PMB, the TACTIC model correctly predicts that PMB yields stronger synergies when paired with aztreonam (AZT), fosfomycin (FOS), minocycline (MIN), and rifampicin (RIF) compared to other drugs.

The conclusions above indicate that the predictions generated by the TACTIC model can be generally trusted and may align with experimental and/or clinical outcomes.

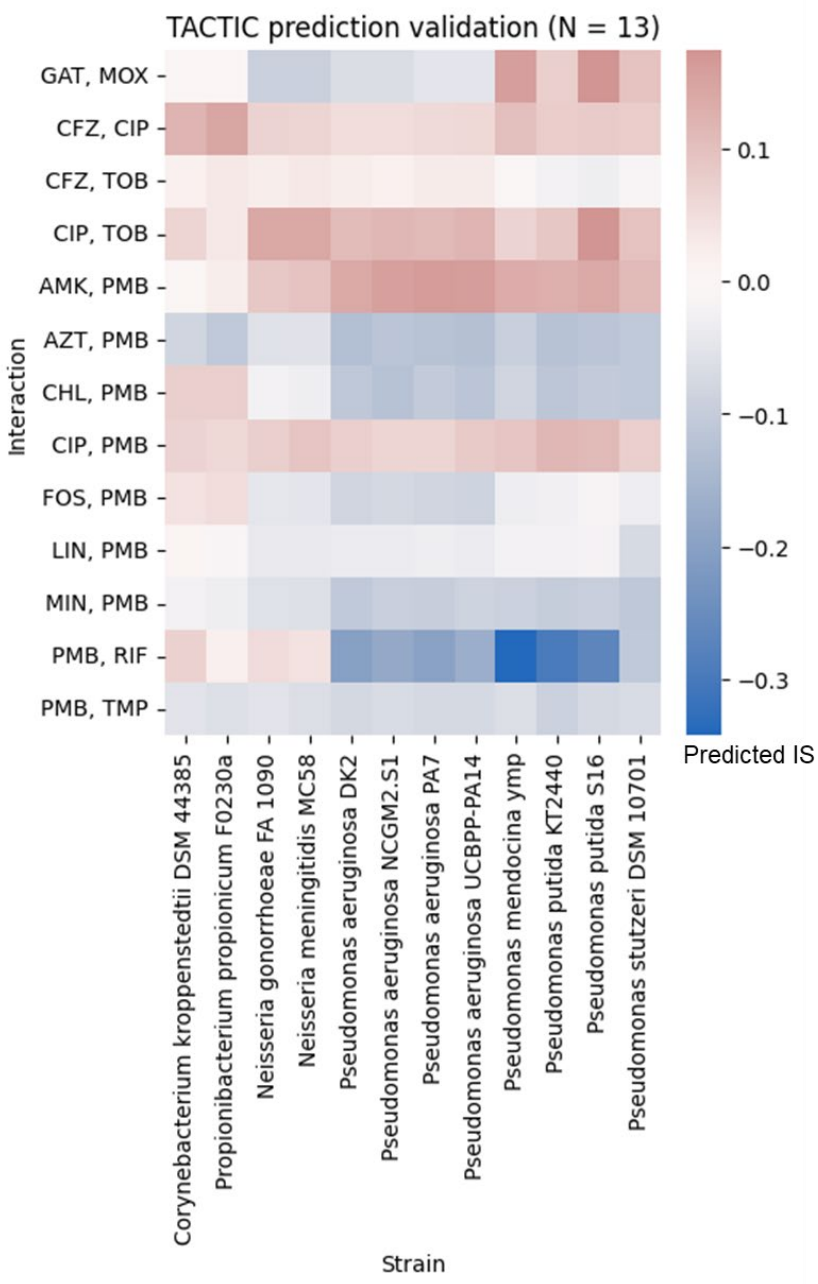

Figure 4-7 TACTIC prediction of 13 clinically or experimentally measured drug interactions. TACTIC model predictions across two commensal residents of the ocular microbiome and ten causative agents for clinical cases of endophthalmitis for 13 drug interactions with clinical or experimental data. Negative (blue) predicted interaction scores (IS) indicate synergy while positive (red) predictions indicate antagonism. Refer to **Dataset 3-2** for more information on abbreviated drug names.

Based on the assurance provided above, I next inspected the prediction landscape for drug combinations with narrow-spectrum synergy against pathogenic strains. To conduct this investigation, I first assessed the correlation between model predictions generated for different

strains (**Figure 4-8**). As expected, predictions for different *P. aeruginosa* strains were highly correlated with one another (R ~ 1). Predictions for the two *Neisseria* strains were also highly correlated (R ~ 1). Interestingly, the correlation between *P. aeruginosa* predictions and those for other *Pseudomonas* species was lower (R ~ 0.9) than the correlations determined within the latter set (R ~ 0.95). Importantly, the predictions for *C. kroppenstedtii* and *P. propionicum* correlated well with each other (R ~ 0.95) and were dissimilar from predictions for all pathogenic strains (R < 0.9). These trends indicated that drug combinations with narrow-spectrum synergy against pathogenic bacteria may indeed exist within the prediction landscape generated by the TACTIC model. Drug combinations with narrow-spectrum synergy against pathogenic strains were defined as those having a predicted IS ≥ 0 (indicative of outcomes towards antagonism) for commensal strains while having a predicted IS < 0 (indicative of outcomes towards synergy) for all pathogenic strains. Based on these criteria, I identified 48 out of 2,628 possible drug combinations having narrow-spectrum synergy against pathogenic bacteria (**Figure 4-9**, **Dataset 4-8**). A quick inspection of the ten most synergistic drug interactions against pathogenic strains (most negative mean predicted IS, top ten rows in **Figure 4-9**) revealed a few combinations that involve gentamicin (GEN) and CFZ, which are commonly used to treat endophthalmitis and are more effective against Gram-negative pathogens (Benz et al., 2004). Interestingly, the remaining top synergistic set includes combinations involving at least one antibiotic active against the bacterial cell wall (mechanism of CFZ activity) but these combinations have not yet been investigated in treating endophthalmitis caused by bacterial agents. Considering that the effectiveness of CFZ in treating endophthalmitis has steadily decreased over the past few decades (Joseph et al., 2019), the proposed set of 48 drug interactions predicted to be selectively synergistic against *Pseudomonas* and *Neisseria* species may be worth exploring for clinical use.

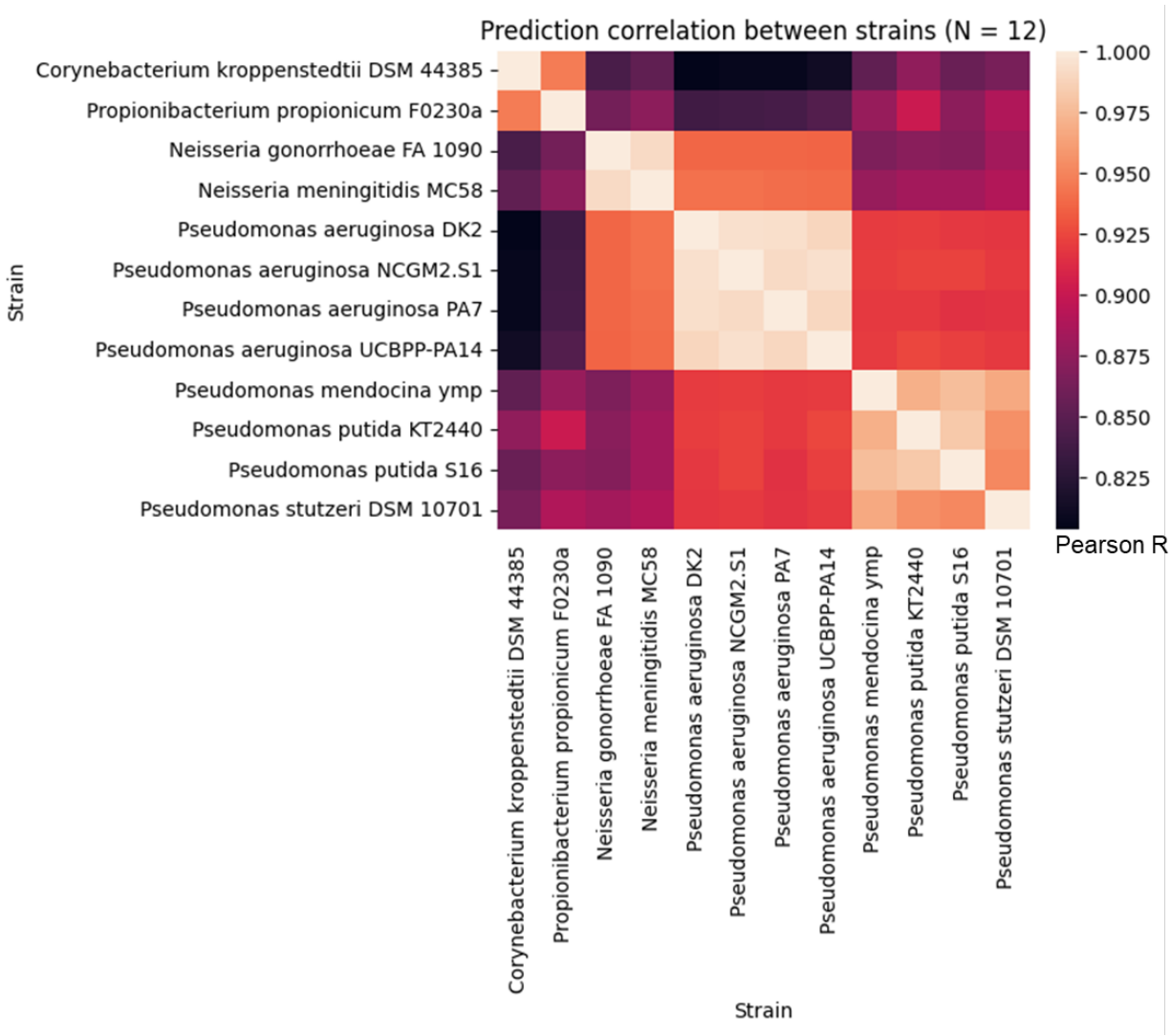

Figure 4-8 Correlation between species-specific drug interaction predictions. Heatmap visualization of the Pearson correlation between drug interaction score predictions for two commensal strains of the ocular microbiome and ten pathogenic strains in clinical cases of endophthalmitis.

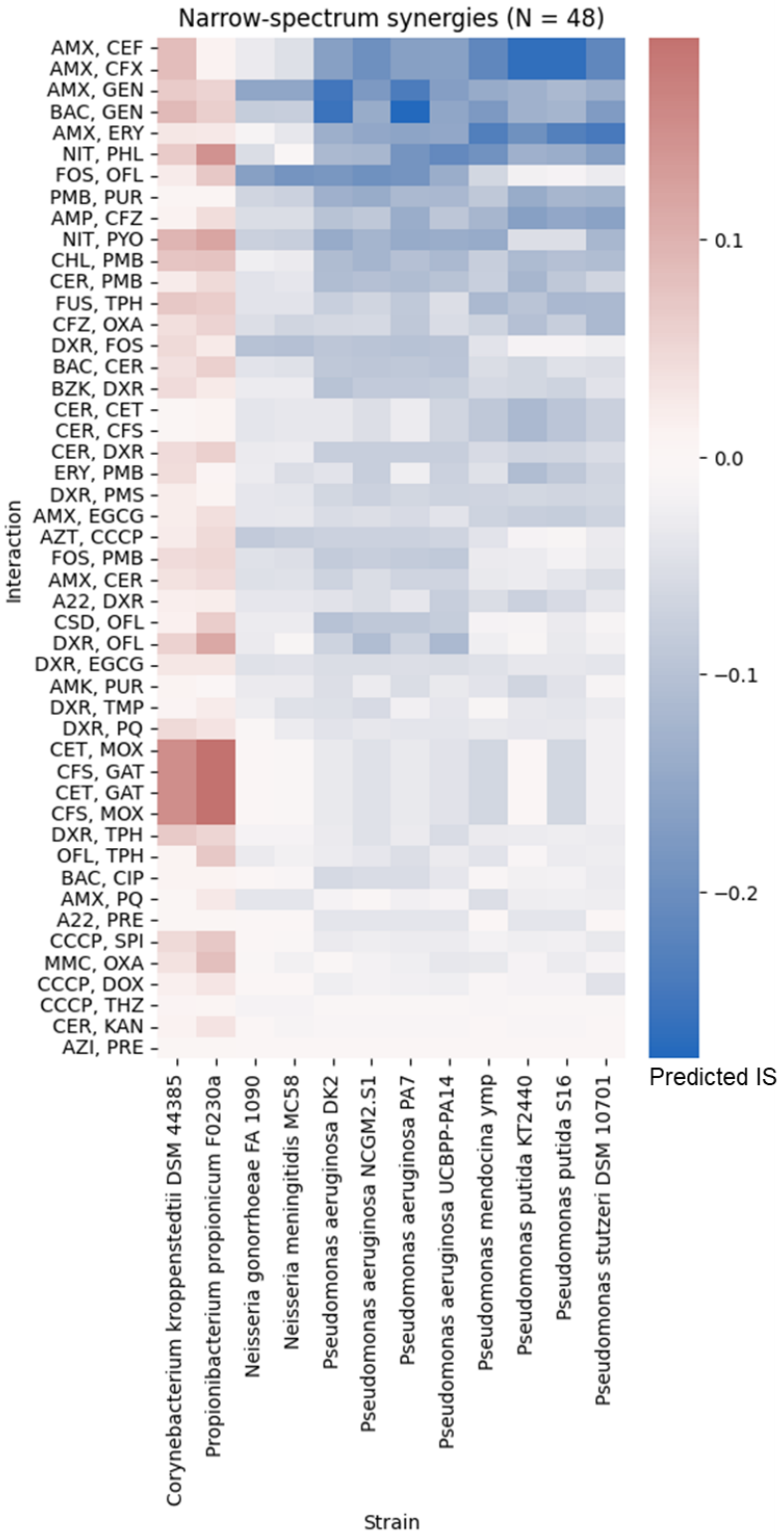

Figure 4-9 Drug combinations predicted to have arrow-spectrum synergy against pathogenic strains. Out of 2,628 drug combinations, 48 were predicted to have narrow-spectrum synergy against causative agents for endophthalmitis (predicted IS < 0 against pathogenic strains, predicted IS ≥ 0 for commensal strains). Refer to **Dataset 3-2** for more information on abbreviated drug names.

4.2.4 Discussion

For this project, I sought to identify drug combinations that are selectively synergistic against causative agents for internal cases of endophthalmitis at the U-M KEC. To complete this task, I applied the fully trained TACTIC model (described in **Chapter 3**) to generate drug interaction outcome predictions across a selection of pathogenic and commensal bacteria of the eye. In collaboration with Dr. Karthik Srinivasan at the U-M KEC, we identified species belonging to the *Pseudomonas* and *Neisseria* genera to be the primary pathogens for internal cases of endophthalmitis (**Table 4-3**). Based on literature characterizing the normal ocular microbiome (Doan et al., 2016; Ozkan et al., 2017) and genomic information available in OrtholugeDB (Whiteside et al., 2013), I designated *C. kroppenstedtii* and *P. propionicum* as representative commensals of the eye microbiome.

In total, I generated outcome predictions for 2,628 drug pairs across a panel of 12 bacterial strains (10 pathogens and 2 commensals). Before scanning this prediction landscape for narrow-spectrum synergies, I validated that TACTIC model predictions aligned with observed outcomes for internal cases of endophthalmitis treated with GAT + MOX as well as experimental data measuring drug interaction outcomes for clinical strains of *P. aeruginosa* (P. Kapoor & Murphy, 2018; Olsson et al., 2020). I then inspected the prediction landscape for drug interactions predicted to be synergistic ($IS < 0$) against pathogenic strains and additive or antagonistic ($IS \geq 0$) against commensal strains. Based on these two criteria, I identified 48 drug combinations that are selectively synergistic against pathogens that were identified for internal cases of endophthalmitis. A few of the most selectively synergistic drug combinations (AMoXicillin + GEN, BACitracin + GEN, AMPicillin + CFZ) involve antibiotics that are commonly used to treat endophthalmitis (Benz et al., 2004). Although the remaining combinations of the 48-set of narrow-spectrum

synergy involve antibiotics that have not previously been investigated for treating endophthalmitis, they serve as a manageable starting point for discovering new combination therapies that effectively treat bacterial cases of endophthalmitis.

4.3 Datasets

All supplementary data files from this chapter are available in the following external location:

https://www.dropbox.com/s/m8zwd7297ho5yh8/Chung_Carolina_Dissertation_Data.xlsx?dl=0

Dataset 4-1 Curated and processed bulk *M. tb* transcriptomics data used for CARAMeL-Mtb (1009 x 95).

Dataset 4-2 Gene essentiality (GE) predictions for all iEK1008 genes across all caseum-mimicking conditions (N = 11) and a broth control, with values scaled by media-corresponding gene-intact references. Includes metadata on gene names, description, and associated pathways (1010 x 16).

Dataset 4-3 Drug-media interaction outcome predictions made with CARAMeL-Mtb for 12 anti-TB drugs across all caseum conditions (N = 42). Includes metadata on drug names and MBC_{90} measurements in broth and caseum (13 x 47).

Dataset 4-4 Drug-media prediction accuracy against MBC_{90} measurements across all caseum conditions (N = 42). Includes information on the caseum condition type (mimics vs. rabbit) (43 x 3).

Dataset 4-5 Multi-drug interaction outcomes predictions made by CARAMeL-Mtb for 57 regimens across all clinically relevant media conditions (N = 47) and a no media reference. Includes metadata on clinical outcome measurements (58 x 50).

Dataset 4-6 Pairwise drug interaction outcome predictions made by CARAMeL for all possible drug pairs among 43 drugs (N = 903) across four clinical strain types and 47 media conditions. Includes p-values calculated from a 2-way ANOVA test evaluating strain-only, media-only, or strain-media effect on the predicted outcome (904 x 192).

Dataset 4-7 Pairwise drug interaction outcome predictions made by TACTIC for all possible drug pairs among X drugs (N = 2628) across 12 strains related to clinical cases of endophthalmitis or the normal ocular microbiome (2629 x 13).

Dataset 4-8 The set of 48 drug pairs predicted to have narrow-spectrum synergy activity against pathogenic strains for clinical cases of endophthalmitis (49 x 13).

Chapter 5 Conclusions and Future Directions

5.1 Summary of Findings

Broadly speaking, my dissertation research focused on tackling the problem of antibiotic resistance (AR), a major global health crisis with detrimental consequences if left unaddressed (Centers for Disease Control and Prevention, 2019; World Health Organization, 2014). Specifically, I set out to optimize the design of antibiotic combination therapies, which offer a promising solution to AR but are difficult to translate into clinical use (Farha & Brown, 2019; Tyers & Wright, 2019). The challenges implicated with developing this therapeutic option include: (a) the exponential explosion in the combinatorial space to search as the number of drugs and dosage levels to screen increases, (b) the heterogeneity in bacterial drug response due to cell-specific genetic and phenotypic states, and (c) the limited mechanistic insight that empirical methods for combination therapy design currently offer. To overcome these barriers, I developed two computational methods that predict drug interaction outcomes in precise cell state and cellular growth contexts.

The first approach is CARAMeL (**Chapter 2**), which stands for *Condition-specific Antibiotic Regimen Assessment using Mechanistic Learning*. This approach leverages genome-scale metabolic models (GEMs) (Price et al., 2004) and machine learning (ML) (Greener et al., 2021) to generate condition-specific drug interaction outcome predictions. This is computationally achieved by simulating the metabolic response to individual conditions (e.g., single drug treatments, growth in minimal media) and using this data to engineer ML features for a drug interaction to predict its outcome (e.g., synergy, additivity, or antagonism). Although similar

computational methods that predict drug synergy have been developed before (Chandrasekaran et al., 2016; Cokol et al., 2018; Ma et al., 2019), I show that CARAMeL models generate comparable and sometimes more accurate predictions than previous models. I also demonstrate how CARAMeL can be used to predict media-specific, single-cell, and sequential drug interaction outcomes, which had not been previously done with similar methodologies. Most importantly, I showcase how CARAMeL can be leveraged to expedite and optimize combination therapy design by identifying 24 out of 528 (<5%) drug combinations predicted to be synergistic against *Escherichia coli* across different media conditions and regardless of simultaneous or sequential prescription. Of note, some of these combinations possessed evidence of clinical use.

The second approach that I developed is TACTIC (**Chapter 3**), which stands for *Transfer learning And Crowdsourcing to predict Therapeutic Interactions Cross-species*. As the name implies, this approach implements transfer learning (Torrey & Learning, 2010) and crowdsourcing (Vaughan, 2018) to generate strain-specific drug interaction outcome predictions. This is accomplished by integrating data from multiple organisms (e.g., *E. coli*, *Mycobacterium tuberculosis*) and transferring this information to other organisms (e.g., *Acinetobacter baumannii*, *Staphylococcus aureus*) via orthology mapping to engineer ML features used for predictive modeling. Based on a data collection of drug interaction outcomes measured across 12 bacterial strains, I show that TACTIC models can better predict drug interaction outcomes for unseen microbes compared to INDIGO (Chandrasekaran et al., 2016), a prior computational approach that serves as the inspiration for TACTIC. Using a TACTIC model trained on the entire cross-species data collection, I predict outcomes for 3,828 drug interactions across 18 strains representative of commensal (i.e., health-promoting) or pathogenic (i.e., disease-causing) bacteria. I then inspect this prediction landscape to identify substantially smaller sets of drug interactions (N < 100)

predicted to have narrow-spectrum synergy against all pathogens or specific groups of pathogens (e.g., Gram-negative species, non-tuberculous mycobacteria).

Beyond developing CARAMeL and TACTIC and demonstrating use cases for each one, I apply both approaches to predict combined drug treatment outcomes against causative agents for tuberculosis (TB) (Pai et al., 2016) and endophthalmitis (Simakurthy & Tripathy, 2023) (**Chapter 4**). For the first application regarding TB, I use CARAMeL to predict drug interaction outcomes for clinical strains of *M. tuberculosis* (*M. tb*) simulated at different stages of TB progression. CARAMeL model predictions indicate that drug interaction outcomes differ based on both strain- and growth condition-specific factors, although the latter was found to have a larger impact on predicted outcomes. Specifically, changes in predicted outcomes across growth conditions (proxy for TB progression) imply that therapeutic interventions are most effective when given at early infection timepoints before *M. tb* can adapt to external stresses. This hypothesis aligns with previous studies that have shown greater *M. tb* resistance and tolerance against anti-TB drugs within conditions representative of late-stage TB infection (Gomez & McKinney, 2004; Sarathy et al., 2018; Stewart et al., 2003), often leading to incomplete infection clearance and TB relapse.

For the second application regarding endophthalmitis, I use the TACTIC model developed in **Chapter 3** to predict drug interaction outcomes against bacterial agents that cause endophthalmitis (i.e., *Pseudomonas spp*.) as well as bacterial species believed to serve commensal roles within the ocular microbiome (i.e., *Corynebacterium spp.*) (St. Leger et al., 2017). This selection of organisms was specifically chosen to screen for combination therapies with the potential of achieving precise efficacy against internal cases of endophthalmitis at the U-M Kellogg Eye Center. Out of 2,628 drug interactions that were screened, I identified 48 (~2%) that are predicted to be selectively synergistic against pathogenic strains. Of note, this set includes drug

combinations involving antibiotics that are commonly used to treat endophthalmitis (Benz et al., 2004); but most importantly, this reduced set provides a manageable starting point for developing new combination therapies effective against bacterial cases of endophthalmitis.

CARAMeL and TACTIC are tangible outcomes from my dissertation work. Within the scope of my research, I demonstrated how each approach could be leveraged to discover more effective regimens against tuberculosis and endophthalmitis, two infectious diseases that are clinically challenging to treat. Both computational approaches have the potential to aid in the discovery of new combination therapies with precise efficacy against other infectious diseases, with the long-term goal of mitigating antibiotic resistance. To this end, CARAMeL and TACTIC are both publicly available in adaptable formats that are primed for extended use by other research groups to optimize the design of antibiotic combination therapies.

5.2 Limitations

Though CARAMeL and TACTIC serve as novel methodologies for designing antibiotic combination therapies, it is critical to highlight several data- and computation-related limitations that pertain to both approaches. Data-related issues include the need for integrating more omics data and consolidating discrepancies in the quantification of drug interaction outcomes. Regarding omics data integration, additional information on the drug response for other bacteria that are phylogenetically different from *E. coli* or *M. tuberculosis* (e.g., *S. aureus*) may lead to more accurate predictions for strain-specific drug interaction outcomes. The inclusion of other omics data types (e.g., proteomics) may also help to gain a more holistic picture of the bacterial response to combined drug treatments. Regarding the quantification of drug interaction outcomes, a consensus on which mathematical model to use (e.g., Loewe or Bliss) and what drug dosages to explore (e.g., linear or logarithmic dilutions) does not currently exist. Disagreement over these

choices can lead to different measured outcomes for the same drug interaction, which hinders the development of an accurate predictive model for drug synergy. Computational tools built to automate outcome quantification have recently been introduced to address this concern (Ianevski et al., 2020; Wooten et al., 2021). It is worth exploring whether the unanimous use of one of these tools to quantify drug interactions could improve the utility of aggregated datasets for the computational design of combination therapies.

Regarding computation-related limitations of CARAMeL and TACTIC, both approaches do not yet implement the full capacity for modeling using GEMs and ML. Specifically, the metabolic response to different conditions (e.g., drug treatment) is only simulated at steady-state in the CARAMeL approach. This constraint can only capture the metabolic state of a cell at a single timepoint (i.e., when the organism has adapted to the given condition); hence, it is not suitable for considering dynamic changes in the bacterial drug response. This may explain why CARAMeL predictions for sequential drug interaction outcomes were moderately accurate in comparison to predictions for simultaneous interactions. Several methods that can simulate dynamic metabolic changes using GEMs exist and could be incorporated into the CARAMeL approach to improve the prediction of sequential therapy outcomes (Campit & Chandrasekaran, 2020; Chung et al., 2021; N. E. Lewis et al., 2012). Regarding the ML aspect in CARAMeL and TACTIC, both approaches were developed using random forests (RF) (Breiman, 2001) as the foundational algorithm. Though RF was chosen due to its advantages as a white-box (i.e., explainable) ensemble method that generates robust predictions, it has limited predictive power for unseen situations (e.g., drug combinations involving drugs that it has not been trained on). As a traditional ML method, RF also relies heavily on manual feature engineering. To overcome these limitations, deep learning (DL) algorithms could be used to develop next-generation CARAMeL

and TACTIC models. DL methods provide two advantages over RF: (1) the prediction accuracy improves as more data is integrated into the model, and (2) DL methods can learn to identify informative features from the input data, therefore alleviating some of the effort required in feature engineering (LeCun et al., 2015). It is worth noting that DL methods are more complex, and hence, incur large computation costs and are difficult to interpret. Nonetheless, using DL methods as a new foundation for CARAMeL and TACTIC models holds great potential for generating more accurate predictions for unseen drug interactions. This, in turn, may promote the establishment of predictive modeling as a standard step in the pipeline for designing and developing new antibiotic combination therapies.

5.3 Future Directions for Advancing Combination Therapy Discovery and Design

5.3.1 CARAMeL and TACTIC for anti-fungal and anti-cancer combination therapy design

Within the scope of this work, CARAMeL and TACTIC were developed to specifically aid the design of antibiotic combination therapies. Beyond the bacterial space, the use of combination therapies to overcome drug resistance is a strategy that can be adopted to tackle other disease areas. Here I briefly discuss two diseases for which CARAMeL and TACTIC could be extended to: drug-resistant fungal infections and cancer.

Regarding fungal infections, the Centers for Disease Control and Prevention have begun to recognize certain fungi as emerging public health concerns, namely: azole-resistant *Aspergillus fumigatus* and multi-drug resistant *Candida auris* (Centers for Disease Control and Prevention, 2019). Similar to antibiotic-resistant pathogens, resistant strains of *A. fumigatus* and *C. auris* pose serious threats that could unexpectedly claim thousands of lives annually if left unchecked (Rayens & Norris, 2022). The concern over rising drug resistance in fungal pathogens is exacerbated by the fact that, compared to antibiotics, few anti-fungal treatment options are available (McDermott,

2022). Within the past few decades, there has been growing interest in designing combination therapies to more effectively treat fungal infections (Baddley & Pappas, 2005; Johnson & Perfect, 2010; Kontoyiannis & Lewis, 2004). At the same time, drug response and drug interaction data have been measured in tangentially related fungal species such as *Saccharomyces cerevisiae* and *Candida albicans* (Shrestha et al., 2015; Wildenhain et al., 2016). Considering that these data types have not yet been widely measured in *A. fumigatus* nor *C. auris*, the TACTIC approach could be integrated with *S. cerevisiae* and *C. albicans* data to predict drug interaction outcomes against drug-resistant fungal pathogens, and in turn, deduce combinations to explore as potential therapeutic options to treat fungal infections.

The search for combination therapy to treat cancer dates back farther than its application to address antibiotic resistance, with the first combination therapy suggested for clinical use proposed in 1965 to treat leukemia (Frei E 3rd et al., 1965). Since then, combination therapy design has been a mainstay strategy for combating various cancer types (Mokhtari et al., 2017; Webster, 2016). Operating based on the understanding that cancer arises from dysregulation of multiple signaling pathways, anti-cancer combination therapy design is traditionally guided by empirical knowledge of how to target multiple pathways in parallel (Jia et al., 2009; Mokhtari et al., 2017). However, the successful clinical translation of combination therapy candidates identified *in vitro* is extremely low (Schmidt et al., 2023), possibly due to the complexity and heterogeneity in cancer cell response to drug treatments. Considering the abundance of drug response and drug interaction data that is available for multiple cancer types (Barretina et al., 2012; H. Liu et al., 2020; Shtar et al., 2022), coupled with the systemic-level of complexity and heterogeneity entailed in this disease area (Junttila & De Sauvage, 2013; Vasan et al., 2019), the CARAMeL approach may prove to be useful in designing anti-cancer combination therapies with these factors in mind.

5.3.2 Accounting for host-specific factors during combination therapy design

A critical component that is lacking in CARAMeL and TACTIC, as well as other computational methods for combination therapy design, is the consideration of host-specific factors that influence bacterial or cancer cell response to treatment. Here I highlight the importance of understanding how the host-specific microbiome and immune system interact with disease-causing cells. In context of AR, the microbiome may play a spectrum of roles where on one end, it may provide a reservoir of antibiotic resistance genes that bacterial pathogens could adopt via horizontal gene transfer (Baron et al., 2018). On the other end, further understanding of the host microbiome could be harnessed to more effectively clear problematic infections, such as the case where fecal microbiota transplantation (FMT) was shown to effectively overcome recurring infection by *Clostridium difficile* (Bakken et al., 2011). In tandem with the microbiome, the host immune system also plays a significant role in fighting against malignant cells. In relation to AR, there is interest in investigating the use of immune-boosting compounds that could indirectly fight pathogens by disarming their virulence factors and enhancing immune-based bactericidal activity (Munguia & Nizet, 2017). In fact, immunotherapy (i.e., the stimulation of the immune system to treat a disease) has widely gained traction for the treatment of cancer within the past decade (Couzin-Frankel, 2013). Considering the unexpected yet successful stories of FMT and cancer immunotherapy, the role of the host microbiome and immune system is warranted for antibiotic and anti-cancer drug design. Hence, computational methods like CARAMeL and TACTIC, which aim to optimize combination therapy design, would benefit from incorporating host-specific information. Ultimately, this advancement may lead to more accurate identification of promising therapeutic candidates that are clinically proven to overcome drug resistance.

Bibliography

American Thoracic Society. (2005). Guidelines for the management of adults with hospital-acquired, ventilator-associated, and healthcare-associated pneumonia. In *American Journal of Respiratory and Critical Care Medicine* (Vol. 171, Issue 4). Am J Respir Crit Care Med. https://doi.org/10.1164/rccm.200405-644ST

Ankomah, P., Johnson, P. J. T., & Levin, B. R. (2013). The Pharmaco –, Population and Evolutionary Dynamics of Multi-drug Therapy: Experiments with S. aureus and E. coli and Computer Simulations. *PLOS Pathogens*, *9*(4), e1003300. https://doi.org/10.1371/JOURNAL.PPAT.1003300

Baddley, J. W., & Pappas, P. G. (2005). Antifungal combination therapy: Clinical potential. *Drugs*, *65*(11), 1461–1480. https://doi.org/10.2165/00003495-200565110-00002

Bakken, J. S., Borody, T., Brandt, L. J., Brill, J. V., Demarco, D. C., Franzos, M. A., Kelly, C., Khoruts, A., Louie, T., Martinelli, L. P., Moore, T. A., Russell, G., & Surawicz, C. (2011). Treating Clostridium difficile Infection With Fecal Microbiota Transplantation. *Clinical Gastroenterology and Hepatology*, *9*(12), 1044–1049. https://doi.org/10.1016/J.CGH.2011.08.014

Balaban, N. Q., Gerdes, K., Lewis, K., & McKinney, J. D. (2013). A problem of persistence: still more questions than answers? *Nature Reviews Microbiology 2013 11:8*, *11*(8), 587–591. https://doi.org/10.1038/nrmicro3076

Barberis, I., Bragazzi, N. L., Galluzzo, L., & Martini, M. (2017). The history of tuberculosis:

from the first historical records to the isolation of Koch's bacillus. *Journal of Preventive Medicine and Hygiene*, *58*(1), E9. /pmc/articles/PMC5432783/

Baron, S. A., Diene, S. M., & Rolain, J. M. (2018). Human microbiomes and antibiotic resistance. *Human Microbiome Journal*, *10*, 43–52. https://doi.org/10.1016/J.HUMIC.2018.08.005

Barretina, J., Caponigro, G., Stransky, N., Venkatesan, K., Margolin, A. A., Kim, S., Wilson, C. J., Lehár, J., Kryukov, G. V., Sonkin, D., Reddy, A., Liu, M., Murray, L., Berger, M. F., Monahan, J. E., Morais, P., Meltzer, J., Korejwa, A., Jané-Valbuena, J., … Garraway, L. A. (2012). The Cancer Cell Line Encyclopedia enables predictive modelling of anticancer drug sensitivity. *Nature*, *483*(7391), 603–607. https://doi.org/10.1038/nature11003

Baym, M., Stone, L. K., & Kishony, R. (2016). Multidrug evolutionary strategies to reverse antibiotic resistance. *Science*, *351*(6268), aad3292–aad3292. https://doi.org/10.1126/science.aad3292

Benjamini, Y., & Hochberg, Y. (1995). Controlling the False Discovery Rate: A Practical and Powerful Approach to Multiple Testing. *Journal of the Royal Statistical Society: Series B (Methodological)*, *57*(1), 289–300. https://doi.org/10.1111/J.2517-6161.1995.TB02031.X

Benz, M. S., Scott, I. U., Flynn, H. W., Unonius, N., & Miller, D. (2004). Endophthalmitis isolates and antibiotic sensitivities: a 6-year review of culture-proven cases. *American Journal of Ophthalmology*, *137*(1), 38–42. https://doi.org/10.1016/S0002-9394(03)00896-1

Bernstein, D. B., Sulheim, S., Almaas, E., & Segrè, D. (2021). Addressing uncertainty in genome-scale metabolic model reconstruction and analysis. In *Genome Biology* (Vol. 22, Issue 1, pp. 1–22). BioMed Central Ltd. https://doi.org/10.1186/s13059-021-02289-z

Bhusal, Y., Shiohira, C. M., & Yamane, N. (2005). Determination of in vitro synergy when three

antimicrobial agents are combined against Mycobacterium tuberculosis. *International Journal of Antimicrobial Agents*, *26*(4), 292–297. https://doi.org/10.1016/J.IJANTIMICAG.2005.05.005

Blair, J. M. A., Webber, M. A., Baylay, A. J., Ogbolu, D. O., & Piddock, L. J. V. (2015). Molecular mechanisms of antibiotic resistance. In *Nature Reviews Microbiology* (Vol. 13, Issue 1, pp. 42–51). Nature Publishing Group. https://doi.org/10.1038/nrmicro3380

Bliss, C. I. (1939). The Toxicity of Poisons Applied Jointly. *Annals of Applied Biology*, *26*(3), 585–615. https://doi.org/10.1111/j.1744-7348.1939.tb06990.x

Bochner, B. R., Gadzinski, P., & Panomitros, E. (2001). Phenotype Microarrays for high-throughput phenotypic testing and assay of gene function. *Genome Research*, *11*(7), 1246–1255. https://doi.org/10.1101/gr.186501

Bonnett, L. J., Ken-Dror, G., Koh, G. C. K. W., & Davies, G. R. (2017). Comparing the Efficacy of Drug Regimens for Pulmonary Tuberculosis: Meta-analysis of Endpoints in Early-Phase Clinical Trials. *Clinical Infectious Diseases*, *46*(1), 46–54. https://doi.org/10.1093/cid/cix247

Bonora, M., Patergnani, S., Rimessi, A., de Marchi, E., Suski, J. M., Bononi, A., Giorgi, C., Marchi, S., Missiroli, S., Poletti, F., Wieckowski, M. R., & Pinton, P. (2012). ATP synthesis and storage. *Purinergic Signalling*, *8*(3), 343–357. https://doi.org/10.1007/S11302-012-9305-8

Boyd, N., & Nailor, M. D. (2011). Combination Antibiotic Therapy for Empiric and Definitive Treatment of Gram-Negative Infections: Insights from the Society of Infectious Diseases Pharmacists. *Pharmacotherapy: The Journal of Human Pharmacology and Drug Therapy*, *31*(11), 1073–1084. https://doi.org/10.1592/PHCO.31.11.1073

Brauner, A., Fridman, O., Gefen, O., & Balaban, N. Q. (2016). Distinguishing between resistance, tolerance and persistence to antibiotic treatment. *Nature Reviews Microbiology*, *14*(5), 320–330. https://doi.org/10.1038/nrmicro.2016.34

Breijyeh, Z., Jubeh, B., & Karaman, R. (2020). Resistance of Gram-Negative Bacteria to Current Antibacterial Agents and Approaches to Resolve It. *Molecules*, *25*(6), 1340. https://doi.org/10.3390/MOLECULES25061340

Breiman, L. (2001). Random forests. *Machine Learning*, *45*(1), 5–32. https://doi.org/10.1023/A:1010933404324

Brochado, A. R., Telzerow, A., Bobonis, J., Banzhaf, M., Mateus, A., Selkrig, J., Huth, E., Bassler, S., Zamarreño Beas, J., Zietek, M., Ng, N., Foerster, S., Ezraty, B., Py, B., Barras, F., Savitski, M. M., Bork, P., Göttig, S., & Typas, A. (2018). Species-specific activity of antibacterial drug combinations. *Nature*, *559*(7713), 259–263. https://doi.org/10.1038/s41586-018-0278-9

Brown, S. A., Palmer, K. L., & Whiteley, M. (2008). Revisiting the host as a growth medium. In *Nature Reviews Microbiology* (Vol. 6, Issue 9, pp. 657–666). Nature Publishing Group. https://doi.org/10.1038/nrmicro1955

Bumann, D. (2015). Heterogeneous Host-Pathogen Encounters: Act Locally, Think Globally. *Cell Host & Microbe*, *17*(1), 13–19. https://doi.org/10.1016/J.CHOM.2014.12.006

Campit, S., & Chandrasekaran, S. (2020). Inferring metabolic flux from time-course metabolomics. In *Methods in Molecular Biology* (Vol. 2088, pp. 299–313). Humana Press Inc. https://doi.org/10.1007/978-1-0716-0159-4_13

Cantrell, J. M., Chung, C. H., & Chandrasekaran, S. (2022). Machine learning to design antimicrobial combination therapies: Promises and pitfalls. *Drug Discovery Today*, *27*(6),

1639–1651. https://doi.org/10.1016/J.DRUDIS.2022.04.006

Carter, J. D., Espinoza, L. R., Inman, R. D., Sneed, K. B., Ricca, L. R., Vasey, F. B., Valeriano, J., Stanich, J. A., Oszust, C., Gerard, H. C., & Hudson, A. P. (2010). Combination antibiotics as a treatment for chronic Chlamydia-induced reactive arthritis: A double-blind, placebo-controlled, prospective trial. *Arthritis and Rheumatism*, *62*(5), 1298–1307. https://doi.org/10.1002/art.27394

Centers for Disease Control and Prevention. (2019). *Antibiotic Resistance Threats in the United States*. https://doi.org/http://dx.doi.org/10.15620/cdc:82532

Chambers, H. F., & DeLeo, F. R. (2009). Waves of resistance: Staphylococcus aureus in the antibiotic era. *Nature Reviews Microbiology*, *7*(9), 629–641. https://doi.org/10.1038/nrmicro2200

Chandramohan, Y., Padmanaban, V., Bethunaickan, R., Tripathy, S., Swaminathan, S., & Ranganathan, U. D. (2019). In vitro interaction profiles of the new antitubercular drugs bedaquiline and delamanid with moxifloxacin against clinical Mycobacterium tuberculosis isolates. *Journal of Global Antimicrobial Resistance*, *19*, 348–353. https://doi.org/10.1016/J.JGAR.2019.06.013

Chandrasekaran, S., Cokol-Cakmak, M., Sahin, N., Yilancioglu, K., Kazan, H., Collins, J. J., & Cokol, M. (2016). Chemogenomics and orthology-based design of antibiotic combination therapies. *Molecular Systems Biology*, *12*(5), 872. https://doi.org/10.15252/msb.20156777

Chua, H. E., Bhowmick, S. S., & Tucker-Kellogg, L. (2017). Synergistic target combination prediction from curated signaling networks: Machine learning meets systems biology and pharmacology. *Methods*, *129*, 60–80. https://doi.org/10.1016/j.ymeth.2017.05.015

Chung, C. H., & Chandrasekaran, S. (2022). A flux-based machine learning model to simulate

the impact of pathogen metabolic heterogeneity on drug interactions. *PNAS Nexus*, *1*(3), 1–14. https://doi.org/10.1093/PNASNEXUS/PGAC132

Chung, C. H., Lin, D.-W., Eames, A., & Chandrasekaran, S. (2021). Next-Generation Genome-Scale Metabolic Modeling through Integration of Regulatory Mechanisms. *Metabolites*, *11*(9), 606. https://doi.org/10.3390/METABO11090606

Cicchese, J. M., Sambarey, A., Kirschner, D., Linderman, J. J., & Chandrasekaran, S. (2021). A multi-scale pipeline linking drug transcriptomics with pharmacokinetics predicts in vivo interactions of tuberculosis drugs. *Scientific Reports*, *11*(1), 5643. https://doi.org/10.1038/s41598-021-84827-0

Coelho, T., Machado, D., Couto, I., Maschmann, R., Ramos, D., Groll, A. von, Rossetti, M. L., Silva, P. A., & Viveiros, M. (2015). Enhancement of antibiotic activity by efflux inhibitors against multidrug resistant Mycobacterium tuberculosis clinical isolates from Brazil. *Frontiers in Microbiology*, *6*(APR), 330. https://doi.org/10.3389/FMICB.2015.00330

Cohen, N. R., Lobritz, M. A., & Collins, J. J. (2013). Microbial Persistence and the Road to Drug Resistance. *Cell Host & Microbe*, *13*(6), 632–642. https://doi.org/10.1016/J.CHOM.2013.05.009

Cokol, M., Li, C., & Chandrasekaran, S. (2018). Chemogenomic model identifies synergistic drug combinations robust to the pathogen microenvironment. *PLOS Computational Biology*, *14*(12), e1006677. https://doi.org/10.1371/journal.pcbi.1006677

Colangeli, R., Jedrey, H., Kim, S., Connell, R., Ma, S., Chippada Venkata, U. D., Chakravorty, S., Gupta, A., Sizemore, E. E., Diem, L., Sherman, D. R., Okwera, A., Dietze, R., Boom, W. H., Johnson, J. L., Mac Kenzie, W. R., & Alland, D. (2018). Bacterial Factors That Predict Relapse after Tuberculosis Therapy. *New England Journal of Medicine*, *379*(9),

823–833. https://doi.org/10.1056/NEJMOA1715849

Comas, I., Coscolla, M., Luo, T., Borrell, S., Holt, K. E., Kato-Maeda, M., Parkhill, J., Malla, B., Berg, S., Thwaites, G., Yeboah-Manu, D., Bothamley, G., Mei, J., Wei, L., Bentley, S., Harris, S. R., Niemann, S., Diel, R., Aseffa, A., … Gagneux, S. (2013). Out-of-Africa migration and Neolithic coexpansion of Mycobacterium tuberculosis with modern humans. *Nature Genetics*, *45*(10), 1176–1182. https://doi.org/10.1038/ng.2744

Couzin-Frankel, J. (2013). Cancer immunotherapy. *Science*, *342*(6165), 1432–1433. https://doi.org/10.1126/SCIENCE.342.6165.1432

Cowman, S., Burns, K., Benson, S., Wilson, R., & Loebinger, M. R. (2016). The antimicrobial susceptibility of non-tuberculous mycobacteria. *Journal of Infection*, *72*(3), 324–331. https://doi.org/10.1016/J.JINF.2015.12.007

Dahal, S., Yurkovich, J. T., Xu, H., Palsson, B. O., & Yang, L. (2020). Synthesizing Systems Biology Knowledge from Omics Using Genome-Scale Models. In *Proteomics* (Vol. 20, Issues 17–18, p. 1900282). Wiley-VCH Verlag. https://doi.org/10.1002/pmic.201900282

Das, P., Delost, M. D., Qureshi, M. H., Smith, D. T., & Njardarson, J. T. (2019). A Survey of the Structures of US FDA Approved Combination Drugs. *Journal of Medicinal Chemistry*, *62*(9), 4265–4311. https://doi.org/10.1021/ACS.JMEDCHEM.8B01610

Das, T. (2020). Endophthalmitis Management: Stain-Culture, Empirical Treatment, and Beyond. *Asia-Pacific Journal of Ophthalmology*, *9*(1), 1. https://doi.org/10.1097/01.APO.0000617904.11979.AE

Deeks, S. G. (2003). Treatment of antiretroviral-drug-resistant HIV-1 infection. In *Lancet* (Vol. 362, Issue 9400, pp. 2002–2011). Elsevier B.V. https://doi.org/10.1016/S0140-6736(03)15022-2

Dekel, E., & Alon, U. (2005). Optimality and evolutionary tuning of the expression level of a protein. *Nature*, *436*(7050), 588–592. https://doi.org/10.1038/nature03842

Dellinger, R. P., Levy, M., Rhodes, A., Annane, D., Gerlach, H., Opal, S. M., Sevransky, J. E., Sprung, C. L., Douglas, I. S., Jaeschke, R., Osborn, T. M., Nunnally, M. E., Townsend, S. R., Reinhart, K., Kleinpell, R. M., Angus, D. C., Deutschman, C. S., Machado, F. R., Rubenfeld, G. D., … Zimmerman, J. L. (2013). Surviving sepsis campaign: International guidelines for management of severe sepsis and septic shock: 2012. *Critical Care Medicine*, *41*(2), 580–637. https://doi.org/10.1097/CCM.0b013e31827e83af

Dharmaraja, A. T. (2017). Role of Reactive Oxygen Species (ROS) in Therapeutics and Drug Resistance in Cancer and Bacteria. *Journal of Medicinal Chemistry*, *60*(8), 3221–3240. https://doi.org/10.1021/acs.jmedchem.6b01243

Dheda, K., Barry, C. E., & Maartens, G. (2016). Tuberculosis. *The Lancet*, *387*(10024), 1211–1226. https://doi.org/10.1016/S0140-6736(15)00151-8

Doan, T., Akileswaran, L., Andersen, D., Johnson, B., Ko, N., Shrestha, A., Shestopalov, V., Lee, C. S., Lee, A. Y., & Van Gelder, R. N. (2016). Paucibacterial Microbiome and Resident DNA Virome of the Healthy Conjunctiva. *Investigative Ophthalmology & Visual Science*, *57*(13), 5116–5126. https://doi.org/10.1167/IOVS.16-19803

Drapeau, C. M. J., Grilli, E., & Petrosillo, N. (2010). Rifampicin combined regimens for Gram-negative infections: data from the literature. *International Journal of Antimicrobial Agents*, *35*(1), 39–44. https://doi.org/10.1016/j.ijantimicag.2009.08.011

Dwyer, D. J., Kohanski, M. A., & Collins, J. J. (2009). Role of reactive oxygen species in antibiotic action and resistance. *Current Opinion in Microbiology*, *12*(5), 482–489. https://doi.org/10.1016/J.MIB.2009.06.018

Edwards, J. S., Ibarra, R. U., & Palsson, B. O. (2001). In silico predictions of Escherichia coli metabolic capabilities are consistent with experimental data. *Nature Biotechnology*, *19*(2), 125–130. https://doi.org/10.1038/84379

Eisenreich, W., Dandekar, T., Heesemann, J., & Goebel, W. (2010). Carbon metabolism of intracellular bacterial pathogens and possible links to virulence. In *Nature Reviews Microbiology* (Vol. 8, Issue 6, pp. 401–412). Nature Publishing Group. https://doi.org/10.1038/nrmicro2351

El Zahed, S. S., & Brown, E. D. (2018). Chemical-Chemical Combinations Map Uncharted Interactions in Escherichia coli under Nutrient Stress. *IScience*, *2*, 168–181. https://doi.org/10.1016/J.ISCI.2018.03.018

Fabiani, C., Agarwal, M., Dogra, M., Tosi, G. M., & Davis, J. L. (2022). Exogenous Endophthalmitis. *Ocular Immunology and Inflammation*. https://doi.org/10.1080/09273948.2022.2152699

Fàbrega, A., Madurga, S., Giralt, E., & Vila, J. (2009). Mechanism of action of and resistance to quinolones. *Microbial Biotechnology*, *2*(1), 40–61. https://doi.org/10.1111/j.1751-7915.2008.00063.x

Fang, X., Lloyd, C. J., & Palsson, B. O. (2020). Reconstructing organisms in silico: genome-scale models and their emerging applications. In *Nature Reviews Microbiology* (pp. 1–13). Nature Research. https://doi.org/10.1038/s41579-020-00440-4

Farha, M. A., & Brown, E. D. (2019). Drug repurposing for antimicrobial discovery. In *Nature Microbiology* (Vol. 4, Issue 4, pp. 565–577). Nature Publishing Group. https://doi.org/10.1038/s41564-019-0357-1

Feist, A. M., & Palsson, B. O. (2010). The biomass objective function. *Current Opinion in*

Microbiology, *13*(3), 344–349. https://doi.org/10.1016/J.MIB.2010.03.003

Forrest, G. N., & Tamura, K. (2010). Rifampin combination therapy for nonmycobacterial infections. *Clinical Microbiology Reviews*, *23*(1), 14–34. https://doi.org/10.1128/CMR.00034-09

Forster, S. C., Liu, J., Kumar, N., Gulliver, E. L., Gould, J. A., Escobar-Zepeda, A., Mkandawire, T., Pike, L. J., Shao, Y., Stares, M. D., Browne, H. P., Neville, B. A., & Lawley, T. D. (2022). Strain-level characterization of broad host range mobile genetic elements transferring antibiotic resistance from the human microbiome. *Nature Communications*, *13*(1), 1–9. https://doi.org/10.1038/s41467-022-29096-9

Frei E 3rd, Karon M, Levin RH, Freireich EJ, Taylor RJ, Selawry O, Holland JF, Hoogstraten B, Wolman IJ, Abir E, Sawitsky A, Lee S, Mills SD, Burgert EO Jr, Spurr CL, Patterson RB, Ebaugh FG, James GW 3rd, & Moon JH. (1965). The Effectiveness of Combinations of Antileukemic Agents in Inducing and Maintaining Remission in Children with Acute Leukemia. *Blood*, *26*(5), 642–656.

Fuchs, T. M., Eisenreich, W., Heesemann, J., & Goebel, W. (2012). Metabolic adaptation of human pathogenic and related nonpathogenic bacteria to extra- and intracellular habitats. In *FEMS Microbiology Reviews* (Vol. 36, Issue 2, pp. 435–462). Oxford Academic. https://doi.org/10.1111/j.1574-6976.2011.00301.x

Gadamski, G., Ciarka, D., Gressel, J., & Gawronski, S. W. (2000). Negative cross-resistance in triazine-resistant biotypes of Echinochloa crus-galli and Conyza canadensis. *Weed Science*, *48*(2), 176–180. https://doi.org/10.1614/0043-1745(2000)048[0176:NCRITR]2.0.CO;2

Gentile, R. C., Shukla, S., Shah, M., Ritterband, D. C., Engelbert, M., Davis, A., & Hu, D. N. (2014). Microbiological spectrum and antibiotic sensitivity in endophthalmitis: A 25-year

review. *Ophthalmology*, *121*(8), 1634–1642. https://doi.org/10.1016/j.ophtha.2014.02.001

Gill, E. E., Franco, O. L., & Hancock, R. E. W. (2015). Antibiotic Adjuvants: Diverse Strategies for Controlling Drug-Resistant Pathogens. *Chemical Biology & Drug Design*, *85*(1), 56–78. https://doi.org/10.1111/CBDD.12478

Gomez, J. E., & McKinney, J. D. (2004). M. tuberculosis persistence, latency, and drug tolerance. *Tuberculosis*, *84*(1–2), 29–44. https://doi.org/10.1016/J.TUBE.2003.08.003

Gonzalo, X., Casali, N., Broda, A., Pardieu, C., & Drobniewski, F. (2015). Combination of amikacin and doxycycline against multidrug-resistant and extensively drug-resistant tuberculosis. *International Journal of Antimicrobial Agents*, *45*(4), 406–412. https://doi.org/10.1016/J.IJANTIMICAG.2014.11.017

Gramatica, P., & Sangion, A. (2016). A Historical Excursus on the Statistical Validation Parameters for QSAR Models: A Clarification Concerning Metrics and Terminology. *Journal of Chemical Information and Modeling*, *56*(6), 1127–1131. https://doi.org/10.1021/ACS.JCIM.6B00088

Greener, J. G., Kandathil, S. M., Moffat, L., & Jones, D. T. (2021). A guide to machine learning for biologists. *Nature Reviews Molecular Cell Biology*, 1–16. https://doi.org/10.1038/s41580-021-00407-0

Gutierrez, A., Jain, S., Bhargava, P., Hamblin, M., Lobritz, M. A., & Collins, J. J. (2017). Understanding and Sensitizing Density-Dependent Persistence to Quinolone Antibiotics. *Molecular Cell*, *68*(6), 1147-1154.e3. https://doi.org/10.1016/J.MOLCEL.2017.11.012

Güvenç Paltun, B., Kaski, S., & Mamitsuka, H. (2021). Machine learning approaches for drug combination therapies. *Briefings in Bioinformatics*, *22*(6), 1–16. https://doi.org/10.1093/BIB/BBAB293

Holmes, A. H., Moore, L. S. P., Sundsfjord, A., Steinbakk, M., Regmi, S., Karkey, A., Guerin, P. J., & Piddock, L. J. V. (2016). Understanding the mechanisms and drivers of antimicrobial resistance. *The Lancet*, *387*(10014), 176–187. https://doi.org/10.1016/S0140-6736(15)00473-0

Hornef, M. (2015). Pathogens, Commensal Symbionts, and Pathobionts: Discovery and Functional Effects on the Host. *ILAR Journal*, *56*(2), 159–162. https://doi.org/10.1093/ILAR/ILV007

Hutchings, M., Truman, A., & Wilkinson, B. (2019). Antibiotics: past, present and future. In *Current Opinion in Microbiology* (Vol. 51, pp. 72–80). Elsevier Ltd. https://doi.org/10.1016/j.mib.2019.10.008

Ianevski, A., Giri, A. K., & Aittokallio, T. (2020). SynergyFinder 2.0: visual analytics of multi-drug combination synergies. *Nucleic Acids Research*, *48*(W1), W488–W493. https://doi.org/10.1093/NAR/GKAA216

Imamovic, L., & Sommer, M. O. A. (2013). Use of collateral sensitivity networks to design drug cycling protocols that avoid resistance development. *Science Translational Medicine*, *5*(204), 204ra132-204ra132. https://doi.org/10.1126/scitranslmed.3006609

Jamal-Hanjani, M., Quezada, S. A., Larkin, J., & Swanton, C. (2015). Translational Implications of Tumor Heterogeneity. *Clinical Cancer Research*, *21*(6), 1258–1266. https://doi.org/10.1158/1078-0432.CCR-14-1429

Janausch, I. G., Zientz, E., Tran, Q. H., Kröger, A., & Unden, G. (2002). C4-dicarboxylate carriers and sensors in bacteria. *Biochimica et Biophysica Acta (BBA) - Bioenergetics*, *1553*(1–2), 39–56. https://doi.org/10.1016/S0005-2728(01)00233-X

Jia, J., Zhu, F., Ma, X., Cao, Z. W., Li, Y. X., & Chen, Y. Z. (2009). Mechanisms of drug

combinations: interaction and network perspectives. *Nature Reviews Drug Discovery*, *8*(2), 111–128. https://doi.org/10.1038/nrd2683

Jiang, T., Gradus, J. L., & Rosellini, A. J. (2020). Supervised Machine Learning: A Brief Primer. *Behavior Therapy*, *51*(5), 675–687. https://doi.org/10.1016/J.BETH.2020.05.002

Johansen, M. D., Herrmann, J. L., & Kremer, L. (2020). Non-tuberculous mycobacteria and the rise of Mycobacterium abscessus. *Nature Reviews Microbiology*, *18*(7), 392–407. https://doi.org/10.1038/s41579-020-0331-1

Johnson, M. D., & Perfect, J. R. (2010). Use of antifungal combination therapy: Agents, order, and timing. *Current Fungal Infection Reports*, *4*(2), 87–95. https://doi.org/10.1007/S12281-010-0018-6

Joseph, J., Sontam, B., Guda, S. J. M., Gandhi, J., Sharma, S., Tyagi, M., Dave, V. P., & Das, T. (2019). Trends in microbiological spectrum of endophthalmitis at a single tertiary care ophthalmic hospital in India: a review of 25 years. *Eye*, *33*(7), 1090–1095. https://doi.org/10.1038/s41433-019-0380-8

Junttila, M. R., & De Sauvage, F. J. (2013). Influence of tumour micro-environment heterogeneity on therapeutic response. *Nature*, *501*(7467), 346–354. https://doi.org/10.1038/nature12626

Kanehisa, M., & Goto, S. (2000). KEGG: Kyoto Encyclopedia of Genes and Genomes. *Nucleic Acids Research*, *28*(1), 27–30. https://doi.org/10.1093/NAR/28.1.27

Kapoor, G., Saigal, S., & Elongavan, A. (2017). Action and resistance mechanisms of antibiotics: A guide for clinicians. *Journal of Anaesthesiology Clinical Pharmacology*, *33*(3), 300. https://doi.org/10.4103/joacp.JOACP_349_15

Kapoor, P., & Murphy, P. (2018). Combination antibiotics against Pseudomonas aeruginosa,

representing common and rare cystic fibrosis strains from different Irish clinics. *Heliyon*, *4*(3), e00562. https://doi.org/10.1016/j.heliyon.2018.e00562

Katzir, I., Cokol, M., Aldridge, B. B., & Alon, U. (2019). Prediction of ultra-high-order antibiotic combinations based on pairwise interactions. *PLOS Computational Biology*, *15*(1), e1006774. https://doi.org/10.1371/journal.pcbi.1006774

Kavvas, E. S., Seif, Y., Yurkovich, J. T., Norsigian, C., Poudel, S., Greenwald, W. W., Ghatak, S., Palsson, B. O., & Monk, J. M. (2018). Updated and standardized genome-scale reconstruction of Mycobacterium tuberculosis H37Rv, iEK1011, simulates flux states indicative of physiological conditions. *BMC Systems Biology*, *12*(1), 25. https://doi.org/10.1186/s12918-018-0557-y

Kerantzas, C. A., & Jacobs, W. R. (2017). Origins of Combination Therapy for Tuberculosis: Lessons for Future Antimicrobial Development and Application. *MBio*, *8*(2). https://doi.org/10.1128/MBIO.01586-16

Kim, S., Lieberman, T. D., & Kishony, R. (2014). Alternating antibiotic treatments constrain evolutionary paths to multidrug resistance. *Proceedings of the National Academy of Sciences of the United States of America*, *111*(40), 14494–14499. https://doi.org/10.1073/pnas.1409800111

Kim, Y., Kim, G. B., & Lee, S. Y. (2021). Machine learning applications in genome-scale metabolic modeling. *Current Opinion in Systems Biology*, *25*, 42–49. https://doi.org/10.1016/J.COISB.2021.03.001

Kohanski, M. A., Dwyer, D. J., Hayete, B., Lawrence, C. A., & Collins, J. J. (2007). A Common Mechanism of Cellular Death Induced by Bactericidal Antibiotics. *Cell*, *130*(5), 797–810. https://doi.org/10.1016/j.cell.2007.06.049

Kontoyiannis, D. P., & Lewis, R. E. (2004). Toward more effective antifungal therapy: the prospects of combination therapy. *British Journal of Haematology*, *126*(2), 165–175. https://doi.org/10.1111/J.1365-2141.2004.05007.X

Krause, K. M., Serio, A. W., Kane, T. R., & Connolly, L. E. (2016). Aminoglycosides: An overview. *Cold Spring Harbor Perspectives in Medicine*, *6*(6). https://doi.org/10.1101/cshperspect.a027029

Kussell, E., Kishony, R., Balaban, N. Q., & Leibler, S. (2005). Bacterial PersistenceA Model of Survival in Changing Environments. *Genetics*, *169*(4), 1807–1814. https://doi.org/10.1534/GENETICS.104.035352

Labhsetwar, P., Cole, J. A., Roberts, E., Price, N. D., & Luthey-Schulten, Z. A. (2013). Heterogeneity in protein expression induces metabolic variability in a modeled Escherichia coli population. *Proceedings of the National Academy of Sciences*, *110*(34), 14006–14011. https://doi.org/10.1073/PNAS.1222569110

Lázár, V., Martins, A., Spohn, R., Daruka, L., Grézal, G., Fekete, G., Számel, M., Jangir, P. K., Kintses, B., Csörgő, B., Nyerges, Á., Györkei, Á., Kincses, A., Dér, A., Walter, F. R., Deli, M. A., Urbán, E., Hegedűs, Z., Olajos, G., … Pál, C. (2018). Antibiotic-resistant bacteria show widespread collateral sensitivity to antimicrobial peptides. *Nature Microbiology*. https://doi.org/10.1038/s41564-018-0164-0

LeCun, Y., Bengio, Y., & Hinton, G. (2015). Deep learning. *Nature*, *521*(7553), 436–444. https://doi.org/10.1038/nature14539

Lee, J.-H., Kim, D. G., Bae, T. J., Rho, K., Kim, J.-T., Lee, J.-J., Jang, Y., Kim, B. C., Park, K. M., & Kim, S. (2012). CDA: Combinatorial Drug Discovery Using Transcriptional Response Modules. *PLoS ONE*, *7*(8), e42573. https://doi.org/10.1371/journal.pone.0042573

Leimbach, A., Hacker, J., & Dobrindt, U. (2013). E. coli as an all-rounder: The thin line between commensalism and pathogenicity. *Current Topics in Microbiology and Immunology*, *358*, 3–32. https://doi.org/10.1007/82_2012_303

Levy, S. B. (2002). Active efflux, a common mechanism for biocide and antibiotic resistance. *Journal of Applied Microbiology*, *92*(1), 65S-71S. https://doi.org/10.1046/j.1365-2672.92.5s1.4.x

Lewis, K. (2006). Persister cells, dormancy and infectious disease. *Nature Reviews Microbiology*, *5*(1), 48–56. https://doi.org/10.1038/nrmicro1557

Lewis, N. E., Hixson, K. K., Conrad, T. M., Lerman, J. A., Charusanti, P., Polpitiya, A. D., Adkins, J. N., Schramm, G., Purvine, S. O., Lopez-Ferrer, D., Weitz, K. K., Eils, R., König, R., Smith, R. D., & Palsson, B. Ø. (2010). Omic data from evolved *E. coli* are consistent with computed optimal growth from genome-scale models. *Molecular Systems Biology*, *6*(1), 390. https://doi.org/10.1038/msb.2010.47

Lewis, N. E., Nagarajan, H., & Palsson, B. O. (2012). Constraining the metabolic genotype-phenotype relationship using a phylogeny of in silico methods. In *Nature Reviews Microbiology* (Vol. 10, Issue 4, pp. 291–305). Nature Publishing Group. https://doi.org/10.1038/nrmicro2737

Liu, H., Zhang, W., Zou, B., Wang, J., Deng, Y., & Deng, L. (2020). DrugCombDB: a comprehensive database of drug combinations toward the discovery of combinatorial therapy. *Nucleic Acids Research*, *48*(D1), D871–D881. https://doi.org/10.1093/NAR/GKZ1007

Liu, Y., Yang, K., Jia, Y., Shi, J., Tong, Z., Fang, D., Yang, B., Su, C., Li, R., Xiao, X., & Wang, Z. (2021). Gut microbiome alterations in high-fat-diet-fed mice are associated with

antibiotic tolerance. *Nature Microbiology*, *6*(7), 874–884. https://doi.org/10.1038/s41564-021-00912-0

Livengood, S. J., Drew, R. H., & Perfect, J. R. (2020). Combination Therapy for Invasive Fungal Infections. *Current Fungal Infection Reports*, *14*(1), 40–49. https://doi.org/10.1007/S12281-020-00369-4

Loewe, S., & Muischnek, H. (1926). Über Kombinationswirkungen - Mitteilung: Hilfsmittel der Fragestellung. *Archiv Für Experimentelle Pathologie Und Pharmakologie*, *114*(5–6), 313–326. https://doi.org/10.1007/BF01952257

Lopatkin, A. J., Stokes, J. M., Zheng, E. J., Yang, J. H., Takahashi, M. K., You, L., & Collins, J. J. (2019). Bacterial metabolic state more accurately predicts antibiotic lethality than growth rate. *Nature Microbiology*, *4*, 2109–2117. https://doi.org/10.1038/s41564-019-0536-0

Lu, T. K., & Koeris, M. S. (2011). The next generation of bacteriophage therapy. In *Current Opinion in Microbiology* (Vol. 14, Issue 5, pp. 524–531). Elsevier Current Trends. https://doi.org/10.1016/j.mib.2011.07.028

Lukens, A. K., Ross, L. S., Heidebrecht, R., Gamo, F. J., Lafuente-Monasterio, M. J., Booker, M. L., Hartl, D. L., Wiegand, R. C., & Wirth, D. F. (2014). Harnessing evolutionary fitness in Plasmodium falciparum for drug discovery and suppressing resistance. *Proceedings of the National Academy of Sciences of the United States of America*, *111*(2), 799–804. https://doi.org/10.1073/pnas.1320886110

Lyczak, J. B., Cannon, C. L., & Pier, G. B. (2000). Establishment of Pseudomonas aeruginosa infection: lessons from a versatile opportunist. *Microbes and Infection*, *2*(9), 1051–1060. https://doi.org/10.1016/S1286-4579(00)01259-4

Ma, S., Jaipalli, S., Larkins-Ford, J., Lohmiller, J., Aldridge, B. B., Sherman, D. R., &

Chandrasekaran, S. (2019). Transcriptomic signatures predict regulators of drug synergy and clinical regimen efficacy against tuberculosis. *MBio*, *10*(6). https://doi.org/10.1128/mBio.02627-19

Machado, D., & Herrgård, M. (2014). Systematic Evaluation of Methods for Integration of Transcriptomic Data into Constraint-Based Models of Metabolism. *PLoS Computational Biology*, *10*(4), e1003580. https://doi.org/10.1371/journal.pcbi.1003580

Maeda, T., Iwasawa, J., Kotani, H., Sakata, N., Kawada, M., Horinouchi, T., Sakai, A., Tanabe, K., & Furusawa, C. (2020). High-throughput laboratory evolution reveals evolutionary constraints in Escherichia coli. *Nature Communications*, *11*(1), 5970. https://doi.org/10.1038/s41467-020-19713-w

Mann, R., Mediati, D. G., Duggin, I. G., Harry, E. J., & Bottomley, A. L. (2017). Metabolic adaptations of Uropathogenic E. coli in the urinary tract. *Frontiers in Cellular and Infection Microbiology*, *7*(JUN), 241. https://doi.org/10.3389/fcimb.2017.00241

Manor, O., Dai, C. L., Kornilov, S. A., Smith, B., Price, N. D., Lovejoy, J. C., Gibbons, S. M., & Magis, A. T. (2020). Health and disease markers correlate with gut microbiome composition across thousands of people. *Nature Communications*, *11*(1), 1–12. https://doi.org/10.1038/s41467-020-18871-1

Martínez, J. L., & Rojo, F. (2011). Metabolic regulation of antibiotic resistance. *FEMS Microbiology Reviews*, *35*(5), 768–789. https://doi.org/10.1111/j.1574-6976.2011.00282.x

McDermott, A. (2022). Drug-resistant fungi on the rise. *Proceedings of the National Academy of Sciences of the United States of America*, *119*(48), e2217948119. https://doi.org/10.1073/PNAS.2217948119

Megchelenbrink, W., Huynen, M., & Marchiori, E. (2014). optGpSampler: An Improved Tool

for Uniformly Sampling the Solution-Space of Genome-Scale Metabolic Networks. *PLoS ONE*, *9*(2), 86587. https://doi.org/10.1371/JOURNAL.PONE.0086587

Melander, R. J., Zurawski, D. V., & Melander, C. (2018). Narrow-spectrum antibacterial agents. *MedChemComm*, *9*(1), 12. https://doi.org/10.1039/C7MD00528H

Meyer, C. T., Wooten, D. J., Lopez, C. F., & Quaranta, V. (2020). Charting the fragmented landscape of drug synergy. *Trends in Pharmacological Sciences*, *41*(4), 266. https://doi.org/10.1016/J.TIPS.2020.01.011

Mirzayev, F., Viney, K., Linh, N. N., Gonzalez-Angulo, L., Gegia, M., Jaramillo, E., Zignol, M., & Kasaeva, T. (2021). World Health Organization recommendations on the treatment of drug-resistant tuberculosis, 2020 update. *European Respiratory Journal*, *57*(6). https://doi.org/10.1183/13993003.03300-2020

Mokhtari, R. B., Homayouni, T. S., Baluch, N., Morgatskaya, E., Kumar, S., Das, B., & Yeger, H. (2017). Combination therapy in combating cancer. *Oncotarget*, *8*(23), 38022. https://doi.org/10.18632/ONCOTARGET.16723

Morales, E. F., & Escalante, H. J. (2022). A brief introduction to supervised, unsupervised, and reinforcement learning. *Biosignal Processing and Classification Using Computational Learning and Intelligence: Principles, Algorithms, and Applications*, 111–129. https://doi.org/10.1016/B978-0-12-820125-1.00017-8

Mori, M., Zhang, Z., Banaei-Esfahani, A., Lalanne, J., Okano, H., Collins, B. C., Schmidt, A., Schubert, O. T., Lee, D., Li, G., Aebersold, R., Hwa, T., & Ludwig, C. (2021). From coarse to fine: the absolute Escherichia coli proteome under diverse growth conditions. *Molecular Systems Biology*, *17*(5), e9536. https://doi.org/10.15252/msb.20209536

Munguia, J., & Nizet, V. (2017). Pharmacological Targeting of the Host–Pathogen Interaction:

Alternatives to Classical Antibiotics to Combat Drug-Resistant Superbugs. *Trends in Pharmacological Sciences*, *38*(5), 473–488. https://doi.org/10.1016/J.TIPS.2017.02.003

Muthukrishnan, N., Maleki, F., Ovens, K., Reinhold, C., Forghani, B., & Forghani, R. (2020). Brief History of Artificial Intelligence. *Neuroimaging Clinics of North America*, *30*(4), 393–399. https://doi.org/10.1016/J.NIC.2020.07.004

Namasivayam, S., Sher, A., Glickman, M. S., & Wipperman, M. F. (2018). The microbiome and tuberculosis: Early evidence for cross talk. In *mBio* (Vol. 9, Issue 5). American Society for Microbiology. https://doi.org/10.1128/mBio.01420-18

Nemeth, J., Oesch, G., & Kuster, S. P. (2015). Bacteriostatic versus bactericidal antibiotics for patients with serious bacterial infections: systematic review and meta-analysis. *Journal of Antimicrobial Chemotherapy*, *70*(2), 382–395. https://doi.org/10.1093/JAC/DKU379

Nichols, R. J., Sen, S., Choo, Y. J., Beltrao, P., Zietek, M., Chaba, R., Lee, S., Kazmierczak, K. M., Lee, K. J., Wong, A., Shales, M., Lovett, S., Winkler, M. E., Krogan, N. J., Typas, A., & Gross, C. A. (2011). Phenotypic landscape of a bacterial cell. *Cell*, *144*(1), 143–156. https://doi.org/10.1016/j.cell.2010.11.052

Ocampo, P. S., Lázár, V., Papp, B., Arnoldini, M., Zur Wiesch, P. A., Busa-Fekete, R., Fekete, G., Pál, C., Ackermann, M., & Bonhoeffer, S. (2014). Antagonism between bacteriostatic and bactericidal antibiotics is prevalent. *Antimicrobial Agents and Chemotherapy*, *58*(8), 4573–4582. https://doi.org/10.1128/AAC.02463-14

Olsson, A., Wistrand-Yuen, P., Nielsen, E. I., Friberg, L. E., Sandegren, L., Lagerbäck, P., & Tängdén, T. (2020). Efficacy of antibiotic combinations against multidrug-resistant pseudomonas aeruginosa in automated time-lapse microscopy and static time-kill experiments. *Antimicrobial Agents and Chemotherapy*, *64*(6).

https://doi.org/10.1128/AAC.02111-19

Orth, J. D., Conrad, T. M., Na, J., Lerman, J. A., Nam, H., Feist, A. M., & Palsson, B. Ø. (2011). A comprehensive genome-scale reconstruction of *Escherichia coli* metabolism—2011. *Molecular Systems Biology*, *7*(1), 535. https://doi.org/10.1038/msb.2011.65

Orth, J. D., Thiele, I., & Palsson, B. Ø. (2010). What is flux balance analysis? *Nature Biotechnology*, *28*(3), 245–248. https://doi.org/10.1038/nbt.1614

Oz, T., Guvenek, A., Yildiz, S., Karaboga, E., Tamer, Y. T., Mumcuyan, N., Ozan, V. B., Senturk, G. H., Cokol, M., Yeh, P., & Toprak, E. (2014). Strength of selection pressure is an important parameter contributing to the complexity of antibiotic resistance evolution. *Molecular Biology and Evolution*, *31*(9), 2387–2401. https://doi.org/10.1093/molbev/msu191

Ozkan, J., Nielsen, S., Diez-Vives, C., Coroneo, M., Thomas, T., & Willcox, M. (2017). Temporal Stability and Composition of the Ocular Surface Microbiome. *Scientific Reports*, *7*(1), 1–11. https://doi.org/10.1038/s41598-017-10494-9

Pai, M., Behr, M. A., Dowdy, D., Dheda, K., Divangahi, M., Boehme, C. C., Ginsberg, A., Swaminathan, S., Spigelman, M., Getahun, H., Menzies, D., & Raviglione, M. (2016). Tuberculosis. *Nature Reviews Disease Primers*, *2*(1), 1–23. https://doi.org/10.1038/nrdp.2016.76

Pál, C., Papp, B., & Lázár, V. (2015). Collateral sensitivity of antibiotic-resistant microbes. In *Trends in Microbiology* (Vol. 23, Issue 7, pp. 401–407). Elsevier Ltd. https://doi.org/10.1016/j.tim.2015.02.009

Palmblad, J., & Lönnqvist, B. (1982). Combination of Amikacin and either Ampicillin or Cephalotin as Initial Treatment of Febrile Neutropenic Patients. *Acta Medica Scandinavica*,

212(6), 379–384. https://doi.org/10.1111/j.0954-6820.1982.tb03233.x

Panchal, P., Budree, S., Scheeler, A., Medina, G., Seng, M., Wong, W. F., Eliott, R., Mitchell, T., Kassam, Z., Allegretti, J. R., & Osman, M. (2018). Scaling Safe Access to Fecal Microbiota Transplantation: Past, Present, and Future. In *Current Gastroenterology Reports* (Vol. 20, Issue 4, pp. 1–11). Current Medicine Group LLC 1. https://doi.org/10.1007/s11894-018-0619-8

Pedregosa, F., Varoquaux, G., Gramfort, A., Michel, V., Thirion, B., Grisel, O., Blondel, M., Prettenhofer, P., Weiss, R., Dubourg, V., Vanderplas, J., Passos, A., Cournapeau, D., Brucher, M., Perrot, M., & Duchesnay, É. (2011). Scikit-learn: Machine Learning in Python. *Journal of Machine Learning Research*, *12*(85), 2825–2830. http://jmlr.org/papers/v12/pedregosa11a.html

Peterson, E. J., Bailo, R., Rothchild, A. C., Arrieta-Ortiz, M. L., Kaur, A., Pan, M., Mai, D., Abidi, A. A., Cooper, C., Aderem, A., Bhatt, A., & Baliga, N. S. (2019). Path-seq identifies an essential mycolate remodeling program for mycobacterial host adaptation. *Molecular Systems Biology*, *15*(3), e8584. https://doi.org/10.15252/MSB.20188584

Pisu, D., Huang, L., Grenier, J. K., & Russell, D. G. (2020). Dual RNA-Seq of Mtb-Infected Macrophages In Vivo Reveals Ontologically Distinct Host-Pathogen Interactions. *Cell Reports*, *30*(2), 335-350.e4. https://doi.org/10.1016/J.CELREP.2019.12.033

Pluchino, K. M., Hall, M. D., Goldsborough, A. S., Callaghan, R., & Gottesman, M. M. (2012). Collateral sensitivity as a strategy against cancer multidrug resistance. *Drug Resistance Updates*, *15*(1–2), 98–105. https://doi.org/10.1016/j.drup.2012.03.002

Poirel, L., Madec, J.-Y., Lupo, A., Schink, A.-K., Kieffer, N., Nordmann, P., & Schwarz, S. (2018). Antimicrobial Resistance in Escherichia coli. *Microbiology Spectrum*, *6*(4).

https://doi.org/10.1128/MICROBIOLSPEC.ARBA-0026-2017

Price, N. D., Reed, J. L., & Palsson, B. (2004). Genome-scale models of microbial cells: Evaluating the consequences of constraints. In *Nature Reviews Microbiology* (Vol. 2, Issue 11, pp. 886–897). Nature Publishing Group. https://doi.org/10.1038/nrmicro1023

Raad, I., Darouiche, R., Hachem, R., Sacilowski, M., & Bodey, G. P. (1995). Antibiotics and prevention of microbial colonization of catheters. *Antimicrobial Agents and Chemotherapy*, *39*(11), 2397. https://doi.org/10.1128/AAC.39.11.2397

Ramakrishnan, L. (2012). Revisiting the role of the granuloma in tuberculosis. *Nature Reviews Immunology*, *12*(5), 352–366. https://doi.org/10.1038/nri3211

Ramon, C., Gollub, M. G., & Stelling, J. (2018). Integrating -omics data into genome-scale metabolic network models: principles and challenges. *Essays in Biochemistry*, *62*(4), 563–574. https://doi.org/10.1042/EBC20180011

Rayens, E., & Norris, K. A. (2022). Prevalence and Healthcare Burden of Fungal Infections in the United States, 2018. *Open Forum Infectious Diseases*, *9*(1). https://doi.org/10.1093/OFID/OFAB593

Regan-Fendt, K. E., Xu, J., DiVincenzo, M., Duggan, M. C., Shakya, R., Na, R., Carson, W. E., Payne, P. R. O., & Li, F. (2019). Synergy from gene expression and network mining (SynGeNet) method predicts synergistic drug combinations for diverse melanoma genomic subtypes. *Npj Systems Biology and Applications*, *5*(1), 1–15. https://doi.org/10.1038/s41540-019-0085-4

Reimers, A. M., & Reimers, A. C. (2016). The steady-state assumption in oscillating and growing systems. *Journal of Theoretical Biology*, *406*, 176–186. https://doi.org/10.1016/J.JTBI.2016.06.031

Rey-Jurado, E., Tudó, G., De La Bellacasa, J. P., Espasa, M., & González-Martín, J. (2013). In vitro effect of three-drug combinations of antituberculous agents against multidrug-resistant Mycobacterium tuberculosis isolates. *International Journal of Antimicrobial Agents*, *41*(3), 278–280. https://doi.org/10.1016/J.IJANTIMICAG.2012.11.011

Rey-Jurado, E., Tudó, G., Martínez, J. A., & González-Martín, J. (2012). Synergistic effect of two combinations of antituberculous drugs against Mycobacterium tuberculosis. *Tuberculosis*, *92*(3), 260–263. https://doi.org/10.1016/J.TUBE.2012.01.005

Ribeiro da Cunha, B., Fonseca, L. P., & Calado, C. R. C. (2021). Simultaneous elucidation of antibiotic mechanism of action and potency with high-throughput Fourier-transform infrared (FTIR) spectroscopy and machine learning. *Applied Microbiology and Biotechnology*, *105*(3), 1269–1286. https://doi.org/10.1007/s00253-021-11102-7

Rittershaus, E. S. C., Baek, S. H., & Sassetti, C. M. (2013). The Normalcy of Dormancy: Common Themes in Microbial Quiescence. *Cell Host & Microbe*, *13*(6), 643–651. https://doi.org/10.1016/J.CHOM.2013.05.012

Roemhild, R., & Andersson, D. I. (2021). Mechanisms and therapeutic potential of collateral sensitivity to antibiotics. *PLOS Pathogens*, *17*(1), e1009172. https://doi.org/10.1371/journal.ppat.1009172

Roy, K., Kar, S., & Das, R. N. (2015). Statistical Methods in QSAR/QSPR. In *A Primer on QSAR/QSPR Modeling* (pp. 37–59). Springer, Cham. https://doi.org/10.1007/978-3-319-17281-1_2

Russ, D., & Kishony, R. (2018). Additivity of inhibitory effects in multidrug combinations. *Nature Microbiology*, *3*(12), 1339–1345. https://doi.org/10.1038/s41564-018-0252-1

Saa, P. A., & Nielsen, L. K. (2017). Formulation, construction and analysis of kinetic models of

metabolism: A review of modelling frameworks. In *Biotechnology Advances* (Vol. 35, Issue 8, pp. 981–1003). Elsevier Inc. https://doi.org/10.1016/j.biotechadv.2017.09.005

Sadiq, M. A., Hassan, M., Agarwal, A., Sarwar, S., Toufeeq, S., Soliman, M. K., Hanout, M., Sepah, Y. J., Do, D. V., & Nguyen, Q. D. (2015). Endogenous endophthalmitis: diagnosis, management, and prognosis. *Journal of Ophthalmic Inflammation and Infection*, *5*(1), 1–11. https://doi.org/10.1186/S12348-015-0063-Y

Sarathy, J. P., & Dartois, V. (2020). Caseum: a Niche for Mycobacterium tuberculosis Drug-Tolerant Persisters. *Clinical Microbiology Reviews*, *33*(3). https://doi.org/10.1128/CMR.00159-19

Sarathy, J. P., Via, L. E., Weiner, D., Blanc, L., Boshoff, H., Eugenin, E. A., Barry, C. E., & Dartois, V. A. (2018). Extreme drug tolerance of mycobacterium tuberculosis in Caseum. *Antimicrobial Agents and Chemotherapy*, *62*(2). https://doi.org/10.1128/AAC.02266-17

Sarathy, J. P., Xie, M., Jones, R. M., Chang, A., Osiecki, P., Weiner, D., Tsao, W.-S., Dougher, M., Blanc, L., Fotouhi, N., Via, L. E., BarryIII, C. E., Vlaminck, I. De, Sherman, D. R., & Dartois, V. A. (2023). A Novel Tool to Identify Bactericidal Compounds against Vulnerable Targets in Drug-Tolerant M. tuberculosis found in Caseum. *MBio*, *14*(2). https://doi.org/10.1128/MBIO.00598-23

Schmidt, E. V., Sun, L. Z., Palmer, A. C., & Chen, C. (2023). Rationales for Combining Therapies to Treat Cancer: Independent Action, Response Correlation, and Collateral Sensitivity Versus Synergy. *Annual Review of Cancer Biology*, *7*, 247–263. https://doi.org/10.1146/ANNUREV-CANCERBIO-061421-020411

Schuetz, R., Kuepfer, L., & Sauer, U. (2007). Systematic evaluation of objective functions for predicting intracellular fluxes in Escherichia coli. *Molecular Systems Biology*, *3*(1), 119.

https://doi.org/10.1038/msb4100162

Seung, K. J., Keshavjee, S., & Rich, M. L. (2015). Multidrug-Resistant Tuberculosis and Extensively Drug-Resistant Tuberculosis. *Cold Spring Harbor Perspectives in Medicine*, *5*(9). https://doi.org/10.1101/CSHPERSPECT.A017863

Sharma, S. K., Mohan, A., & Kohli, M. (2021). Extrapulmonary tuberculosis. *Expert Review of Respiratory Medicine*, *15*(7), 931–948. https://doi.org/10.1080/17476348.2021.1927718

Shen, F., Boccuto, L., Pauly, R., Srikanth, S., & Chandrasekaran, S. (2019). Genome-scale network model of metabolism and histone acetylation reveals metabolic dependencies of histone deacetylase inhibitors. *Genome Biology*, *20*(1), 49. https://doi.org/10.1186/s13059-019-1661-z

Shen, F., Cheek, C., & Chandrasekaran, S. (2019). Dynamic Network Modeling of Stem Cell Metabolism. *Methods in Molecular Biology*, *1975*, 305–320. https://doi.org/10.1007/978-1-4939-9224-9_14

Shlomi, T., Cabili, M. N., Herrgård, M. J., Palsson, B., & Ruppin, E. (2008). Network-based prediction of human tissue-specific metabolism. In *Nature Biotechnology* (Vol. 26, Issue 9, pp. 1003–1010). Nature Publishing Group. https://doi.org/10.1038/nbt.1487

Shrestha, S. K., Fosso, M. Y., & Garneau-Tsodikova, S. (2015). A combination approach to treating fungal infections. *Scientific Reports*, *5*(1), 1–11. https://doi.org/10.1038/srep17070

Shtar, G., Azulay, L., Nizri, O., Rokach, L., & Shapira, B. (2022). CDCDB: A large and continuously updated drug combination database. *Scientific Data*, *9*(1), 1–11. https://doi.org/10.1038/s41597-022-01360-z

Silhavy, T. J., Kahne, D., & Walker, S. (2010). The Bacterial Cell Envelope. *Cold Spring Harbor Perspectives in Biology*, *2*(5). https://doi.org/10.1101/CSHPERSPECT.A000414

Silva, A., Lee, B. Y., Clemens, D. L., Kee, T., Ding, X., Ho, C. M., & Horwitz, M. A. (2016). Output-driven feedback system control platform optimizes combinatorial therapy of tuberculosis using a macrophage cell culture model. *Proceedings of the National Academy of Sciences of the United States of America*, *113*(15), E2172–E2179. https://doi.org/10.1073/pnas.1600812113

Simakurthy, S., & Tripathy, K. (2023). Endophthalmitis. *StatPearls*. https://www.ncbi.nlm.nih.gov/books/NBK559079/

Solomkin, J. S., Mazuski, J. E., Bradley, J. S., Rodvold, K. A., Goldstein, E. J. C., Baron, E. J., O'Neill, P. J., Chow, A. W., Dellinger, E. P., Eachempati, S. R., Gorbach, S., Hilfiker, M., May, A. K., Nathens, A. B., Sawyer, R. G., & Bartlett, J. G. (2010). Diagnosis and Management of Complicated Intra-Abdominal Infection in Adults and Children: Guidelines by the Surgical Infection Society and the Infectious Diseases Society of America. *Surgical Infections*, *11*(1), 79–109. https://doi.org/10.1089/SUR.2009.9930

Sorbara, M. T., & Pamer, E. G. (2022). Microbiome-based therapeutics. *Nature Reviews Microbiology*, 1–16. https://doi.org/10.1038/s41579-021-00667-9

St. Leger, A. J., Desai, J. V., Drummond, R. A., Kugadas, A., Almaghrabi, F., Silver, P., Raychaudhuri, K., Gadjeva, M., Iwakura, Y., Lionakis, M. S., & Caspi, R. R. (2017). An Ocular Commensal Protects against Corneal Infection by Driving an Interleukin-17 Response from Mucosal γδ T Cells. *Immunity*, *47*(1), 148-158.e5. https://doi.org/10.1016/j.immuni.2017.06.014

Stewart, G. R., Robertson, B. D., & Young, D. B. (2003). Tuberculosis: a problem with persistence. *Nature Reviews Microbiology*, *1*(2), 97–105. https://doi.org/10.1038/nrmicro749

Stokes, J. M., Lopatkin, A. J., Lobritz, M. A., & Collins, J. J. (2019). Bacterial Metabolism and Antibiotic Efficacy. *Cell Metabolism*. https://doi.org/10.1016/J.CMET.2019.06.009

Stokes, J. M., Yang, K., Swanson, K., Jin, W., Cubillos-Ruiz, A., Donghia, N. M., MacNair, C. R., French, S., Carfrae, L. A., Bloom-Ackerman, Z., Tran, V. M., Chiappino-Pepe, A., Badran, A. H., Andrews, I. W., Chory, E. J., Church, G. M., Brown, E. D., Jaakkola, T. S., Barzilay, R., & Collins, J. J. (2020). A Deep Learning Approach to Antibiotic Discovery. *Cell*, *180*(4), 688–702. https://doi.org/10.1016/j.cell.2020.01.021

Suzuki, S., Horinouchi, T., & Furusawa, C. (2014). Prediction of antibiotic resistance by gene expression profiles. *Nature Communications*, *5*(1), 5792. https://doi.org/10.1038/ncomms6792

Taniguchi, Y., Choi, P. J., Li, G. W., Chen, H., Babu, M., Hearn, J., Emili, A., & Sunney Xie, X. (2010). Quantifying E. coli proteome and transcriptome with single-molecule sensitivity in single cells. *Science*, *329*(5991), 533–538. https://doi.org/10.1126/SCIENCE.1188308

Tansarli, G. S., Andreatos, N., Pliakos, E. E., & Mylonakis, E. (2019). A Systematic Review and Meta-analysis of Antibiotic Treatment Duration for Bacteremia Due to Enterobacteriaceae. *Antimicrobial Agents and Chemotherapy*, *63*(5). https://doi.org/10.1128/AAC.02495-18

Thiele, I., & Palsson, B. (2010). A protocol for generating a high-quality genome-scale metabolic reconstruction. *Nature Protocols*, *5*(1), 93–121. https://doi.org/10.1038/nprot.2009.203

Torrey, L., & Learning, J. S. (2010). Transfer learning. In *Handbook of research on machine applications and trends: algorithms, methods, and techniques* (pp. 242–264). IGI global. https://www.igi-global.com/chapter/transfer-learning/36988

Tyers, M., & Wright, G. D. (2019). Drug combinations: a strategy to extend the life of antibiotics

in the 21st century. In *Nature Reviews Microbiology* (Vol. 17, Issue 3, pp. 141–155). Nature Publishing Group. https://doi.org/10.1038/s41579-018-0141-x

Umaña, M. A., Odio, C. M., Castro, E., Salas, J. L., & McCracken, G. H. (1990). Evaluation of aztreonam and ampicillin vs. amikacin and ampicillin for treatment of neonatal bacterial infections. *Pediatric Infectious Disease Journal*, *9*(3), 175–180. https://doi.org/10.1097/00006454-199003000-00006

Vasan, N., Baselga, J., & Hyman, D. M. (2019). A view on drug resistance in cancer. *Nature*, *575*(7782), 299–309. https://doi.org/10.1038/s41586-019-1730-1

Vaughan, J. W. (2018). Making Better Use of the Crowd: How Crowdsourcing Can Advance Machine Learning Research. *Journal of Machine Learning Research*, *18*(193), 1–46. http://jmlr.org/papers/v18/17-234.html

Verma, S., Bhatt, K., Lovey, A., Ribeiro-Rodrigues, R., Durbin, J., Jones-López, E. C., Palaci, M., Vinhas, S. A., Alland, D., Dietze, R., Ellner, J. J., & Salgame, P. (2019). Transmission phenotype of Mycobacterium tuberculosis strains is mechanistically linked to induction of distinct pulmonary pathology. *PLOS Pathogens*, *15*(3), e1007613. https://doi.org/10.1371/JOURNAL.PPAT.1007613

Vijayaraghavalu, S., Dermawan, J. K., Cheriyath, V., & Labhasetwar, V. (2013). Highly synergistic effect of sequential treatment with epigenetic and anticancer drugs to overcome drug resistance in breast cancer cells is mediated via activation of p21 gene expression leading to G2/M cycle arrest. *Molecular Pharmaceutics*, *10*(1), 337–352. https://doi.org/10.1021/mp3004622

Watson, S., Cabrera-Aguas, M., & Khoo, P. (2018). Common eye infections. *Australian Prescriber*, *41*(3), 67–72. https://doi.org/10.18773/AUSTPRESCR.2018.016

Webster, R. M. (2016). Combination therapies in oncology. *Nature Reviews Drug Discovery*, *15*(2), 81–82. https://doi.org/10.1038/NRD.2016.3

Wertheim, H. F. L., Melles, D. C., Vos, M. C., Van Leeuwen, W., Van Belkum, A., Verbrugh, H. A., & Nouwen, J. L. (2005). The role of nasal carriage in Staphylococcus aureus infections. *The Lancet Infectious Diseases*, *5*(12), 751–762. https://doi.org/10.1016/S1473-3099(05)70295-4

White, J. M., Schiffer, J. T., Ignacio, R. A. B., Xu, S., Kainov, D., Ianevski, A., Aittokallio, T., Frieman, M., Olinger, G. G., & Polyak, S. J. (2021). Drug Combinations as a First Line of Defense against Coronaviruses and Other Emerging Viruses. *MBio*, *12*(6). https://doi.org/10.1128/MBIO.03347-21

Whiteside, M. D., Winsor, G. L., Laird, M. R., & Brinkman, F. S. L. (2013). OrthologueDB: a bacterial and archaeal orthology resource for improved comparative genomic analysis. *Nucleic Acids Research*, *41*(Database issue). https://doi.org/10.1093/NAR/GKS1241

Wildenhain, J., Spitzer, M., Dolma, S., Jarvik, N., White, R., Roy, M., Griffiths, E., Bellows, D. S., Wright, G. D., & Tyers, M. (2016). Systematic chemical-genetic and chemical-chemical interaction datasets for prediction of compound synergism. *Scientific Data*, *3*(1), 1–9. https://doi.org/10.1038/sdata.2016.95

Wooten, D. J., Meyer, C. T., Lubbock, A. L. R., Quaranta, V., & Lopez, C. F. (2021). MuSyC is a consensus framework that unifies multi-drug synergy metrics for combinatorial drug discovery. *Nature Communications*, *12*(1), 1–16. https://doi.org/10.1038/s41467-021-24789-z

World Health Organization. (2014). *Antimicrobial resistance: global report on surveillance*. https://doi.org/10.1007/s13312-014-0374-3

World Health Organization. (2015). *Global tuberculosis report 2015*. https://apps.who.int/iris/handle/10665/191102

Yang, J. H., Bening, S. C., & Collins, J. J. (2017). Antibiotic efficacy — context matters. *Current Opinion in Microbiology*, *39*, 73–80. https://doi.org/10.1016/J.MIB.2017.09.002

Yang, J. H., Bhargava, P., McCloskey, D., Mao, N., Palsson, B. O., & Collins, J. J. (2017). Antibiotic-Induced Changes to the Host Metabolic Environment Inhibit Drug Efficacy and Alter Immune Function. *Cell Host & Microbe*, *22*(6), 757-765.e3. https://doi.org/10.1016/J.CHOM.2017.10.020

Yang, J. H., Wright, S. N., Hamblin, M., Palsson, B. O., Walker, G. C., & Collins, J. J. (2019). A White-Box Machine Learning Approach for Revealing Antibiotic Mechanisms of Action. *Cell*, *177*, 1649–1661. https://doi.org/10.1016/j.cell.2019.04.016

Yang, J., Pu, J., Lu, S., Bai, X., Wu, Y., Jin, D., Cheng, Y., Zhang, G., Zhu, W., Luo, X., Rosselló-Móra, R., & Xu, J. (2020). Species-Level Analysis of Human Gut Microbiota With Metataxonomics. *Frontiers in Microbiology*, *11*, 2029. https://doi.org/10.3389/FMICB.2020.02029/BIBTEX

Yeh, P., Tschumi, A. I., & Kishony, R. (2006). Functional classification of drugs by properties of their pairwise interactions. *Nature Genetics*, *38*(4), 489–494. https://doi.org/10.1038/ng1755

Yilancioglu, K., & Cokol, M. (2019). Design of high-order antibiotic combinations against M. tuberculosis by ranking and exclusion. *Scientific Reports*, *9*(1), 1–11. https://doi.org/10.1038/s41598-019-48410-y

Yuan, B., Shen, C., Luna, A., Korkut, A., Marks, D. S., Ingraham, J., & Sander, C. (2021). CellBox: Interpretable Machine Learning for Perturbation Biology with Application to the

Design of Cancer Combination Therapy. *Cell Systems*, *12*(2), 128-140.e4. https://doi.org/10.1016/j.cels.2020.11.013

Zampieri, G., Vijayakumar, S., Yaneske, E., & Angione, C. (2019). Machine and deep learning meet genome-scale metabolic modeling. *PLOS Computational Biology*, *15*(7), e1007084. https://doi.org/10.1371/journal.pcbi.1007084

Zhang, T., Zhang, L., Payne, P. R. O., & Li, F. (2021). Synergistic Drug Combination Prediction by Integrating Multiomics Data in Deep Learning Models. *Methods in Molecular Biology*, *2194*, 223–238. https://doi.org/10.1007/978-1-0716-0849-4_12

Zhao, W., Zheng, M., Wang, B., Mu, X., Li, P., Fu, L., Liu, S., & Guo, Z. (2016). Interactions of linezolid and second-line anti-tuberculosis agents against multidrug-resistant Mycobacterium tuberculosis in vitro and in vivo. *International Journal of Infectious Diseases*, *52*, 23–28. https://doi.org/10.1016/j.ijid.2016.08.027

Zhao, X.-M., Iskar, M., Zeller, G., Kuhn, M., van Noort, V., & Bork, P. (2011). Prediction of Drug Combinations by Integrating Molecular and Pharmacological Data. *PLoS Computational Biology*, *7*(12), e1002323. https://doi.org/10.1371/journal.pcbi.1002323

Zhu, M., & Dai, X. (2018). On the intrinsic constraint of bacterial growth rate: M. tuberculosis's view of the protein translation capacity. *Critical Reviews in Microbiology*, *44*(4), 455–464. https://doi.org/10.1080/1040841X.2018.1425672

Zhu, Z., Surujon, D., Ortiz-Marquez, J. C., Huo, W., Isberg, R. R., Bento, J., & van Opijnen, T. (2020). Entropy of a bacterial stress response is a generalizable predictor for fitness and antibiotic sensitivity. *Nature Communications*, *11*(1), 1–15. https://doi.org/10.1038/s41467-020-18134-z

Zimmerli, W., Trampuz, A., & Ochsner, P. E. (2004). Current concepts: Prosthetic-joint

infections. *The New England Journal of Medicine*, *351*(16), 1645–1654. https://doi.org/10.1056/NEJMra040181